TAP2 - PAT2

Functional properties by mixed nano-organic/metal oxide systems

FOMOS

F. BRUSCIOTTI, I. DE GRAEVE, J. VEREECKEN, H. TERRYN (VUB)
A. BATAN, F. RENIERS (ULB)
M. WENKIN, M. PIENS (CORI)
A. BATAN, J.J. PIREAUX (FUNDP)

STANDARDISATION

TELECOMMUNICATIONS

SPACE SECTOR

CLEAN TECHNOLOGIES

NEW MATERIALS

.be

PROGRAMME TO STIMULATE KNOWLEDGE TRANSFER IN AREAS OF STRATEGIC IMPORTANCE

TAP2

FINAL REPORT

FUNCTIONAL PROPERTIES BY MIXED NANO ORGANIC/METAL OXIDE SYSTEMS
FOMOS

P2/00/04

Promoters

Herman Terryn
Vrije Universiteit Brussel (VUB), Electrochemical and Surface Engineering (SURF)
Pleinlaan 2, B-1050 Brussels

François Reniers
Université Libre de Bruxelles (ULB), Analytical and Interfacial Chemistry
Bld Triomphe 2, B-1050 Brussels

Jean-Jacques Pireaux
University of Namur (FUNDP), Research centre in Physics of Matter and Radiation (PMR)
Rue de Bruxelles 61, B-5000 Namur

Marcel Piens
Coating Research Institute (CoRI)
Av. P. Holoffe 21, B-1342 Limelette

Authors
Fabiola Brusciotti, Iris De Graeve, Jean Vereecken, Herman Terryn (VUB)
Abdelkrim Batan, François Reniers (ULB)
Mireille Wenkin, Marcel Piens (CoRI)
Abdelkrim Batan, Jean-Jacques Pireaux (FUNDP)

TABLE OF CONTENTS

RESUME

Les couches minces de silane sont appliquées aux surfaces métalliques pour former par exemple une couche de protection contre la corrosion, ou servir comme couche intermédiaire pour des revêtements ultérieurs. Le précurseur bis-1, 2 - (triethoxysilyl) éthane (BTSE) est utilisé pour déposer des couches minces de silane sur l'aluminium (99,99%) en utilisant trois techniques différentes: dipcoating, plasma à basse pression et plasma à pression atmosphérique.

L'objectif de cette étude est, d'une part, de comparer les caractéristiques de surface de couches déposées par les différentes méthodes de dépôt afin d'obtenir des informations sur la façon dont la molécule de BTSE est modifiée suivant la technique utilisée, et d'autre part, d'étudier l'interface entre les couches de silane déposées par plasma et le substrat d'aluminium.

En général, la méthode de dépôt par voie humide (dipcoating) nécessite de l'eau pour hydrolyser les groupements alcoxy de la molécule de silane formant ainsi des silanols. La présence de ces silanols et des groupements hydroxyles à la surface du métal est essentielle pour la formation d'une liaison covalente Si-O-métal à l'interface métal/couche mince. Une fois la couche de silane déposée, il est nécessaire d'appliquer un traitement thermique afin d'obtenir une couche dense de silane constituant une barrière efficace contre la corrosion, et de renforcer la réticulation de la couche de silane. Cette couche réticulée agira comme une barrière physique entre le substrat métallique et l'environnement agressif.

Une variété de silanes déposés par dipcoating a été étudiée jusqu'à présent pour des traitements d'aluminium et de ses alliages. Ces silanes ont fourni une forte adhésion au substrat d'aluminium et ont présenté des performances exceptionnelles de protection contre la corrosion de l'aluminium, comparable au traitement par les couches de conversion chimique. Cependant, la technique dipcoating présente quelques inconvénients tels que l'utilisation de solvants organiques et une cinétique lente (environ deux jours) pour hydrolyser la solution de silane. De plus, il est possible que des molécules d'eau restent piégées dans les couches de silanes ce qui diminuerait les propriétés anticorrosion du revêtement. La technologie plasma a été utilisée dans ce travail comme une alternative au dipcoating. Le plasma est utilisé pour décomposer chimiquement la vapeur du précurseur du silane formant ainsi les espèces actives impliquées dans la croissance de la couche. Les avantages des techniques plasmas sont nombreux : le contrôle facile des paramètres expérimentaux et son approche respectueuse de l'environnement car aucun solvant n'est nécessaire. Dans le cas des dépôts de couches de silanes comme protection contre la corrosion, l'utilisation des plasmas pourrait être avantageuse car elle évite les réactions de condensation, c'est-à-dire la libération d'eau à l'origine de la dégradation des propriétés barrières de la couche.

Le premier objectif atteint dans ce projet est la mise au point de dépôt de couches minces de silane sur l'aluminium par trois méthodes différentes : dipcoating, plasma à basse pression et plasma à pression atmosphérique. La déposition de films de BTSE par déposition plasma n'avait pas été encore rapportée dans la littérature. Avec ces trois différentes techniques, nous somme capable de déposer des couches minces de silane homogènes, similaires et ayant toutes la même épaisseur. Cette similarité est un bon point de départ afin de comparer les propriétés physico-chimiques de ces couches minces de silane en fonction de la méthode de dépôt.

Les mesures XPS ont montré que les valeurs de la composition atomique des couches de silanes déposées par dipcoating et plasma à basse pression sont comparables. En revanche, la teneur en carbone dans les couches des silanes déposées par plasma à pression atmosphère est trop faible (environ 6,7%). L'énergie de liaison du pic XPS du silicium 2p dans les couches de silanes déposées par plasma à pression atmosphérique est plus élevée et présente une valeur de 103,2 eV. Ces mesures XPS sont en accord avec les mesures infrarouges. En effet, le spectre infrarouge des couches de silane déposées par plasma à pression atmosphérique montre que la bande caractéristique du mode de vibration élongation du groupement siloxane est décalée vers les valeurs plus élevées du nombre d'onde. En revanche, le pic caractéristique du mode de vibration de balancement de la liaison Si-C dans le groupe Si-CH$_3$ est atténué, ce qui suggère la suppression par oxydation des hydrocarbures. De plus, l'absence du pic caractéristique du mode de vibration élongation CH dans le spectre des couches de silane déposées par plasma à pression atmosphérique fournit également une preuve de la perte préférentielle de la matière organique lors du traitement par plasma à pression atmosphérique.

L'adhérence de ces couches de silanes sur le métal a été aussi évaluée, elle dépend de la liaison chimique à l'interface métal-couche de silane.

Un des objectifs de ce projet est de déterminer si la liaison covalente AlOSi est formée à l'interface aluminium/couches de silane déposées par plasma puisque ces dernières sont obtenues en décomposant par plasma la vapeur de la solution de silane (BTSE) non hydrolysée. Dans ce cas-ci aucune réaction de condensation n'a eu lieu, et donc une étude approfondie de l'interface est nécessaire afin de mettre en évidence la formation ou non des liaisons chimiques réelles entre les couches de silanes déposées par plasma et le substrat d'aluminium.

Les mesures ToF-SIMS à haute résolution des ions positifs ont permis d'identifier la présence du fragment Al-O-Si à travers la présence de l'ion AlOSi$^+$ à la masse nominale 70.9539 uma. Cet ion est révélateur de la présence de la liaison covalente Al-O-Si à l'interface. La masse expérimentale observée pour le fragment AlOSi diffère de la masse théorique (70.9534) par 0.0005 uma, et elle est bien séparée (de

plus de 0.01 uma) des autres espèces qui peuvent être identifiés à la même masse nominale de 71 uma, à savoir AlSiCH$_4^+$ (70.9898) et Al$_2$OH$^+$ (70.9658).

Les profils ToF-SIMS et images ToF-SIMS ont confirmé la présence de la couche interfaciale due au fragment AlOSi et donc des liaisons covalentes à l'interface.

Jusqu'à présent, cette forte interaction silane/aluminium n'a jamais été observée à l'interface métal/couche déposée par plasma.

Après avoir confirmé par ToF-SIMS la présence d'une liaison chimique à l'interface des couches de silane déposées par plasma et de l'aluminium, nous avons testé la stabilité relative de ces couches en les plaçant dans un bain à ultrason. La comparaison des aires des pics XPS Al2p et Si2p avant et après le traitement a permis de confirmer indirectement une bonne adhésion des couches sur l'aluminium et ainsi la formation de la liaison covalente AlOSi à l'interface.

Les revêtements de BTSE déposés selon les trois différents méthodes ont aussi été comparés en matière de propriétés barrières et de résistance à la corrosion à l'aide de la spectroscopie d'impédance électrochimique (SIE) en milieu Na$_2$SO$_4$ et NaCl. Seul un écart mineur différencie les trois types de film. Dans tous les cas, le comportement anticorrosion disparaît après un jour d'immersion. Ceci est dû à la très petite épaisseur de ces couches. En effet, cette faible épaisseur affecte bien plus les propriétés anticorrosion des couches que leur chimie et leur composition.

Le précurseur héxaméthylsiloxane (HMDSO) est utilisé pour déposer des couches minces de SiO$_x$ sur le substrat d'aluminium (99.99%) (système 2) par plasma à basse et à pression atmosphérique afin d'être utilisées comme des couches intermédiaires entre le substrat métallique et des couches organiques (peintures).

Les résultats ont montré que des couches minces de SiO$_2$, SiO$_x$ et SiO$_x$C$_y$ peuvent être sélectivement déposées par plasma à basse et à pression atmosphérique en utilisant HMDSO en tant que précurseur.

Le rapport du mélange gazeux (HMDSO/O$_2$) dans le plasma a un effet crucial sur l'environnement chimique de l'atome du silicium dans le dépôt. En effet, les couches minces déposées par plasma HMDSO sans oxygène sont organiques et possédant une surface riche en espèces carbonés, tandis que les couches minces déposées à partir d'un plasma (HMDSO/O$_2$) sont inorganiques avec une très faible quantité de carbone à la surface.

Une caractéristique intéressante des couches déposées par plasma à basse pression et à pression atmosphérique est la similitude de leur composition atomique.

La porosité des couches déposées peut être suivie par la présence de groupements hydroxyles dans les spectres infrarouges.

La nouveauté et l'originalité majeure de ce travail est l'étude de couches minces (moins de 100 nm) formées á partir de BTSE en solution aqueuse, dans laquelle des nanoparticules nano dispersées de $CeCO_2$ ont été incorporées (système 3), avec une distribution uniforme dans film, afin d'améliorer les propriétés barrières. La faible épaisseur du revêtement ainsi que la nature aqueuse de la solution de BTSE sont deux importantes finalités pour l'industrie dans l'optique de réduire le coût et le poids des matériaux, mais aussi l'impact sur la santé humaine et sur l'environnement.

De nombreuses mesures ont été réalisées afin de comprendre comment la présence de nanoparticules pourrait affecter le silane étudié. Des analyses de la solution de déposition utilisant la RMN du ^{29}Si ont montré que la présence de CeO_2 ne modifiait ni la stabilité, ni le vieillissement de la solution de BTSE sur une période de plus de 4 mois. Les interactions chimiques entre les nanoparticules de CeO2 et le silane dans le revêtement réticulé ont été étudiées par XPS. La modification de la forme des pics, ainsi que leurs décalages dans le spectre, entre les différents composants individuels et le revêtement complet indique la formation possible d'une liaison entre les silanes du BTSE et le Ce dans le film après réticulation.

Un des problèmes critique à gérer dans l'élaboration de ces couches minces hybrides est la formation d'agglomérat de nanoparticules de taille similaire à l'épaisseur du film, ce qui conduit à l'apparition de monticules à la surface de l'échantillon affectant l'uniformité et l'homogénéité de la couche et pouvant générer des chemins préférentiels pour les espèces agressives. La formation de couches minces uniformes et homogènes a été réalisée avec succès en ajoutant dans la solution de BTSE les nanoparticules de CeO_2 sous forme de nano-suspension aqueuse.

Les informations sur la structure de la couche ont été obtenues en combinant les résultats provenant des mesures de MEB-FEG, AES-FEG et FIB-MET/EDX. Elles confirment la présence de particules de CeO_2 nano dispersées au sein de la couche de BTSE, et montrent que ces nano oxydes sont toujours recouverts par un film uniforme de silane. En d'autres mots, ces nanoparticules sont bien insérées dans la matrice de silane. Ceci explique les résultats obtenus lors des mesures de SIE en milieu Na_2SO_4 qui montrent que l'incorporation de nanoparticules de CeO_2 modifie les propriétés barrières des couches minces de BTSE. Les meilleures performances sont observées pour les revêtements contenant les nanoparticules nano dispersées fournissant ainsi une couche plus homogène et plus uniforme.

Des mesures supplémentaires de SIE sur des films déposés sur un substrat AA2024-T3 ont été réalisées en milieu NaCl afin d'étudier leurs propriétés de résistance à la corrosion, en présence d'inhibiteurs de corrosion (Ce^{3+}). Bien que les échantillons montrent dans un premier temps un (léger) comportement barrière, en comparaison du blanc, ils perdent tout leur pouvoir protecteur après 1 jour

d'immersion dans la solution de NaCl. Ces résultats sont une confirmation supplémentaire du fait que la faible épaisseur des couches est la principale raison expliquant les faibles performances anticorrosion des échantillons, bien plus que la composition des films et/ou la présence d'additifs.

L'observation d'aluminium nu et des systèmes 1 et 3 (avec ou sans nitrate de cérium) après une exposition au brouillard salin acétique de 24 et de 48h montre que le dépôt d'une couche de silane sur la surface de l'aluminium augmente la résistance du substrat à la corrosion.

L'aluminium nu et les systèmes 1 et 3 ont été revêtus de quatre peintures (une peinture aqueuse commerciale, une peinture UV aqueuse, une peinture UV sans solvants ou une peinture en poudre commerciale). L'influence des dépôts de silane sur l'adhérence des peintures et sur leur résistance à la corrosion a été déterminée.

Seule l'adhérence de la peinture aqueuse commerciale sur un des deux supports en aluminium testés a été accrue en présence d'une couche de BTSE. Dans les autres cas, aucune amélioration significative de l'adhérence n'a été constatée. Une nette diminution de l'adhérence de la peinture poudre a même été observée lorsque celle-ci est appliquée sur les systèmes 1 et 3.

Cependant, les tests de résistance à une exposition au brouillard salin acétique et les mesures de spectroscopie d'impédance électrochimique ont mis en évidence que l'addition de nanoparticules d'oxyde de cérium et de nitrate de cérium dans la couche de BTSE permettait d'accroître la résistance à la corrosion des plaques peintes.

Mots-Clés: *Aluminium, couches minces, BTSE en solution aqueuse, BTSE polymérisation plasma, déposition plasma, nanoparticules CeO$_2$, XPS, IRRAS, ToF-SIMS, propriétés barrière*

SAMENVATTING

Silaandeklagen worden om verscheidene redenen aangebracht op metalen, bijvoorbeeld als bescherming tegen corrosie of als primer voor verdere verflaagapplicaties. In dit project wordt bis-1,2-(triethoxysilyl) ethaan of BTSE gebruikt als precursor om deklagen aan te brengen op aluminium door middel van drie applicatiemethodes: dipcoating (water-gebaseerd BTSE), vacuüm plasma en atmosferische plasma depositie.

De algemene doelstelling van deze studie is om dunne deklagen (< 100 nm), bekomen met deze drie methodes te vergelijken in termen van chemische samenstelling, morfologie en eigenschappen; de verschillende applicatiemethodes hebben immers een andere invloed op de silaanmoleculen voor en tijdens de depositie. Ook worden hybride laagsystemen aangebracht waarin metaaloxide nanodeeltjes (CeO_2) and andere additieven zoals corrosie-inhibitoren (Ce^{3+}) worden toegevoegd om de eigenschappen te verbeteren.

Tot op heden worden silaandeklagen aangebracht vanuit een oplossing, via dipping, sproei- of rollcoating. De aanwezigheid van water in de oplossing is nodig om de silaanmoleculen te hydrolyseren zodat de aanwezige (m)ethoxygroepen worden omgezet in zeer reactieve silanolgroepen. Deze reageren dan met metaalhydroxidegroepen aan het metaaloppervlak om een covalent gebonden metaal-silaan interface te vormen. Door een thermische curing van het gecoate substraat kan crosslinking, door condensatie tussen nog vrije silanolgroepen, zorgen voor een goede barrière-werking tegen de indringing van agressieve componenten vanuit het milieu om aldus het metaal te beschermen tegen corrosie.

De afzetting van silaanlagen via de natte chemieroute werd reeds uitvoerig bestudeerd, maar deze methode kent meerdere nadelen. Ondermeer zijn er tal van processtappen nodig: eerst de activering van het metaaloppervlak om de hechting met het silaan te bevorderen, daarna de silaanafzetting en daarna de curing van de laag. Verder impliceert deze methode het gebruik van organische solventen indien nog geen watergebaseerde alternatieven voorhanden zijn, en de productie van meerdere afvalstromen. Indien watergebaseerde silanen gebruikt worden, dan blijkt het zeer moeilijk om alle water uit de laag te verwijderen wat ten koste gaat van de corrosieweerstand.

Plasmatechnologie kan een efficiënt alternatief bieden. In een plasma wordt de silaanprecursor opgebroken in reactieve deeltjes voor filmformatie. Er zijn tal van voordelen zoals de hoge controle over de procesparameters en de milieuvriendelijke processing zonder solventen of afvalstromen. Het metaal kan tevens in dezelfde reactoropstelling gereinigd en geactiveerd worden vóór de laagdepositie en er wordt

direct een gecrosslinkte film gevormd, waarvan de mate van crosslinking afhangt van de gebruikte plasmacondities.

De resultaten van dit project tonen dat het mogelijk is om dunne filmen af te zetten vanuit een silaanprecursor via vacuüm en atmosferische plasma processing. De vorming van BTSE lagen via plasmadepositie werd nog niet eerder gerapporteerd in de literatuur. Het is mogelijk met de drie methodes -natte depositie, vacuüm en atmosferische plasma- lagen met vergelijkbare diktes te vormen; dit is een belangrijk resultaat als startpunt om de lagen te kunnen vergelijken in termen van chemie en eigenschappen.

XPS leert ons dat via vacuüm plasma de lagen qua chemie het best overeenstemmen met die van de natte depositie. In de atmosferische plasmacoatings is het koolstofgehalte echter lager (6.7%), en het siliciumgehalte hoger. De Si2p bindingsenergie (103.2 eV) is tevens hoger dan verwacht, in overeenstemming met IRRAS metingen. XPS duidt aan dat de atmosferische plasmacoatings meer geoxideerd zijn, en IR bevestigt dit door een shift van de Si-O-Si stretching band bij 1250-1000 cm^{-1}, en een reductie van de Si-CH$_3$ band bij 1270 cm^{-1} wat wijst op de oxidatieve verwijdering van de methylgroepen. De afwezigheid van de C-H stretching band bij 2950 cm^{-1} versterkt de vaststelling dat de atmosferische plasmacoatings minder organisch van aard zijn. De zuurstof aanwezig tijdens de atmosferische plasma processing is verantwoordelijk voor de vorming van coatings met meer Si-O bindingen dan in de lagen gevormd via natte of vacuüm plasma depositie.

Silanen worden naast als barrièrelagen, ook gebruikt als adhesiepromotors. Gehydrolyseerde silaanmoleculen kunnen immers met metaalhydroxidegroepen een covalente Si-O-Al binding vorming door condensatie; dit resulteert in een sterke hechting tussen metaal en coating. In het project werd nagegaan of deze covalent gebonden interface ook mogelijk is via plasma depositie waar niet in de precursor silanolgroepen aanwezig zijn, aangezien men vertrekt vanuit geconcentreerd BTSE dat wordt gevaporiseerd. Met hoge-resolutie ToF-SIMS wordt de aanwezigheid van een AlOSi$^+$ fragment aan de interface tussen metaal en coating gemeten zowel voor vacuum als atmosferische plasma coatings. De massa van dit fragment is goed gescheiden, met meer dan 0.01 amu, van de andere mogelijke fragmenten met vergelijkbare nominale massa, zijnde Al$_2$OH$^+$ en AlSiCH$_4^+$, en ook contaminatie met koolstof wordt uitgesloten.

Via diepteprofilering wordt bevestigd dat de intensiteit van het AlOSi$^+$ fragment bij massa 71 maximaal is aan de metaal-film interface, en, eenmaal daar voorbij, de intensiteit daalt terwijl de intensiteit van Al$_2$O$^+$ toeneemt door de sputtering van het geoxideerde substraat. Deze waarnemingen werden verder bevestigd door het opstellen van ToF-SIMS beelden van de verschillende fragmenten in functie van de

laagdikte: aan het buitenoppervlak wordt organisch materiaal gemeten, daarna Si_2O^+ ionen van het siloxaan netwerk, daarna de interface $AlOSi^+$ ionen, gevolgd door Al_2O^+ ionen van de oxidelaag, en tot slot Al2p ionen afkomstig van het substraat.

De stabiliteit van de coatings op de substraten wordt bevestigd door ultrasone testing waarbij met XPS voor en na de ultrasone sonificatie de relatieve intensiteiten van de Al2p en Si2p pieken worden vergeleken. Een constante ratio van Si/Al bevestigt dat de filmen goed hechten op het metaal.

De BTSE filmen gemaakt met de drie applicatiemethodes worden verder vergeleken in termen van barrière-eigenschappen en corrosiebescherming met behulp van EIS in Na_2SO_4 en NaCl. De drie types lagen vertonen minimale verschillen in initiële impedantie. Reeds na 1 dag in de oplossing neemt de initiële barrièrewerking af doordat de lagen bijzonder dun zijn (< 100 nm), en bijgevolg niet als finale coating mogen bestemd worden. Eventuele effecten van de verschillen in samenstelling van de lagen gevormd met de verschillende applicatiemethodes komen hierdoor niet tot uiting.

Een deel van het project onderzoekt ook de mogelijkheid om SiO_x filmen (systeem 2) te vormen met vacuüm en atmosferische plasma depositie. Dit type film wordt gebruikt als diëlektrische laag in elektronische componenten of als film met lage brekingsindex in optische systemen zoals anti-reflectie coatings op architecturaal glas of plastic. In dit project werd plasma depositie van een dunne SiO_x film op aluminium bestudeerd, met HMDSO als precursor. De experimenten tonen aan dat SiO_2, SiO_x en SiO_xC_y films selectief kunnen gevormd worden met PECVD bij lage en atmosferische druk. De $HMDSO/O_2$ ratio in het gasmengsel is hierbij van cruciaal belang. Films gevormd met puur HMDSO zijn polymeerachtig met een hoog gehalte aan koolstof aan het oppervlak, terwijl een $HMDSO/O_2$ mengsel resulteert in een silica-achtige film met maar weinig koolstofcomponenten. Filmen gevormd bij lage and atmosferische druk hebben een vergelijkbare samenstelling, met een zekere porositeit die met IR kan gevolgd worden op basis van de hydroxyl-groepen.

Zeer innovatief in dit project zijn de resultaten op systeem 3 waarbij een zeer dunne watergebaseerde BTSE film wordt gevormd met nano-gedisperseerde CeO_2 deeltjes voor verbeterde barrière-eigenschappen. De dunne laagdikte en de water-gebaseerde natuur van de film zijn zeer belangrijk voor de industrie indien natte depositie wordt toegepast, voor economische en ecologische redenen.

Er werd nagegaan met ^{29}Si NMR analyse hoe de aanwezigheid van nano-oxide deeltjes de silaanoplossing beïnvloedt. Er werd waargenomen dat de stabiliteit van de oplossing ongewijzigd blijft voor een periode van minstens 4 maanden, wat de bruikbaarheid voor industriële applicatie mogelijk maakt. De chemische interactie tussen de CeO_2 nanoparticles en silaan in de gecrosslinkte film werd verder bestudeerd

met XPS; shifts in de bindingsenergie en verandering in de piekvormen duiden op een mogelijke binding tussen silicium en cerium.

Een kritische parameter in de vorming van hybride lagen door incorporatie van nano-particles, is de uniforme distributie van de deeltjes doorheen de film, zonder deeltjesagglomeratie. Indien de nanodeeltjes worden toegevoegd aan de silaanoplossing onder droog poedervorm, werd waargenomen dat deeltjes agglomereerden tot particles met een dimensie in de grootteorde van de filmdikte die de film lokaal verstoren en de beschermende eigenschappen verminderen. Dit is een probleem dat alom bekend is bij alle groepen die werken met nano-deeltjes in coatings. Door samenwerking met Umicore, kon echter dit probleem opgelost worden door gebruik te maken van een waterige nano-suspensie van CeO_2 nanoparticles.

Een combinatie van FE-SEM, FE-AES en FIB-TEM/EDX laat toe te bevestigen dat de deeltjes nano-gedispergeerd zijn in de BTSE film en steeds ook bedekt zijn met silaan, of met andere woorden, goed geïncorporeerd in de dunne deklaag. Met EIS in Na_2SO_4, wordt aangetoond dat de incorporatie van CeO_2 nanoparticles de barrier-eigenschappen verbetert indien ze worden toegevoegd als nano-suspensie om een homogene verdeling in de laag te krijgen.

EIS metingen werden ook uitgevoerd in NaCl op coatings aangebracht op AA2024-T3 om de corrosierespons te bestuderen in de aanwezigheid van nano-deeltjes en een corrosie-inhibitor (Ce^{3+}) in de laag. Echter opnieuw bleken de lagen te dun om een goede langdurige bescherming te verkrijgen.

De toegepaste eigenschappen werden bestudeerd door de BTSE coated samples (met en zonder nano-particles en inhibitor) te bekleden met een toplaag. Zoutnevel-tests en pull-off tests werden uitgevoerd, voor respectievelijk corrosiebescherming en hechting te beoordelen.

Zoutnevel-tests bevestigen dat een silaanlaag de weerstand tegen corrosie verbetert in vergelijking met het niet-gecoate substraat.

Meerdere types verflagen werden vervolgens aangebracht: een commerciële water-gebaseerde verf, een UV watergebaseerde verf, een UV curable verfsysteem, en een poedercoating. Uit de testen blijkt dat een onderliggende BTSE laag (als primer) enkel de hechting met de commerciële watergebaseerde verf verbetert. Met de poedercoating werd deze zelfs slechter. Dit komt omdat BTSE wel een goede hechting met het substraat toelaat, evenals een dichte crosslinking in de laag, maar geen bijkomende functionele groepen bezit om te binden met een topcoat.

De zoutneveltesten en EIS metingen tonen wel dat de toevoegingen van ceriumoxide nano-particles en ceriumnitraat inhibitor de weerstand tegen corrosie verhogen.

Trefwoorden: *Aluminium, deklaag, water-gebaseerd BTSE, plasma polymerisatie, plasma depositie, CeO_2 nanoparticles, XPS, IRRAS, ToF-SIMS, barrière-eigenschappen*

SUMMARY

Silane coatings are applied to metal surfaces for various purposes, e.g., to form a protective layer against corrosion or to act as a primer for subsequent coating. In this project bis-1,2-(triethoxysilyl) ethane (BTSE) was used as a precursor to deposit coatings on aluminium substrates with three different techniques: dipcoating (water based solution), vacuum plasma and atmospheric plasma.

The main aim of this investigation is to compare the surface and interface characteristics of thin (less than 100 nm) BTSE films prepared with the three different methods, in order to get information on how the silane molecule is modified by the deposition technique. In addition, metal oxides nanoparticles (CeO_2) and other additives (Ce^{3+}) are included in the silane matrix for improved properties.

As of now, these silane films are mostly deposited from solution through dipcoating, which requires the addition of water to the silane molecules in order to hydrolyse the methoxy or ethoxy groups and form functional silanol groups. Together with the hydroxyl groups on the metal surface, they are essential to the formation of a covalent Si-O-metal bond at the metal/film interface. In addition, thermal treatment of the silane film improves the barrier properties, by enhancing cross-linking (condensation of silanol groups). This cross-linked film will then act as a physical barrier between the metallic substrate and the aggressive environment, by reducing the number of pathways along which penetration of aggressive species could happen. Hence, the barrier properties of the film and as such the corrosion protection properties of the substrate are improved.

Deposition of silanes through wet methods has been widely studied, but the technique presents some drawbacks. First, wet deposition is a multistep processing, requiring dedicated substrate pre-treatments before film deposition to enhance the metal-film bonding, and a post treatment through thermal curing for the creation of barrier properties. Further, wet processing involves the use of solutions (containing organic solvents if not water-based, i.e. hexane, acetone, and ethanol) and the creation of waste flows. It is also possible that some water or solvent remains in the silane film after curing, and this can decrease the anti-corrosion properties.

Plasma technology could be an efficient and good alternative to wet deposition. The plasma is used to chemically decompose the silane vapour precursor and as a source of active species involved in the film growth. The advantages of plasma techniques are numerous: the easy control of the experimental parameters and the environmental friendly approach, as no solvents are needed. It would allow the use of a plasma cleaning procedure before the deposition of the polymer in the same reactor. In the case of the deposition of silane for corrosion protection purposes, the use of plasma could be advantageous, as the condensation reaction could be

avoided by inducing the release of water inside the coating that could be trapped in the film, and therefore limit the barrier properties.

The results show that films could be deposited by both vacuum and atmospheric plasma, besides the more traditional dipcoating. Atmospheric and vacuum plasma deposition of BTSE films has never been reported in the literature before. Very similar homogenous silane coatings with comparable thickness are obtained with the different techniques. This is a good starting point for the comparison of chemical and physical properties of these coatings as a function of deposition methods.

The XPS measurements have shown that the chemical composition values related to dipcoated and vacuum plasma coatings are comparable. The carbon content in the atmospheric plasma BTSE coatings is low (6.7%). The silicon content on the film surface, on the other hand, is higher in the film deposited by atmospheric plasma. The Si2p binding energy for atmospheric plasma films is higher than expected, exhibiting a value (103.2 eV), which is in agreement with IRRAS measurements. Indeed, the XPS shows that BTSE film deposited by atmospheric plasma is more oxidized than those deposited by vacuum plasma and dipcoating, the corresponding IR spectrum shows a shift of the Si-O-Si stretching band at 1250-1000 cm^{-1}, revealing a higher oxidation state. In contrast, the Si-CH$_3$ band at 1270 cm^{-1} is attenuated, suggesting the oxidative removal of the methyl groups and corresponding to a decrease of the atomic concentration of carbon as shown by XPS. The absence of a C-H stretching at 2950 cm^{-1} also provides evidence to support the preferential loss of organic material on the films deposited by atmospheric plasma.

The oxygen present during atmospheric deposition accounts for carbon removal and a corresponding rise in the oxygen concentration. This points out the formation of oxidized coatings richer in Si-O bonds than those deposited by vacuum plasma and dipcoating.

The use of silanes as adhesion promoters is based on the assumption of a specific interaction between the oxidized metal surface and the silane of use. This is achieved in the case of wet deposition methods with the formation of a covalent bond via condensation between hydroxyls present at the surface of the treated metal and silanols of the hydrolysed silane. Another objective in this project is to determine whether a covalent AlOSi bond is formed at the plasma polymer film-aluminium interface, since the plasma deposited films are obtained not from hydrolyzed silane as the case of wet deposition methods but from plasma polymerization of concentrated BTSE silane vapour.

High-resolution positive ToF-SIMS spectra of the aluminium substrate with a plasma polymer BTSE films have shown the presence of a peak at nominal mass amu (m/z= 70.9539 u), which is assigned to the AlOSi$^+$ fragment and is related to the formation of a covalent bond between the plasma polymer BTSE film and the aluminium

substrate. For both plasma polymer films obtained by vacuum and atmospheric plasma, ToF-SIMS indicates the presence of AlOSi bonding, the observed experimental mass for AlOSi differs from the theoretical mass by only 0.0005 amu and is well separated by more than 0.01 amu from other species with the same nominal mass namely: Al_2OH^+ and $AlSiCH_4^+$ and no possible interference with carbon contamination looks possible.

The depth profile clearly indicates that an interfacial layer fingerprinted by the $AlOSi^+$ fragment is present below the outer layer of organic material obtained from plasma polymer film, hence pointing to the presence of silane–aluminium oxide covalent bond between the plasma polymer BTSE film and the aluminium substrate.

The stability of the coatings on the substrate was tested by treating the plasma deposited films in an ultrasonic bath, and by following the relative intensities of the Al2p and Si2p XPS peaks before and after treatment. As the Si/Al intensity ratio is constant, we conclude this layer is strongly adhered to the substrate.

The BTSE films deposited with the three different deposition methods were also compared in terms of barrier and corrosion properties, through electrochemical impedance spectroscopy (EIS) measurements in Na_2SO_4 and NaCl. The three films showed only minor differences and in all cases their corrosion protective behavior disappeared after 1-day immersion, due to the very thin nature of these layers. The small thickness, in fact, affects the corrosion properties of the samples more than their chemistry and composition do.

Part of this research also deals with vacuum and atmospheric plasma deposition of SiO_x films (system 2). These layers are widespread in application as dielectric layers for electronic devices and as layers with low refractive index in optical systems, e.g. in anti-reflective layer stacks on architectural glass panes or plastic films. The current work focuses on the deposition of a thin SiO_x film on aluminium (99.99%) substrate, as a primer layer for subsequent coating using HMDSO as a precursor. The results have shown that SiO_2, SiO_x, and SiO_xC_y films can be selectively grown by PECVD at low and atmospheric pressure using HMDSO as precursor.

The $HMDSO/O_2$ ratio in the gas mixture has a crucial effect on the silicon chemical bond inside the deposits. The films obtained with pure HMDSO plasma are polymeric with a surface rich in carbonated species; whereas the films obtained from $HMDSO/O_2$ plasma are silica-like with a very small amount of carbon. An interesting feature is that the films deposited at low pressure and at atmospheric pressure have a similar composition. The porosity of the deposited films can be followed by the presence of hydroxyl groups (IR-spectra).

A major novelty and originality of this work is the investigation of thin films of water-based BTSE (less than 100 nm), with the incorporation of nano-dispersed CeO_2

particles (system 3), uniformly distributed in the layer, for improved barrier properties. The small thickness of the film and the water-based nature of the silane are both key issues for industry, in the aim of saving on costs and material weight and reducing the impact on human health and the environment.

Measurements were performed in order to understand how the presence of the nano-oxides might affect the silane under study. ^{29}Si NMR analysis on the coating solutions shows that the presence of CeO_2 does not affect the stability and ageing of the BTSE solution over a period of 4 months. The chemical interactions between the CeO_2 nanoparticles and the silane in the cured coating were investigated by XPS. Shifts of binding energies and change in peaks' shape in the spectra of the individual compounds and of the mixed coating point to the possible formation of a bond between the Si from BTSE and the Ce in the cured film.

A critical issue in the formation of these hybrid thin coatings is the nanoparticles agglomeration to a size comparable to the film thickness, leading to the presence of hillocks on the sample surface, which affect its uniformity and might create preferential paths for corrosion attack. The formation of uniform and homogeneous thin films was successfully achieved by adding the CeO_2 nanoparticles to the coating solution in the form of an aqueous nano-suspension.

Information on the coating structure was collected by combining the results of FE-SEM, FE-AES, FIB-TEM/EDX analyses. They confirm the presence of nano-dispersed CeO_2 particles in the BTSE coating and reveal that these nano-oxides are always covered by a uniform BTSE film, or in other words, well embedded in the silane matrix. This explains the results obtained by EIS investigation in Na_2SO_4, which shows that the incorporation of CeO_2 nanoparticles modifies the barrier properties of the thin BTSE layers, with a better performance observed for the coatings where the particles are nano-dispersed, hence providing a more uniform and homogeneous layer.

Further EIS measurements on these films deposited on AA2024-T3 were performed in NaCl, in order to study their corrosion properties, also in the presence of corrosion inhibitors (Ce^{3+}). Even though at first the samples showed a (minor) barrier behavior compared to the blank, they all lost their protection behavior after 1-day immersion in the NaCl solution. This is a further confirmation that the small thickness of the coating is the main responsible of the poor corrosion behavior of the samples, over the specific coating composition and/or the presence of additives.

In addition, the applied properties of the BTSE films (with and without the presence of additives), coated with a paint layer are also under focus in this project Aluminum substrates are in fact covered by paints for aesthetical reasons but also to ensure their long-term value.

The exposition of uncoated aluminum and of systems 1 and 3 (with or without cerium nitrate) to acetic salt spray during 24h and 48h showed that the deposition of a silane layer on aluminum increases the resistance of the substrate to corrosion.

Bare aluminum and systems 1 and 3 were coated with a paint layer (a commercial water-based paint, a UV water-based paint, a UV-paint or a commercial water-based paint). The influence of the silane layer on the adherence of the paints and on the barrier properties of the coatings were determined.

Only the adherence of the commercial water-based on one of the two selected aluminum substrates was increased by the presence of a silane layer on the substrate. In the other cases, BTSE does not improve significantly the adherence of the paint. The adherence of the powder paint was even decreased when this paint was applied on systems 1 and 3.

However, the tests of resistance to acetic salt spray exposure and the electrochemical impedance spectroscopy measurements (EIS) evidence that the addition of cerium oxide nanoparticles and of cerium nitrate in the silane layer increases the resistance to corrosion of the coated panels.

Key words: *Aluminium, thin films, water-based BTSE, plasma polymerized BTSE, plasma deposition, CeO$_2$ nanoparticles, XPS, IRRAS, ToF-SIMS, barrier properties*

INTRODUCTION

Metals are often coated with organic films (pre-treatment layers, paints, adhesives, etc.) for various applications in packaging, transport, construction, amongst others. Compatibility between the organic medium and the metal substrate covered by its native oxide is crucial and required for durable properties. In the past, hexavalent chromium containing conversion pre-treatments were applied. This compound, though, is highly toxic and carcinogenic, hence for both environmental and work safety reasons, its replacement has become a major priority. Research has been done to develop alternative non-toxic treatment processes. One of them is based on the use of organosilane coupling agents, which are hybrid organic-inorganic compounds. They ensure both adhesion promotion and corrosion protection and can be used on various metals: aluminium and its alloys, iron and steel, copper, zinc and magnesium alloys [1].

In most of the present literature [2-6] the average thickness of these coatings is in the order of hundreds of nanometers to a few micrometers (μm). They usually ensure good barrier properties, but are not congenial to the industry world, where the trend has been to greatly reduce the thickness of the coatings to the order of 100 nm or less in order to save on costs and material weight. It is in this trend that the present work should be placed. The coatings under study are in the range of 50-100 nm, and this is a major point of novelty for this research.

To enhance the corrosion protection of the films, additives can be incorporated into the silane matrix, both for barrier and self-healing enhancement. For this purpose, the inclusion of oxide nanoparticles (such as ceria, silica, zirconia) has been studied [2-5, 7-13], with or without the addition of ions for self-healing properties [3, 4, 10, 14-22].

Oxide nanoparticles are included in the silane in order to enhance the formation of crack-free films with improved mechanical durability and improved corrosion protection properties [9]. The nanoparticles also seem to have a pore blocking effect [3, 4, 10], in the sense that they can fill defects and voids inside the silane film. This leads to a significantly decreased porosity and conductivity and as such to improved barrier properties when compared to a blank silane film. However, when the optimum concentration is exceeded, the film porosity increases and water can intrude, with consequent film delamination [12, 23]. The nature of the nanoparticles has also a great influence on the barrier properties. Montemor et al. [3, 4] compared the performance of CeO_2 and SiO_2 nanoparticles in the silane coatings. The study showed that CeO_2-filled films present better anti-corrosion performance. This is probably due to the low stability of SiO_2 under increased alkaline conditions as those generated at the cathodic sites when corrosion takes place. The SiO_2 nanoparticles

decompose in alkaline pH, leading to the formation of an expansive gel that accelerates silane film degradation and delamination. This behavior contrasts with that of CeO_2, which is very stable in alkaline conditions.

A critical point in the process of including oxide nanoparticles in the silane coating is the formation of particles agglomeration in the dry layer [2, 5, 6, 9, 13]. These agglomerates can reach a few-hundred nanometers in thickness, strongly affecting the homogeneity of the film. In most of the works from other authors [2-6], though, the coatings under study have a thickness of hundreds of nanometers to a few micrometers, which is higher than the agglomerates size. Hence, even though the presence of agglomerates was acknowledged and studies were performed to determine the optimum concentration to be added for best performance, the issue did not have the challenge of the present investigation. Here, the average film thickness is comparable and often smaller than the agglomerates size, so their presence would strongly affect its structure and homogeneity.

A further improvement of the anti-corrosion properties can be achieved by adding corrosion inhibitors [3, 4]. They can be incorporated on the silane matrix or in the oxide nanoparticles. In the latter case, the corrosion inhibitor can also avoid agglomeration of the oxide nanoparticles and as such, avoid the formation of a non-uniform film [9]. Corrosion inhibitors are also added to achieve self-healing properties of the coating. Besides cerium nitrate [3, 9, 10, 18, 19, 22, 24-26], other dopants have been investigated, such as zirconium nitrate [25, 26], lanthanum nitrate [18], tolytriazole [22], benzotriazole [22], etc. In [18] the performance of cerium nitrate and lanthanum nitrate were compared. In both cases, an insoluble oxide/hydroxide film is formed which hinders the corrosion processes. Both dopants increase the total impedance of the film, but cerium is more effective than lanthanum. This can be attributed to a different distribution in the film of the two dopants. During polymerisation and self-assembling of the film, the ions become trapped in the Si-O-Si network. The Ce ions are probably stabilised in the inner layers of the film, whereas La is present in the outermost layers. The nature of the dopant has a great influence on its distribution and on the corrosion protective behaviour of the coating.

A central point of this study is the comparison between different deposition methods: the more traditional wet deposition (dipcoating) and plasma deposition, both in vacuum and atmospheric conditions. Plasma technology could be an efficient and good alternative to wet deposition, in terms of health and environmental issues and flexibility of working parameters. It would also allow the use of a plasma cleaning procedure before the deposition of the polymer in the same reactor. The plasma is used to chemically decompose the silane vapour precursor and as a source of active species involved in the film growth; the plasma polymerization process is usually carried out at low pressure. At present, the main shortcomings of this process in

industrial applications are the high costs related to vacuum systems and the limitations due to the closed vacuum reactor, which makes it harder for samples to be prepared in a continuous process. Considerable efforts are made in order to develop alternative techniques to overcome these disadvantages. Atmospheric plasma is one of the most promising methods to deposit polymer films in a more flexible, reliable, less expensive and continuous way [27].

Plasma deposition of some silane films has already been investigated [28]. Most of these studies deal with the characterization, structure and properties of the deposited polymer films [29-33] and with the plasma polymerization mechanisms of the organosilicon compounds [34]. These films act as corrosion protective coatings, since they are usually branched, highly cross-linked, insoluble, pinhole-free and highly adhesive to most substrates [35, 36]. The silane layers serve as an interfacial modifier for improved adhesion and corrosion resistance.

The silane investigated in this research project is bis-1,2 (triethoxysilyl)ethane (BTSE). Plasma-polymers of this organosilane compound have never been studied, nor are reports available on the comparison between different deposition methods. It is observed how the same precursor results in coatings with different characteristics depending on the technique employed.

BTSE is a non-functional silane, it provides strong adhesion to the substrate and exhibits outstanding corrosion protection performance on Al alloys [12], comparable to that of the hexavalent chromium containing conversion pre-treatments [12, 37]. The solubility, reactivity and stability of BTSE solutions are determined by the hydrolysis and condensation reactions taking place in the solution [38], and they are important parameters for wet deposition. The hydrolysis converts the ethoxy groups into silanol (-SiOH) groups [39], which react with the metal hydroxide groups of the metallic substrate and form covalent oxane (Me-O-Si) bonds at the metal/film interface [40]. The silanol groups also react with each other to form siloxane bonds (condensation), which lead to crosslinking in the bulk of the silane layer. However, the hydrolysed molecules can also react while still in solution to form dimers, trimers and larger species [39].

The hydrolysis of BTSE determines the reactivity of the solution, while the condensation determines its stability [38]. The optimum condition is with the highest solubility, reactivity and stability. Hence, hydrolysis needs to be maximized while the condensation needs to be minimized. The factors influencing the kinetics and equilibrium of hydrolysis and condensation of BTSE in solution are the nature of the functional groups, the concentration of silanes and water, the value of the solution pH, the temperature and the ageing of the solution. The hydrolysis rate increases as a function of the water content while the condensation is related to the concentration

of BTSE. An increment in the temperature as well as ageing of the solution lead to increased hydrolysis and condensation rates [38].

Most of the past work on dipcoating of BTSE [2, 38, 41] was performed on methanol-based solutions due to the low solubility of BTSE in water. However, health issues are associated with methanol and also with the high monomer content of these solutions, since monomers may be absorbed by living organisms, while larger species are not. Hence, for industrial applications, water-based BTSE solutions are considered in this work. Methanol-free BTSE solutions were already used by Palomino and Suegama [42, 43] and in [39] a comparison is made between a water-based and a methanol-based BTSE solution. ^{29}Si NMR measurements showed that the amount of high molecular weight condensed species is higher in a water-based solution compared to a methanol-based solution. This points to a less reactive solution, but it is positive in terms of health issues. FEG-SEM (field emission gun scanning electron microscope) images showed that the film structure is quite similar for the water-based and methanol-based solutions [39].

Another important part of this research is the study of nanoparticles inclusions into silane coatings. This has been already the subject of various studies concentrating on the corrosion performance of such systems, rather than on their structure and the bonds between the different phases. This project focuses on the study of inclusion of CeO_2 nanoparticles, which aim at improving the barrier properties of the silane film and the addition of Ce ions, which aim at introducing corrosion inhibition properties in the bulk of the silane film [10].

Part of this research also deals with vacuum and atmospheric plasma deposition of SiO_x films. These layers are widespread in application as dielectric layers for electronic devices [44, 45] and as layers with low refractive index in optical systems, e.g. in anti-reflective layer stacks on architectural glass panes or plastic films [46, 47]. A large number of publications exist, dealing with plasma-enhanced chemical vapour deposition (PE CVD) processes. These processes are using monomers which will be polymerized by plasma. In many cases the monomer HMDSO [$(CH_3)_3$-Si-O-Si-$(CH_3)_3$] is applied. The current work focuses on the deposition of a thin SiO_x film on an aluminium substrate, as a primer layer for subsequent coating.

Overall, the objective of this research is to gain better fundamental understanding of the compatibility and the interactions between inherently very different material phases (i.e. the aluminium substrate, the BTSE film and the metal oxide nanoparticles) at their connecting interfaces, which will lead to a better understanding of their combined properties. Through the control of materials at the nanometer scale, new innovative structures can be tailored with an improvement of specific or multi-functional properties, such as optical, adhesion, barrier and corrosion properties.

In addition, the applied properties of the BTSE films (with and without the presence of additives), coated with a paint layer are also under focus in this project, Aluminum substrates are in fact covered by paints for aesthetical reasons but also to ensure their long-term value.

Four paints were selected for this purpose: a commercial waterborne adhesion primer, based on acrylic resin dispersed in water, a commercial powder paint dedicated to aluminum applications and two UV paints (a solvent less and an aqueous dispersion). These paints are characterized by different resin natures and curing methods, hence they will interact in a different way with the BTSE leading to a more or less strong adherence of the paint on the substrate and to more or less reinforced barriers properties.

The originality and novelty of the present work is in the fact that thin BTSE films (less than 100 nm) are deposited on Al substrate with three different deposition methods: dipcoating, vacuum plasma and atmospheric plasma. Nano-dispersed CeO_2, agglomerates-free, were also incorporated into the silane matrix. The challenge of this investigation is represented by the very thin nature of the films and the nano-size of the added oxide particles. Most of the characterization tools are much harder to use at the nanometer scale and they need to be adapted or alternative techniques need to be found.

MATERIALS AND METHODS

Three different systems will be studied in this project (see schematic in Figure 1). The considered components are a metallic substrate, a metal oxide phase and an organic layer. System 1 is the reference system, which represents mostly the current status, where a metal substrate is covered by its native oxide, and then coated with an organic layer. In system 2 the native oxide is replaced by a very thin metal oxide, tailored to modify specifically the interfacial properties. In system 3, the metal oxide phase is present as nanosize particles embedded in an organic matrix. The research approach consists of three main steps: system characterization; property analysis; comparison of film deposition methods. Deposition is done either by wet or plasma methods. The main difference between wet and plasma deposition is that in the latter the silane vapour is carried by argon gas into the plasma and eventually decomposed by collision with plasma components (depending on working parameters).
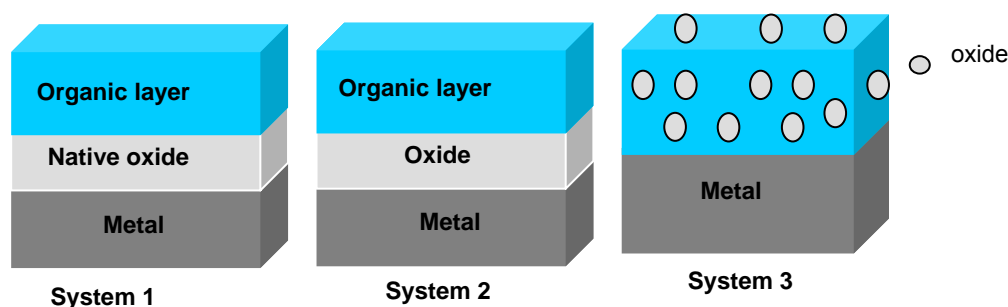
Figure 1 - Schematic of the three systems studied in the project.

The metal substrate under study is aluminium, pure (Al 99.99%, provided by Hydro) or in the commercial alloy AA2024-T3 (provided by Thyssen Krupp). All substrates have been alkaline-treated for surface activation (6-second dipping in 25 g/l NaOH at $70^{o}C$), before silane deposition. When indicated, the substrate has been electropolished, in order to ensure a smooth surface for further analysis.

The silane precursor investigated is a bis-1,2-(triethoxysilyl)ethane (BTSE), provided by Chemetall GmbH as a concentrated (98 wt%) solution or as a water-based solution (10 wt% or 15 wt%). The molecular structure of BTSE is shown in Figure 2.
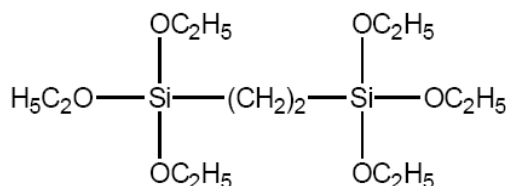
Figure 2 - Molecular structure of bis-1,2-(triethoxysilyl)ethane (BTSE).

The metal oxide under study is CeO_2, and it is added to the coating solution in the form of nanopowder (20-30 nm average size) or nano-dispersed suspension (1 wt% CeO_2, water-based, 20-30 nm), both provided by Umicore.

The coating solutions have been deposited on the aluminium substrate by three different techniques: wet deposition (dipcoating), vacuum plasma and atmospheric plasma deposition.

Wet deposition

For wet deposition, the water-based BTSE solution has been diluted to 5% and 7.5% (depending on the experiment), using distilled water, unless stated otherwise. The metal oxide has been added to the silane matrix in the concentration of 250 ppm as nanoparticles, in the form of nanopowder or nano-dispersed suspension, with the characteristics described above. Each solution was placed in an ultrasonic bath for 30 minutes, and then magnetically stirred to ensure homogeneous distribution of the nanoparticles in the coating solution.

The samples were prepared by manually dipping the substrate into a beaker containing the solution to be coated, for 30 seconds. The samples were then dried in air and cured in the oven at 150° for 1.5 hours, unless stated otherwise.

Atmospheric Plasma deposition

The atmospheric plasma apparatus consists of a SurfX Technologies LLC, A-250D deposition system. Figure 3 shows a schematic of the plasma torch [33], which is cylindrical and ends with a 5 cm^2 showerhead. The system is operated at 13.56 MHz (RF). The plasma is formed by feeding the argon process gas into the system, upstream of the electrodes at a flow rate of 30.0 l/min. The concentrated BTSE precursor is kept in a temperature controlled bath at 373 K and is introduced into the plasma, downstream of the electrodes (in the post-discharge), by bubbling argon through the liquid precursor. A home-made shower ring of 3 cm diameter is used in order to have a homogeneous distribution of the precursor. It is made of a 3 mm diameter aluminium pipe with 24 holes of 1 mm diameter each, drilled on the inside and regularly distributed around the ring (see Figure 3). The gas stream is directed onto a substrate located 0.5 cm downstream. The deposition of plasma films is carried out at 80 W for 2 min.
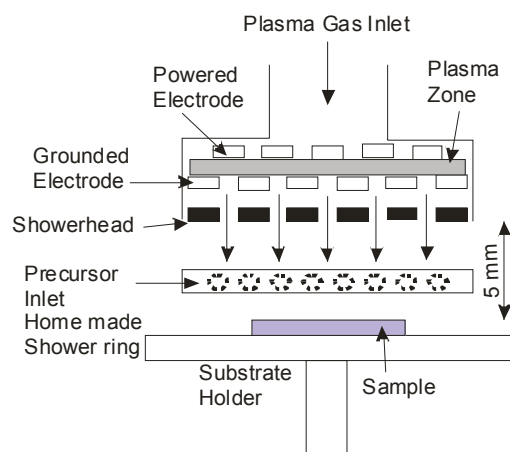
Figure 3 - Schematic of the atmospheric plasma deposition device.

Vacuum Plasma Deposition

The vacuum plasma reactor (Figure 4) consists of three main parts: the planar source (ICP-P 200, JE PlasmaConsult GmbH, Germany), the gas injection system and the vacuum chamber.

The ICP-P 200 is a radiofrequency (13.56 MHz) inductively coupled plasma (ICP) source designed for the efficient production of a high density and low temperature plasma. It consists of a water cooled four-antenna planar copper coil (diameter = 20 cm) whose electromagnetic power is transmitted to the gas through a dielectric window (quartz). It operates in an automatic mode with a RF–power generator (Dressler® Cesar® 1310, Advanced Energy, Germany) and a reflected power below 2 W is achieved within 10 s after plasma ignition.

The gas injection system consists of four flow meters (MKS 1179A types), which are connected to a "shower ring" output, allowing a homogeneous gas distribution in the chamber. The 20 cm diameter in-house shower ring is made of a 6 mm diameter stainless steel pipe with 20 holes of 1 mm diameter each, drilled on the inside and regularly distributed around the ring.

The plasma chamber consists of a 30 cm diameter grounded stainless steel vessel connected to a pumping system (PFEIFFER DUO 20 MC 24 m^3/h primary pump and PFEIFFER TPU 261 PC turbo molecular pump). At the centre of the vacuum chamber, an alumina cylinder is fixed on a four-axis manipulator. The sample holder consists of a 1 mm stainless steel disc inserted inside the alumina cylinder and connected to an electrical feedthrough, in order to apply DC or RF bias voltage on the sample holder, if necessary. Otherwise, the sample may be left at floating potential or grounded. The distance between the sample holder and the quartz window can be adjusted from 0.5 to 17 cm. The pressure is monitored using a Varian gauge (Convector p-type).

Samples are fixed to the sample holder by a carbon tape and placed into the plasma chamber, which is then pumped down to a pressure of 1×10^{-3} Torr. Plasma polymerization is carried out by introducing the concentrated BTSE vapour monomer into the plasma chamber through a leak valve and by adjusting the pressure at 300 mTorr. Polymerization is performed in a continuous wave mode. The deposition of plasma films is carried out at 200 W for 5 min. After the discharge, the chamber is pumped down to 1×10^{-3} mTorr.

In order to avoid post-treatment reaction of residual surface radicals with external reactants, the samples were kept in vacuum or in an inert atmosphere for 4 h prior to transfer in air to the XPS.
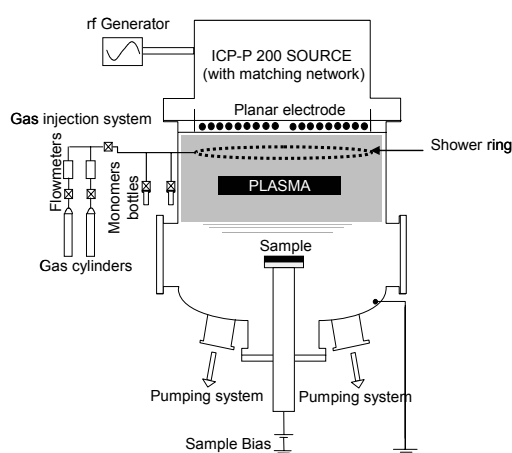
Figure 4 - Schematic diagram of the vacuum plasma reactor.

Coating solution and film characterization

The coating solutions were analyzed with ^{29}Si-NMR (Nuclear Magnetic Resonance), which can provide information about the chemical environment of a nucleus, ^{29}Si in this specific case. As ^{29}Si nuclei in oligomers and polymers resonate at lower frequencies than those in monomeric species, their presence in the sample is easily detected and information on condensation and hence the ageing of the silane can be obtained. NMR spectra were recorded on a Bruker Avance 250 instrument, operating at 49.77 MHz for the ^{29}Si nucleus. The chemical shifts were referenced to external Me$_4$Si (TMS). A T2 filter was applied to suppress the broad background resonance originating from the glass tubes (diameter = 10 mm) and the probe.

X-ray photoelectron spectra (XPS) were obtained by means of a Physical Electronics 5500 photoelectron spectrometer. All spectra were collected using Mg Kα X-rays operating at 300 W. High resolution spectra were obtained using a pass energy of 23.5 eV, which corresponds to a full width at half maximum (FWHM) on the Ag3d5/2 peak of 1.05 eV. XPS spectra were fitted using a Gaussian-Lorentzian product

function and binding energies assigned to the different species were determined after peak fitting. The background subtraction was performed using the Shirley algorithm. The binding energy scale was calibrated by referencing the C1s value at 284.4 eV.

A JEOL JSM – 7000F Field Emission Scanning Electron Microscopy (FE-SEM) was used to characterize the surface morphology of the samples with high spatial resolution. For cross-sectional imaging purposes, the silane coated samples were bent after immersion in liquid nitrogen, in order to ensure a sharp cut of the film.

Samples were also characterized using a JEOL JAMP – 9500F Field Emission Auger Electron Spectroscopy (FE-AES). The electron spectrometer is an electrostatic hemispherical analyzer with a multi-channel detector, for optimal Auger analysis. It provides very high energy resolution without sacrificing sensitivity. In addition, an ion gun is used for high speed sputtering and low energy charge neutralization, in order to perform depth profile analysis.

Visible Light Spectroscopic Ellipsometry (VISSE) was performed with a J.A. Woollam Co VASE (Variable-Angle Spectroscopic Ellipsometer) in the UV-visible and near infrared spectral range (200-1700 nm). Three angles of incidence were used: 65°, 70° and 75°. The spectra were interpreted using the WVASE32 software and the system modelled to estimate thickness of the coating layer.

Cross sectioning of the sample through Focused Ion Beam (FIB) and Transmission Electron Microscope (TEM) measurements were performed at OCAS using a JEOL-SEIKO SMI 3050 TB (Triple Beam) instrument. An energy dispersive X-ray detector (EDX) was used to analyze the chemical composition of the sample. All instruments were calibrated for the magnifications and the EDX peak positions.

Infrared reflection absorption spectra (IRRAS) of BTSE films deposited on Al (99.99%) were measured at 45° with 2 cm^{-1} wave number resolution using a Nicolet 5700 FTIR spectrometer equipped with a MCT detector cooled by liquid nitrogen. The IR spectra were recorded and examined between 4000 and 650 cm^{-1}. One hundred scans were collected to acquire all IRRAS data.

ToF-SIMS (time-of-flight secondary ion mass spectrometry) measurements were performed with a ToF-SIMS IV instrument (ION TOF GmbH, Münster, Germany). A 15 keV Ga^+ (1.5 pA) primary ion beam was used for analysis. To avoid a too strong fluence of gallium, the noninterlaced mode was used (2 s sputtering and 0.3 s pause between sputtering and analysis). The gallium raster area was 61.5 x 61.5 μm^2 or 100 x 100 μm^2. Sputtering was done using a 500 eV Xe^+ source. The Xe^+ current and raster area were 40 nA for 300 x 300 μm^2. These conditions allow to keep a high fluence and to limit chemical effects. Indeed, when more reactive ions are used (Cs^+, O_2^+), artefacts are more important when interfaces are reached [14]. Profiles were rebuilt from raw data. Mass resolution (m/Δm) for the $^{28}Si^+$ and $^{71}AlOSi^+$ ions were,

respectively, around 9600 and 6000. Positions of the particles were confirmed by reconstruction images from the depth profiles raw data.

Electrochemical Impedance Spectroscopy (EIS)

The Electrochemical Impedance Spectroscopy (EIS) measurements were performed at the open circuit potential (OCP) in the 10^5 Hz to 10 mHz frequency range, using an AUTOLAB PGSTAT30 in potentiostatic mode. The amplitude of the perturbation was 10 mV rms. The cell consisted of a three-electrode setup: a saturated calomel electrode (SCE) reference, a platinum grid as a counter electrode, and the working electrode, which is the BTSE-coated aluminium under study (active area: 1.54 cm^2). A Pt wire coupled with a 10 μF capacitance was placed in parallel with the reference electrode, in order to reduce the phase shift induced by the reference electrode in the high frequency range. The tests were performed in 0.4 M Na$_2$SO$_4$ or 0.5 M NaCl, as stated in the results section.

Applied Properties

The Erichsen test was performed to check the flexibility of the samples. A 20 mm diameter steel ball was pressed into the reverse side of a coated panel until fissures appear in the coating. This test was performed 1 month after the application of the water-based paint and 24h after the application of the UV paints.

Adherence of the sample was measured through cross-cut tests and pull-off measurements.

Cross-cut tests (ISO2409) were performed to assess the resistance of the coating to separation from substrate when a right angle lattice pattern is cut into the coating, penetrating through to the substrate. This test method is used to establish whether the adherence is at a generally adequate level. It does not distinguish between higher levels of adherence, for which more sophisticated methods of measurement are required. Paints were examined and classified as described in the norm ISO 2409. Tests were performed 1 month after the application of the water-based paint and 24h after the application of the UV paints.

Pull-off measurements were performed with an Instron 3365 testing machine operating at a crosshead speed of 0.05 mm/min. The experimental set-up allows a perfect alignment of the jaws. Tests were performed in a climate room (50% RH and 21°C) more than 1 month after the application of the water-based paint and more than 24h after the application of the UV paints.

The MEK test consists in rubbing the paint with a MEK soaked cloth or tissue and counting the number of double rubs until the coating is eroded and the substrate is reached. This test is fast and easy to carry out, but is not reproducible since the number of strokes necessary to rub off the paint depends on the operator (applied

pressure, speed of rubbing, texture of the cloth or tissue). However, it does allow a degree of quantification of the resistance of the samples tested toward MEK and enables a ranking order of solvent resistance to be established. Tests were performed 24h after the application of the UV paints.

Two perpendicular scratches of 5 mm were made through the coating to the substrate in order to measure their resistance to acetic salt spray (ISO 9227 method AASS). Panels were exposed to a acetic salt spray (NaCl 5% - CH_3COOH - pH 3.1 to 3.3) at 35°C and examined every day. Tests were performed more than 1 month after the application of the water-based paint and more than 24h after the application of the UV paints.

RESULTS AND DISCUSSION

System 1

Films deposited by dipcoating

The coated samples are transferred to the XPS analysis chamber immediately after film deposition and curing. According to XPS analysis (Figure 5, spectrum A), the composition of the outer surface region of the films corresponds to $SiO_{1.7}C$. The binding energies and atomic percentages of silicon, oxygen and carbon present in the water-based BTSE film are given in Table 1. The film consists of 27.5 at.% silicon, 45.8 at.% oxygen and 26.7 at.% carbon. The oxygen peak at 532.3 eV is characteristic of Si-O bonds [48], the Si peak at 102.3 eV matches energies expected for $R-Si-O_2-$ type silicones [48] and the carbon peak at 284.4 eV does not reveal a significant C-O component.

The infrared absorption spectrum of a dipcoated BTSE film is presented in Figure 6 (spectrum (a)) and the corresponding peak assignment is in Table 2. Peaks of $Si-CH_3$ at 1272 cm^{-1}, the asymmetric Si-O-Si stretching vibration at (1200-1000) cm^{-1} and the $Si-CH_3$ bending vibration at 800 cm^{-1} are observed. The Si-O-C stretching vibration at 1110 cm^{-1} and CH_2 wagging vibrations of $Si–CH_2–Si$ groups at (1000–1020) cm^{-1} might overlap with the $Si–O–Si$ stretching vibration at (1200–1000) cm^{-1}. The signal at 918 cm^{-1} can be identified as Si-OH stretching vibration. Previous studies have shown that upon thermal curing of these layers the IR absorption signal of the Si-O-H bonds decreases and the one of the Si-O-Si bonds increases [1], indicating that condensation reactions take place between the silane molecules in the bulk of the layer, resulting in a cross-linked network. This network formation increases the barrier properties against hydration and corrosion of the substrate, as observed by electrochemical impedance spectroscopy [1].

A cross-section of a water-based 5% BTSE film deposited by dipcoating is shown in Figure 7A. The film thickness is about 50 nm.

	Binding energy (eV)			Atomic concentration %		
	Si_{2p}	C_{1s}	O_{1s}	Si_{2p}	C_{1s}	O_{1s}
Wet deposition	102.3	284.4	532.3	27.5	26.7	45.8
Vacuum plasma	102.7	284.4	532.3	28	24.3	47.6
Atmospheric plasma	103.2	284.4	532.8	34.7	6.7	58.6

Table 1 - Composition and binding energies of BTSE films as for XPS measurements.
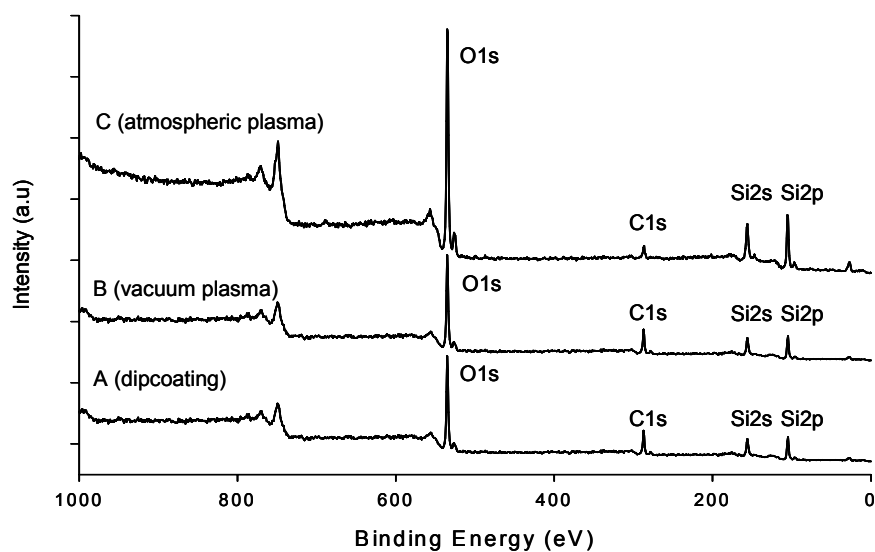
Figure 5 - XPS survey spectra of BTSE films deposited by wet deposition (A), vacuum plasma (B), atmospheric plasma (C).

	Wavenumber (cm^{-1})	Group	Assignment
Wet deposition	1272	Si-CH$_3$	δ_s(CH$_3$)
	1200-1000	Si-O-Si	ν_{as}(Si-O-Si)
	1110	Si-O-C	ν_{as}(Si-O-C)
	1020-1000	SiCH$_2$-Si	CH$_2$ wagg.
	918	Si-OH	δ_s(SiOH)
	800	Si-(CH$_3$)$_2$	r(Si-CH$_3$)
Vacuum plasma	1270	Si-CH$_3$	δ_s(CH$_3$)
	1200-1000	Si-O-Si	ν_{as}(Si-O-Si)
	1110	Si-O-C	ν_{as}(Si-O-C)
	1020-1000	SiCH$_2$-Si	CH$_2$ wagg.
	850	Si-(CH$_3$)$_3$	r(Si-CH$_3$)
	806	Si-(CH$_3$)$_2$	r(Si-CH$_3$)
Atmospheric plasma	1250-1000	Si-O-Si	ν_{as}(Si-O-Si)
	912	Si-OH	δ_s(SiOH)
	712	Si-(CH$_3$)$_2$	r(Si-CH$_3$)

Table 2 - IRRAS peak assignment for the BTSE films.
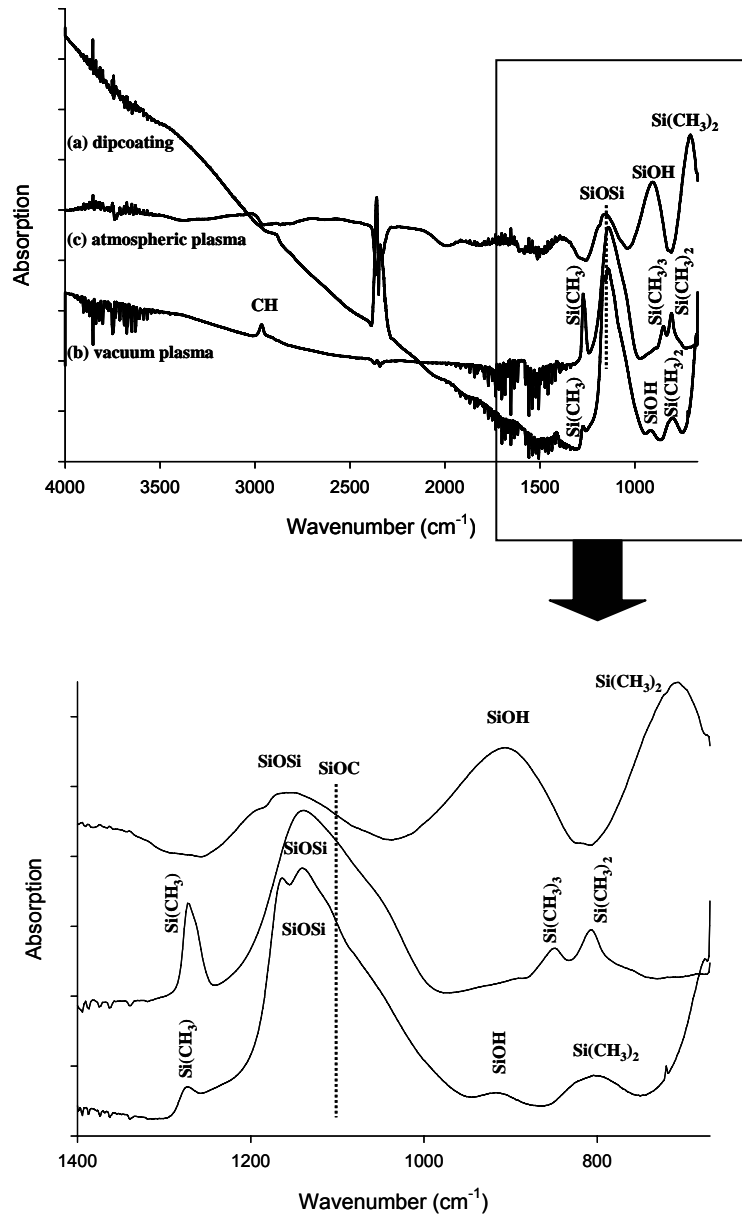
Figure 6 - *Infrared spectra of BTSE films deposited on Al by wet deposition (a), vacuum plasma (b), atmospheric plasma (c).*
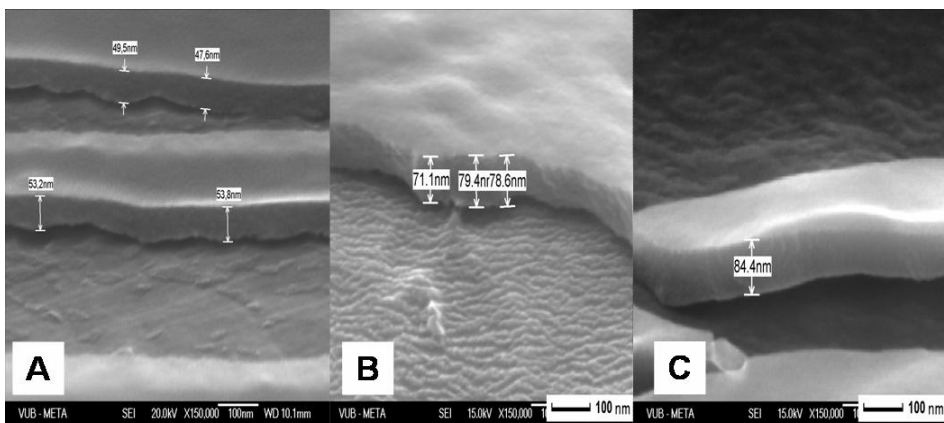
Figure 7 - *SEM micrograph of the cross-section of BTSE films deposited on Al by wet deposition (A), vacuum plasma (B), atmospheric plasma (C).*

Films deposited by vacuum plasma

XPS spectra of the vacuum plasma BTSE films are shown in Figure 5 (spectrum B) and the elemental analysis results are reported in Table 1. The BTSE film contains Si, C, O. The oxygen peak at 532.3 eV is characteristic of Si-O bonds [48], the Si peak at 102.7 eV matches energies expected for $R\text{-}Si\text{-}O_3\text{-}$ type silicones [48] and the carbon peak at 284.4 eV is characteristic of C-C or C-H.

The composition of the film corresponds to $SiO_{1.7}C_{0.9}$ (Figure 5, spectrum B) in comparison to SiO_3C_7 in the case of the unreacted BTSE precursor. This Si:O:C ratio suggests that Si-O bonds formed and Si-C bonds broke during the process, releasing hydrocarbons.

Figure 6 (spectrum (b)) shows the infrared survey spectrum of a plasma-formed BTSE layer deposited at plasma powers of 200 W, 0.3 Torr, with a deposition time of 5 min. The peak assignment is given in Table 2. It reveals the presence of a significant amount of dimethylsilyl groups.

Siloxane (Si-O-Si) at (1200-1000) cm^{-1}, dimethylsilyl ($Si\text{-}(CH_3)_2$) at 806 cm^{-1} and trimethylsilyl ($Si\text{-}(CH_3)_3$) at 850 cm^{-1} are clearly visible. The Si-O-C stretching vibration at 1110 cm^{-1} and CH_2 wagging vibrations of Si–CH_2–Si groups at (1000–1020) cm^{-1} might overlap with the Si–O–Si stretching vibration at (1200–1000) cm^{-1}. However, a comparison of the relative intensities between CH_3 ($v_{as}(CH_3)$ 2960 cm^{-1}, $v_s(CH_3)$ 2903 cm^{-1}) and CH_2 ($v_{as}(CH_2)$ 2928 cm^{-1}, $v_s(CH_2)$ 2860 cm^{-1}) stretching vibrations leads to the conclusion that the concentration of CH_2 is rather low (see Figure 8).

Figure 7B shows the cross section FE-SEM micrograph of a BTSE film deposited on the aluminium substrate by vacuum plasma. The film is continuous and compact and about 70 nm thick. The performed plasma process leads to a topographically homogeneous film.

Films deposited by atmospheric plasma

Films are deposited at plasma powers from 40 to 100 W with deposition times from 2 to 30 min, at atmospheric pressure. Only the XPS and IRRAS spectra at 80 W are presented because no effect is observed on the composition and structure of the film by varying the power and deposition time. Indeed, the infrared spectra recorded on the samples synthesized at these different powers do not reveal any change in the band and peak energy and relative intensities, suggesting a similar chemistry in the films. Due to the particularity of the plasma process, the deposition time has only an effect on the thickness of the films deposited.

The binding energies and atomic percentages of silicon, oxygen and carbon present in the films are given in Table 1, as a result of XPS analysis. The film consists of 34.7

at.% silicon, 58.6 at.% oxygen and 6.7 at.% carbon. The oxygen peak at 532.8 eV is characteristic of Si-O bonds [48] and the Si peak at 103.2 eV matches energies expected for SiO_2 type silicones [48]. The composition measured by XPS (Figure 5, spectrum C) corresponds to $SiO_{1.7}C_{0.2}$.

The infrared spectra of plasma polymer BTSE films is presented in Figure 6 (spectrum (c)) and the peak assignment is given in Table 2. A peak corresponding to the Si-O-Si asymmetric stretching vibration at (1250-1000) cm^{-1} is observed. A band at 912 cm^{-1} is also visible, indicating the presence of Si-OH.

A cross-section of a BTSE film deposited by atmospheric plasma is shown in Figure 7C. The film thickness is about 80 nm (deposition time 30 min). The atmospheric plasma process also leads to a topographically homogeneous film.
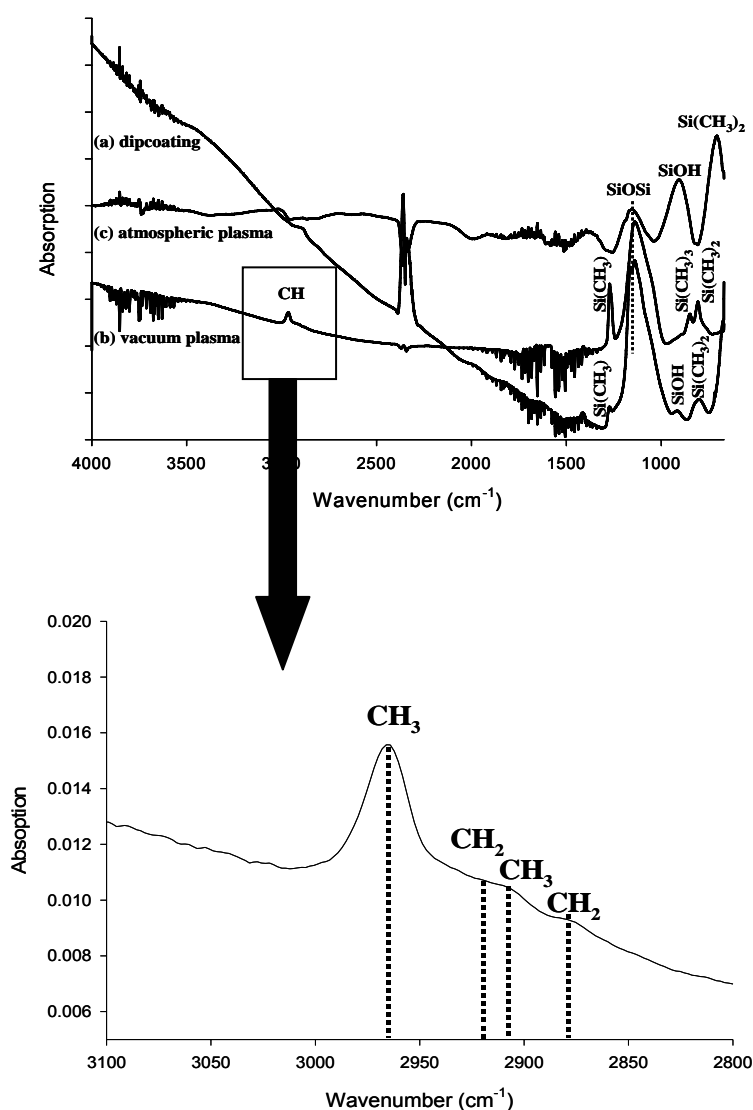
Figure 8 - IRRAS spectrum of plasma polymer BTSE film deposited by vacuum plasma.

Comparison of the films deposited with the different techniques

Table 1 summarizes the XPS results for films deposited with the three methods. While the values related to dipcoated and vacuum plasma films are comparable, the carbon content in the atmospheric plasma BTSE films decreases from 26.7% to 6.7% and the C/O ratio decreases from 0.6 to 0.1. The silicon content on the film surface, on the other hand, increases from 27.5% in the film deposited by dipcoating and vacuum plasma, to 34.7% in the film deposited by atmospheric plasma.

The Si_{2p} binding energy for atmospheric plasma films is higher than expected, exhibiting a value (103.2 eV), which is in agreement with IRRAS measurements. Indeed, the XPS shows that BTSE film deposited by atmospheric plasma is more oxidized than those deposited by vacuum plasma and dipcoating. The corresponding IR spectrum shows a shift of the Si-O-Si stretching band at 1250-1000 cm^{-1}, revealing a higher oxidation state. In contrast, the Si-CH$_3$ band at 1270 cm^{-1} is attenuated, suggesting the oxidative removal of the methyl groups and corresponding to a decrease of the atomic concentration of carbon as shown by XPS. The absence of a C-H stretching at 2950 cm^{-1} also provides evidence to support the preferential loss of organic material on the films deposited by atmospheric plasma.

The characteristics of BTSE films are also studied using curve fitting of the Si_{2p} core level peaks. The Si_{2p} peaks are resolved into four components (Figure 9) according to the method described by Alexander et al [48]. The evolution of the peaks is summarized in Table 3. The component at 102.1 ± 0.1 eV is assigned to silicon bound to two oxygen atoms $R_2Si(-O)_2$ [48], the component at 102.8 ± 0.1 eV to silicon bound to three oxygen atoms $R_2Si(-O)_3$ [48] and the one at 103.4 ± 0.1 eV is assigned to silicon bound to four oxygen atoms $Si(-O)_4$ [48]. In the BTSE film deposited by dipcoating, the component $R_2Si(-O)_2$ is 86%, while in the plasma BTSE film deposited by vacuum plasma, the dominant component is $R_2Si(-O)_3$ (94%). In the plasma BTSE film deposited by atmospheric plasma, the oxidized components $R_2Si(-O)_3$ and $Si(-O)_4$ are 56.5% and 43.4% respectively.

The oxygen present during atmospheric deposition accounts for carbon removal and a corresponding rise in the oxygen concentration. This points out the formation of oxidized coatings richer in Si-O bonds than those deposited by vacuum plasma and dipcoating.
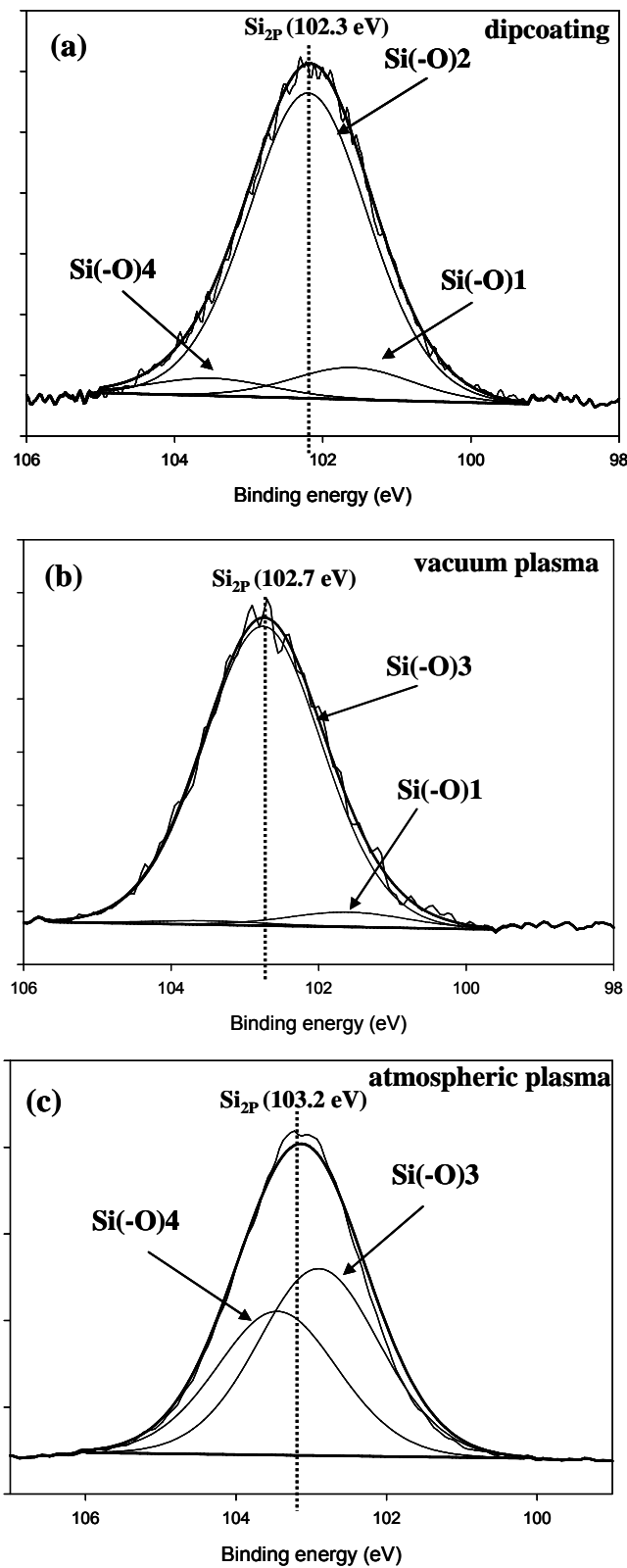
Figure 9 - XPS high resolution spectra (Si₂ₚ) of deposited BTSE films by wet deposition (a), vacuum plasma (b), atmospheric plasma (c).

Element (peak)	Predominant oxidation states (location of peak maximum)		
	dipcoating	vacuum plasma	atmospheric plasma
Si_{2p}	+II (102.3 eV)	+III (102.7 eV)	+III, +IV (103.2 eV)
C_{1s}	0 (284.4 eV)	0 (284.4 eV)	0 (284.4 eV)
O_{1s}	-II (532.3 eV)	-II (532.3 eV)	-II (532.8 eV)

Table 3 - Fitting data from XPS analysis of BTSE films.

Interaction between silane-aluminium at their connecting interface

The emphasis in this part of analysis is to identify with ToF-SIMS the presence of Al–O–Si bonding through the AlOSi$^+$ ion at nominal mass 71 amu in the positive SIMS spectrum (Figure 10).

For each plasma-polymer BTSE film, a search is made in the mass spectrum for the presence of ion fragment indicative of the possible Al-O-Si interfacial bonding. The accuracy of mass assignment is calculated using the formula [49]:

$$\Delta(*) = \frac{\left| M_{\exp} - M_r \right|}{M_r}$$

where: M_{exp} is the experimental mass obtained from the high mass resolution spectrum and M_r is the real mass calculated from exact masses. The assignment of a specific structure and /or formula is thought to be exact when delta is no bigger than a few parts per million [49].

Figure 10 shows the high resolution positive ToF-SIMS spectra of the aluminium substrate with plasma polymer BTSE films. The intense peak at this nominal mass amu (m/z= 70.9539 u) is assigned to the AlOSi$^+$ fragment and is related to the formation of a covalent bond between the plasma polymer BTSE film and the aluminium substrate. For both plasma polymer films obtained by vacuum and atmospheric plasma, ToF-SIMS indicates the presence of AlOSi bonding; the observed experimental masses for AlOSi differs from the theoretical mass by only 7 ppm and no possible interference with carbon contamination looks possible.
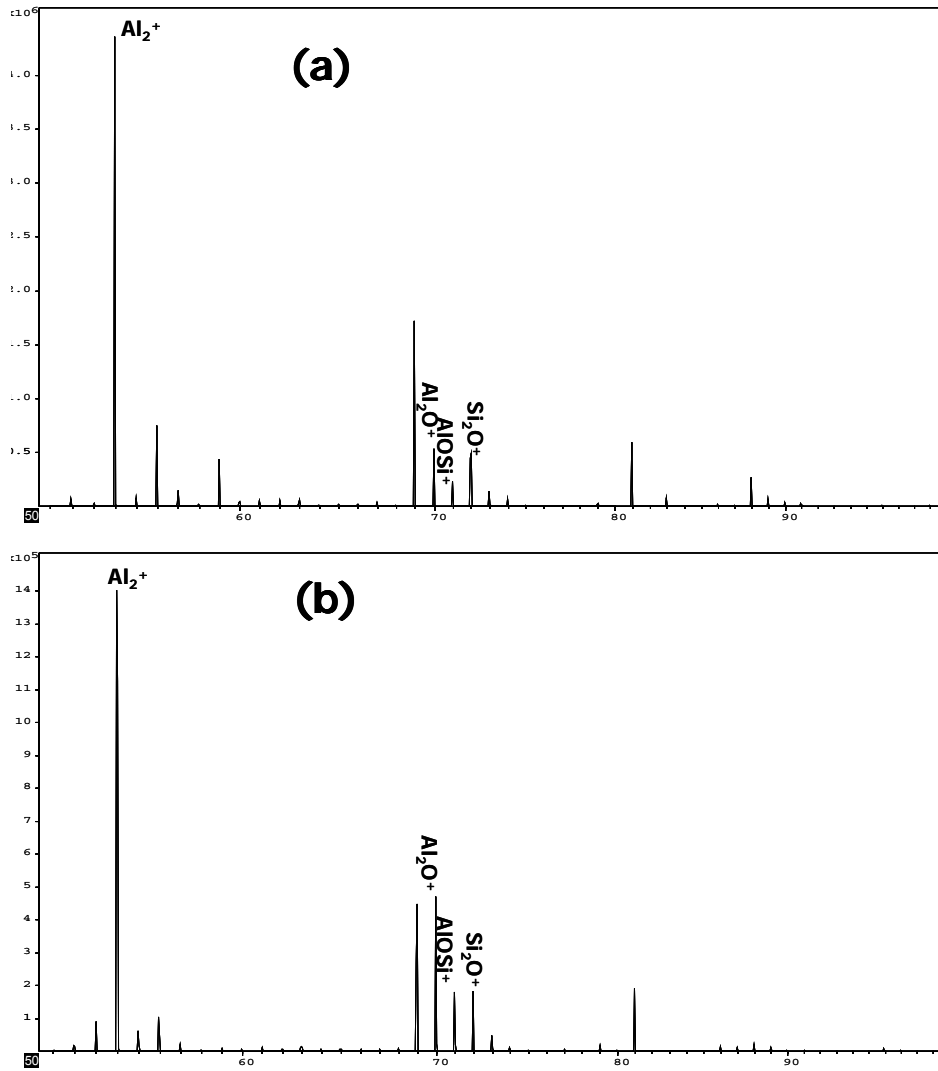
Figure 10 - ***Positive ToF-SIMS spectrum of plasma polymer BTSE film: (a) atmospheric plasma polymer BTSE film: 50-100 amu; (b) vacuum plasma polymer BTSE film: 50-100 amu.***
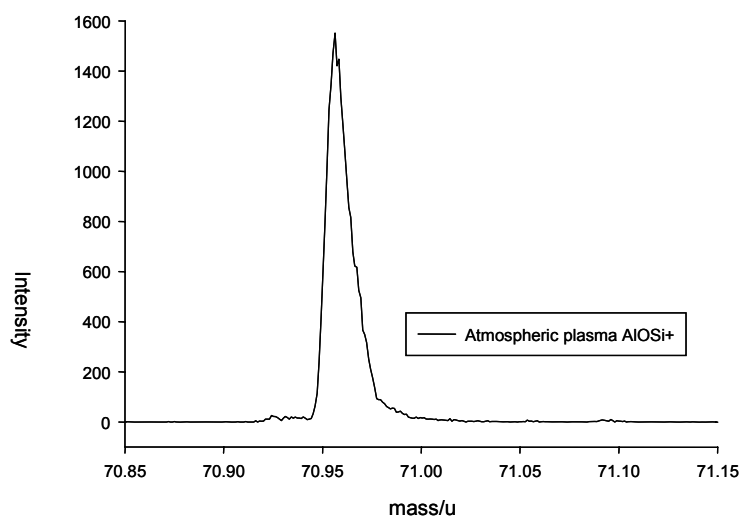
(A) atmospheric plasma polymer BTSE
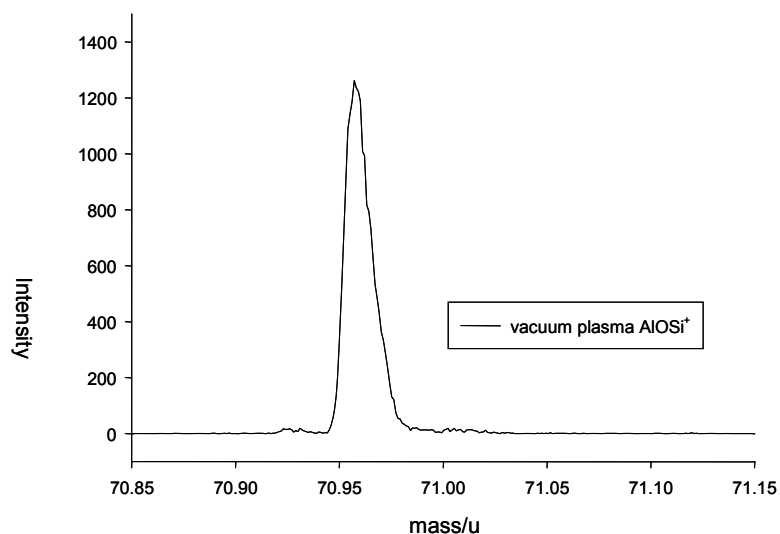
(B) vacuum plasma polymer BTSE

Figure 11 - High-resolution positive ToF-SIMS measurement of AlOSi^{+} near nominal mass m/z equal to 71; (A) atmospheric plasma polymer BTSE, (B) vacuum plasma polymer BTSE.

The use of ToF-SIMS as a tool to analyse interfaces between a silane and a metal substrate is well documented, specifically in the case of silane films deposited from wet deposition methods, but results were often obtained with limited mass resolution (m/Δm < 600 at m/z + 57), which could make the interpretation of the result rather ambiguous. Anyway, Getting and Kinloch found a peak at m/z + 100 when γ-glycidoxypropyltrimethoxysilane (γ-GPS) treated mild steel was studied with ToF-

SIMS and they interpreted this peak as FeOSi$^+$ [50]. In another investigation, the same authors studied the interface between (γ-GPS) and stainless steel and detected ion fragments at m/z + 96 and m/z + 100, which were assigned to CrOSi$^+$ and FeOSi$^+$ respectively [51]. Fang et al. investigated γ-GPS treated aluminium and detected a peak at m/z + 71, which was assigned to AlOSi$^+$ [50]. Cayless and Perry studied the adhesion of polystyrene on mild steel using an aminosilane as adhesion promoter [52]; the presence of peaks at m/z + 100, m/z + 122 and m/z + 148, which were assigned to FeOSi$^+$, FeO$_3$Si$^+$ and FeO$_4$Si$^+$, respectively, was taken as strong evidence for chemical bond formation between the silane and substrate. Abel et al. studied the interface between oxidized aluminium and hydrolyzed γ-GPS [53]. Their work was the first study where a high mass resolution SIMS instrument was used (m/Δm = 3800 at m/z + 41 (C$_3$H$_5^+$)). They were able to show the presence of the AlOSi$^+$ ion at m/z + 71, which evidenced the formation of covalent bonds between the aluminium substrate and the silane. Abel [53] has legitimately pointed out that the nominal mass of 71 amu can arise from other sources, including ion fragments from hydrocarbon contamination and residual chemicals from the sample preparation process. Nevertheless, the same study also reported that, after the outermost layers of the sample had been sputtered off, the main contribution to the peak at nominal mass 71 amu was indeed mainly attributable to the AlOSi$^+$ ion. An additional TOF-SIMS study by Bexell and Olsson [54] and more recently by Shimizu [55] have also confirmed that the peak at 71 amu was predominantly AlOSi$^+$ at the aluminum–silane interface. All these studies have been done on silane films obtained by wet deposition techniques. Taking this information together, we work with the philosophy that it is reasonable to assign a nominal peak at 71 amu to AlOSi$^+$ ion. Our resolution measurements is ((m/Δm = 9600 at m/z + 28 (Si$^+$)) and ((m/Δm = 6000 at m/z + 71 (AlOSi$^+$)).

To complement and support this peak assignment, results from the depth profiling experiments of BTSE film deposited by atmospheric plasma are given in Figure 12. The examination of the intensity of peak 71 (AlOSi$^+$) along the depth profile provides indeed interesting information. As soon as we start to etch the surface, the main fragment remaining at nominal mass 71 is related to the AlOSi$^+$ ion. This fragment has a maximum intensity at the interface. More interestingly, the relative AlOSi$^+$ and Al$_2$O$^+$ ions intensities start arising and then while the AlOSi$^+$ ion mass starts to decrease, the Al$_2$O$^+$ ion peak continues to increase, indicating that the aluminium substrate is being exposed on etching (this last fragment is assumed to arise from the oxidized metal surface).

The depth profile thus clearly indicates that an interfacial layer fingerprinted by the AlOSi$^+$ fragment is present below the outer layer of organic material obtained from plasma polymer film. As shown in the depth profile, when the AlOSi$^+$ peak is reduced

to only a few counts, it is not possible to detect any organics from plasma polymer films and only fragments from the aluminium substrate are detected.

Depth profiles for BTSE film deposited by vacuum plasma show the same trend as for film deposited by atmospheric plasma (see Figure 9).
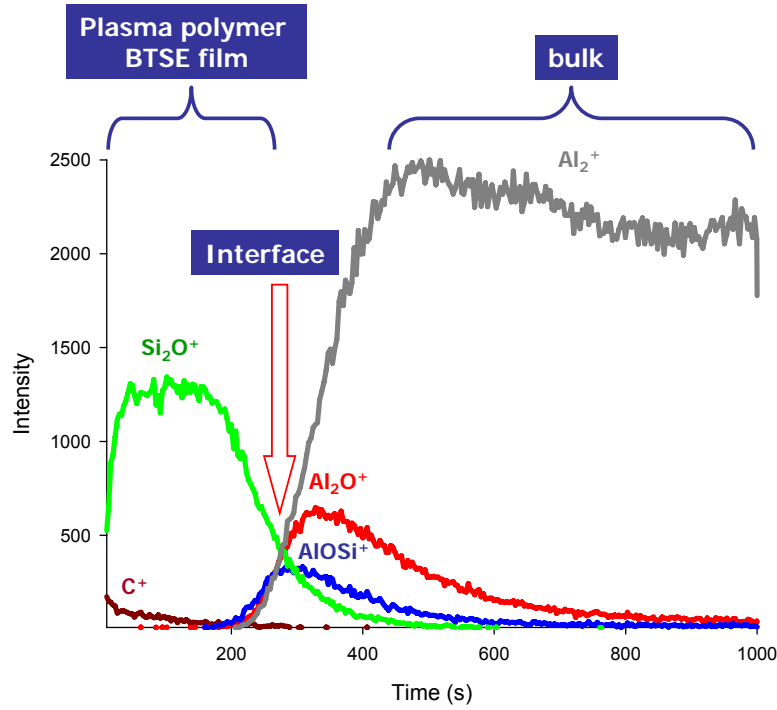
Figure 12 - SIMS depth profile from atmospheric plasma polymer BTSE film on Al (99.99%).
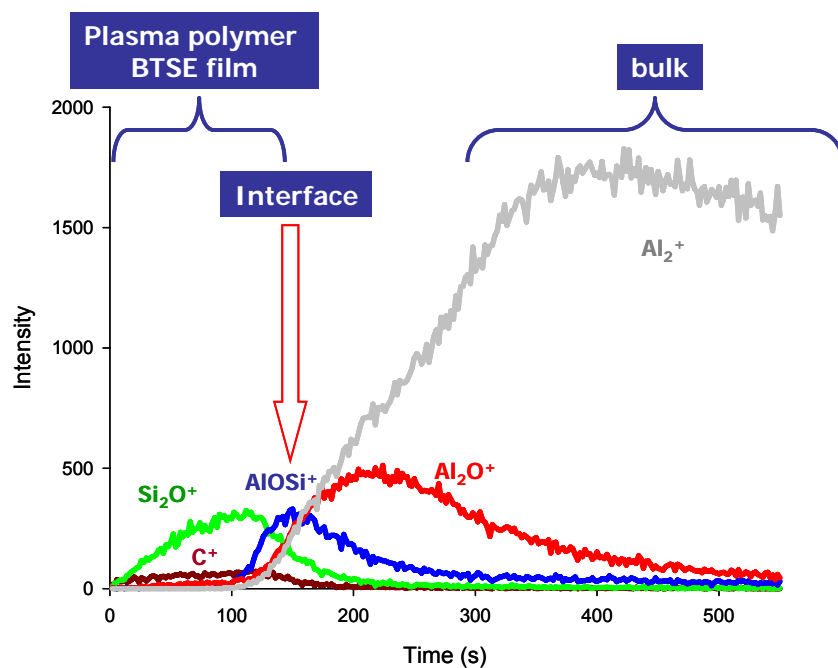
Figure 13 - SIMS depth profile from vacuum plasma polymer BTSE film on Al (99.99%).

In order to confirm the location of different interfaces, additional ToF-SIMS images (Figure 14) are constructed for ions associated with the fragments of interest. Analyzing the particles distribution on a z axis, from top to down, first organics materials (largest counts of C^+ ion) can be observed, then Si_2O^+ ions of the siloxane network. Below these particles the chemical interface is evidenced by the detection of $AlOSi^+$ ions, then Al_2O^+ ions of the substrate oxide are detected and finally the Al_2^+ peak characteristic of metal. These images clearly show the presence of the AlOSi interface layer and thus the presence of silane-aluminium oxide covalent bond between the plasma polymer BTSE film and the aluminium substrate.

The ToF-SIMS images constructed for BTSE film deposited by vacuum plasma show the same tendency as for film deposited by atmospheric plasma (see Figure 15).
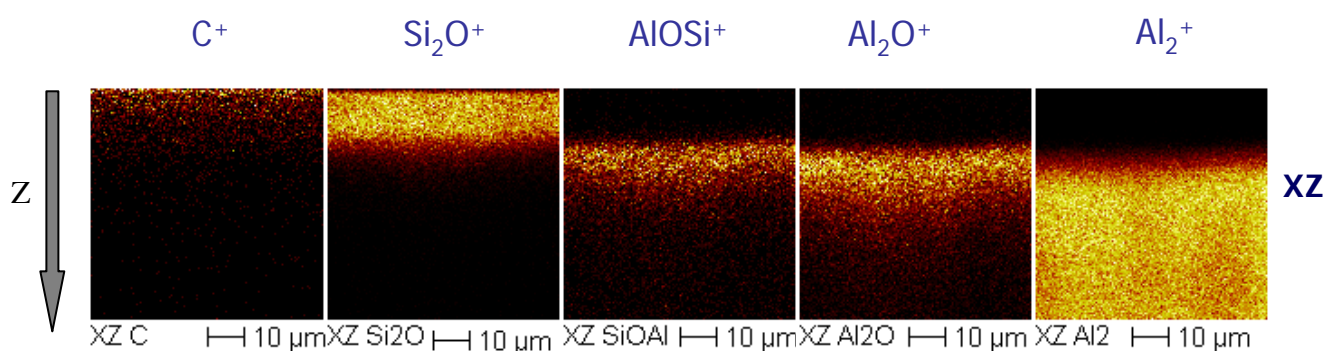
Figure 14 - Ion fragments images from atmospheric plasma polymer BTSE film on Al(99.99%)
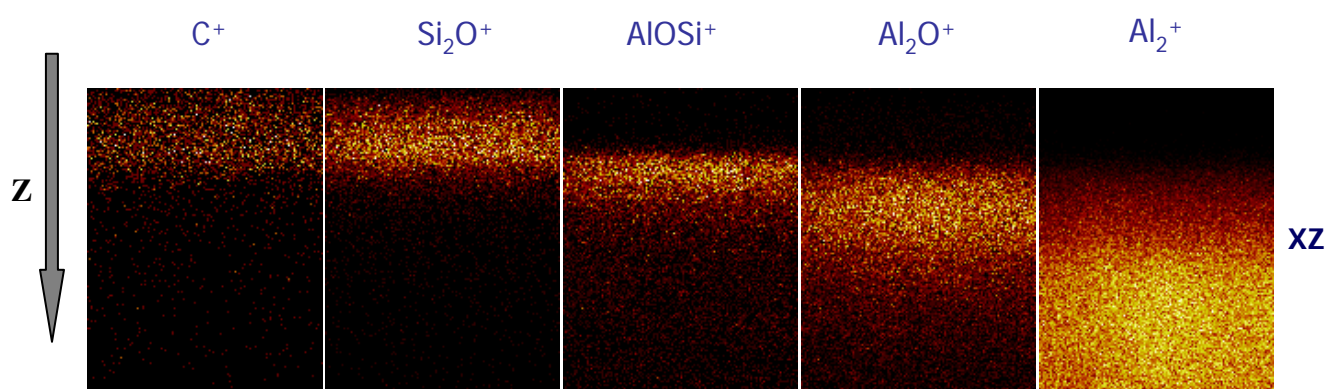
Figure 15 - Ion fragments images of vacuum plasma polymer BTSE film on Al (99.99%).

The bonding between the silane layer and the aluminium oxide of the substrate might be weak, either because the plasma polymer BTSE film is only physically absorbed or only weakly adhering to the substrate; or it might be strong, as a result of a true chemisorption. The quality of the interface has been tested by subjecting the plasma deposited films to a sonication bath, and comparing XPS spectra before and after

this treatment (Figure 16). The Al signal is observed by XPS for both surfaces, which suggests that the film thickness is less than 10 nm. As the Si/Al intensity ratio is constant (see Table 4), it can be concluded that this layer is strongly adhered to the substrate.
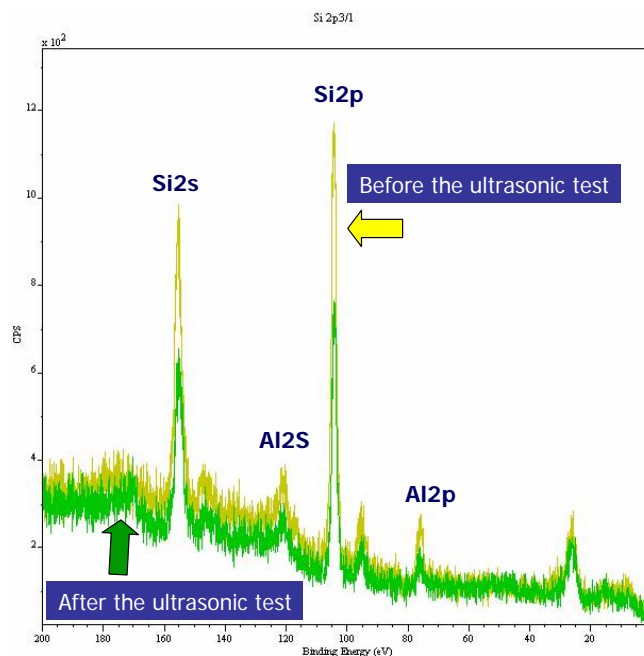
Figure 16 - XPS survey spectra of plasma polymer BTSE film deposited by atmospheric plasma before and after the ultrasonic test.

	(Al/Si) peak area
Before the ultrasonic test	0.23
After the ultrasonic test	0.20

Table 4 - XPS survey spectra of plasma polymer BTSE film deposited by atmospheric plasma before and after the ultrasonic test.

Barrier and corrosion properties

The BTSE films deposited with the three different deposition methods were also compared in terms of barrier and corrosion properties. EIS measurements were performed on the films deposited on AA2024-T3, immersed in 0.5 M NaCl, which is an aggressive electrolyte for aluminium since it induces local corrosion. The thickness of the three layers, deposited by dipcoating, vacuum and atmospheric plasma respectively, are in the same range (75-85 nm).

Figure 17 shows the Bode diagram of the blank and the BTSE films deposited with the three different techniques, at immersion in NaCl. The data show minor

differences between the three coated samples: in particular, as a confirmation of the above results, the dip-coated and the vacuum plasma films have a very similar behavior, and the presence of the layer is clearly shown by the presence of the high-medium frequency peak in the phase angle part of the Bode plot. However, the vacuum plasma layer seems to have better barrier properties. The high frequency relaxation is in fact shifted to the higher frequency domain, compared to the dip-coated film. This means that the film is characterized by a smaller capacity, hence it is more dense (less pores) or has better dielectric properties, which could be due to the different deposition procedure.

On the other side, the layer deposited by atmospheric plasma does not show good corrosion properties, probably due to its inhomogeneity or the presence of pores. However, after two days of immersion in the same electrolyte (Figure 18), the three samples reduce significantly their protective behavior, which becomes comparable to the one of the blank. This quick loss of barrier properties can be attributed to the small thickness of the layers, which affects the corrosion properties of the samples more than their chemistry and composition.

The data scattering at low frequencies is due to pitting of the substrate. Pitting is in fact a quick reaction, with high current density, hence not stable in a slow time interval (as in the case of low frequencies).

Figure 19 shows the impedance behavior of the same films deposited by the three different methods on Al 99.99%, and immersed in $NaSO_4$. This is a less aggressive electrolyte than NaCl, and it has been chosen in order not to damage the substrate, and observe the barrier properties of the BTSE film. In this case, the dip-coated and atmospheric plasma deposited BTSE show similar behavior in term of dielectric properties, while the vacuum plasma layer is comparable to the blank. This might be attributed to the presence of cracks on the sample or to the lack of adhesion of the film to the pure aluminium substrate.

The very thin nature of the films has the highest contribution on their poor protective behavior, hence conclusions cannot be drawn on the barrier and corrosion properties of these specific systems. Anyway, these thin films are meant as pre-treatment only, to which further protective layers will be applied for improved properties.
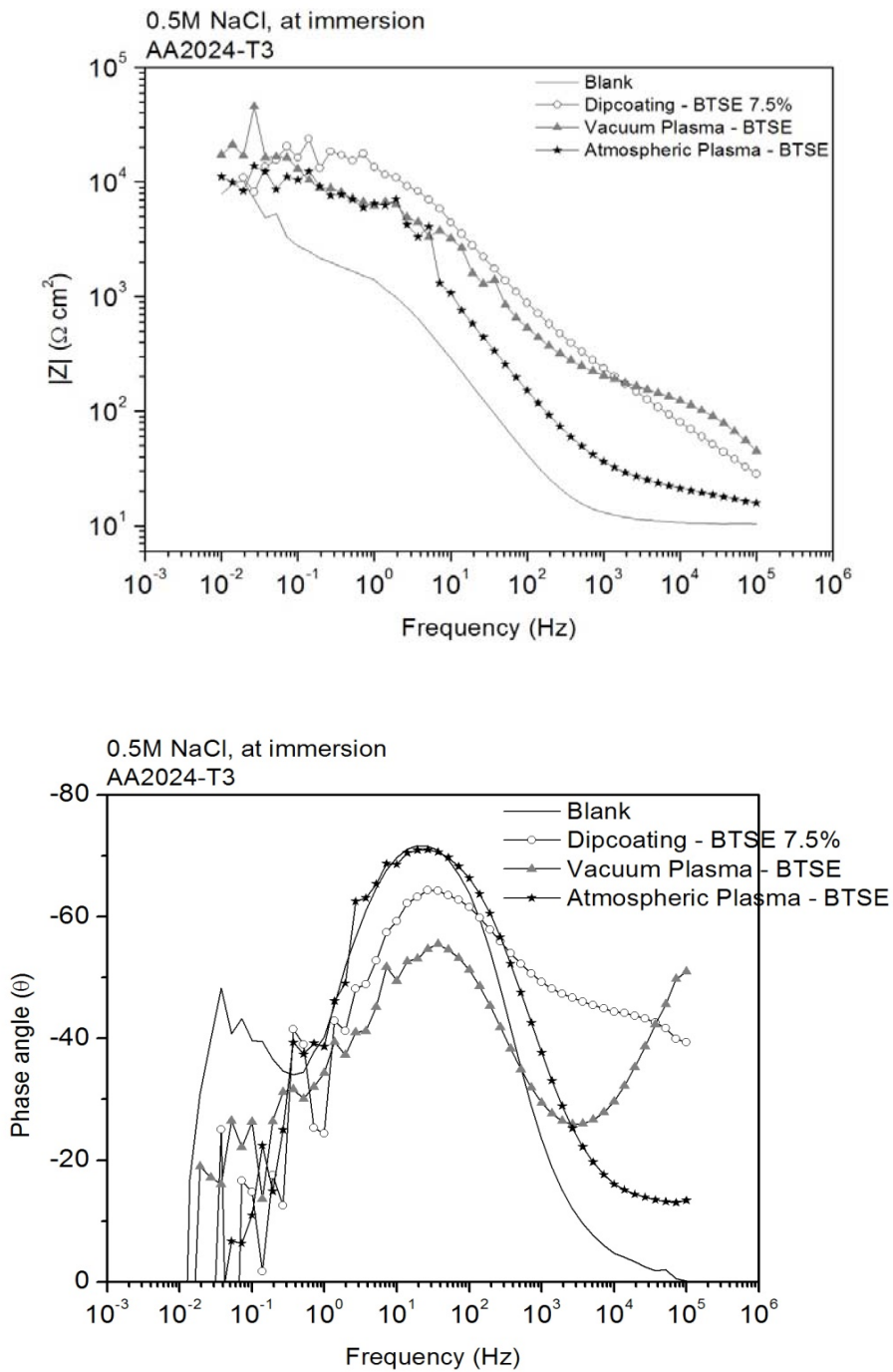
Figure 17 - *Bode diagram of an alkaline pre-treated blank AA2024-T3, and the same substrate coated with BTSE, through dipcoating (BTSE 7.5%), vacuum and atmospheric plasma, at immersion in NaCl.*
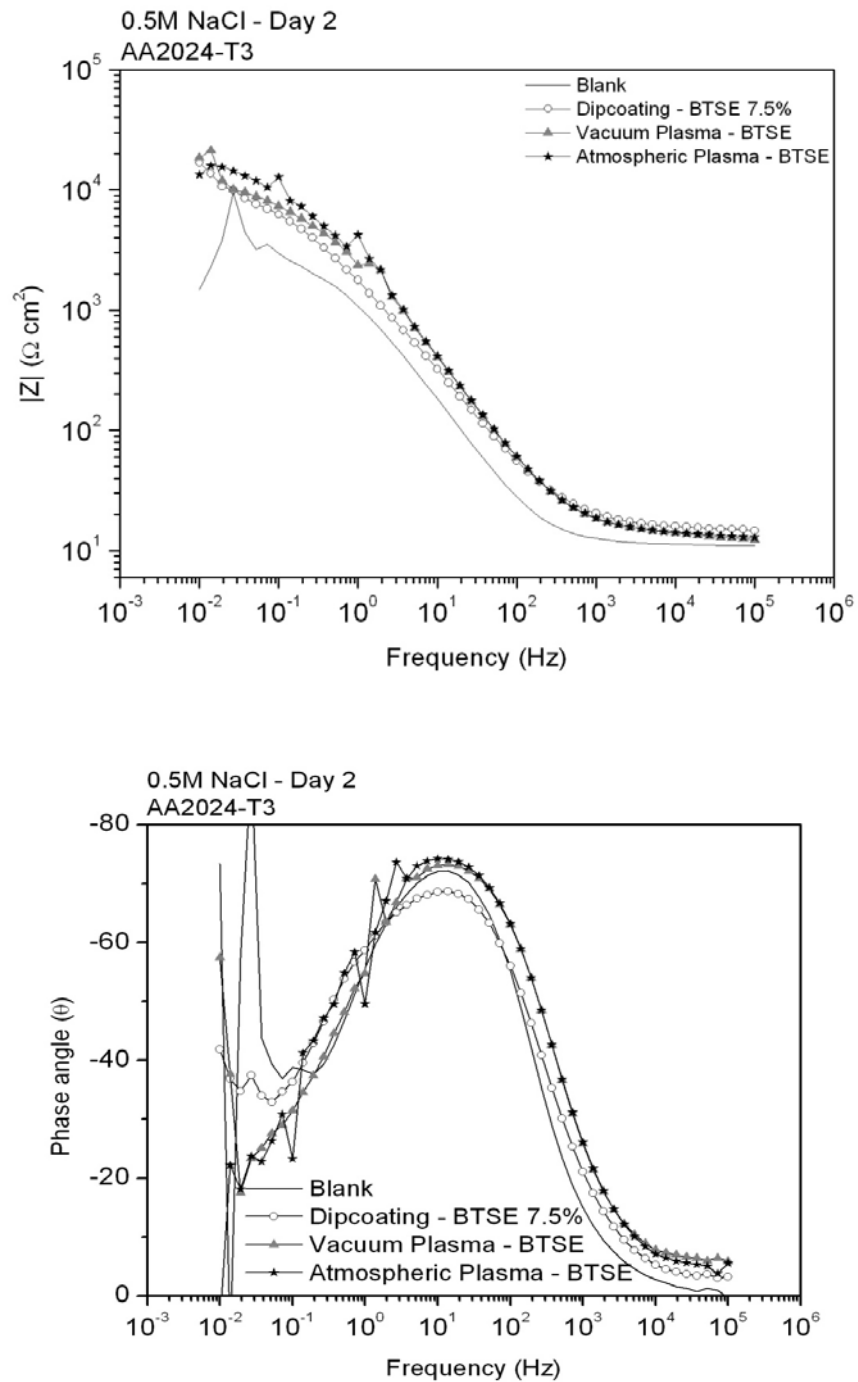
Figure 18 - *Bode diagram of an alkaline pre-treated blank AA2024-T3, and the same substrate coated with BTSE, through dipcoating (BTSE 7.5%), vacuum and atmospheric plasma, after 2-day immersion in NaCl.*
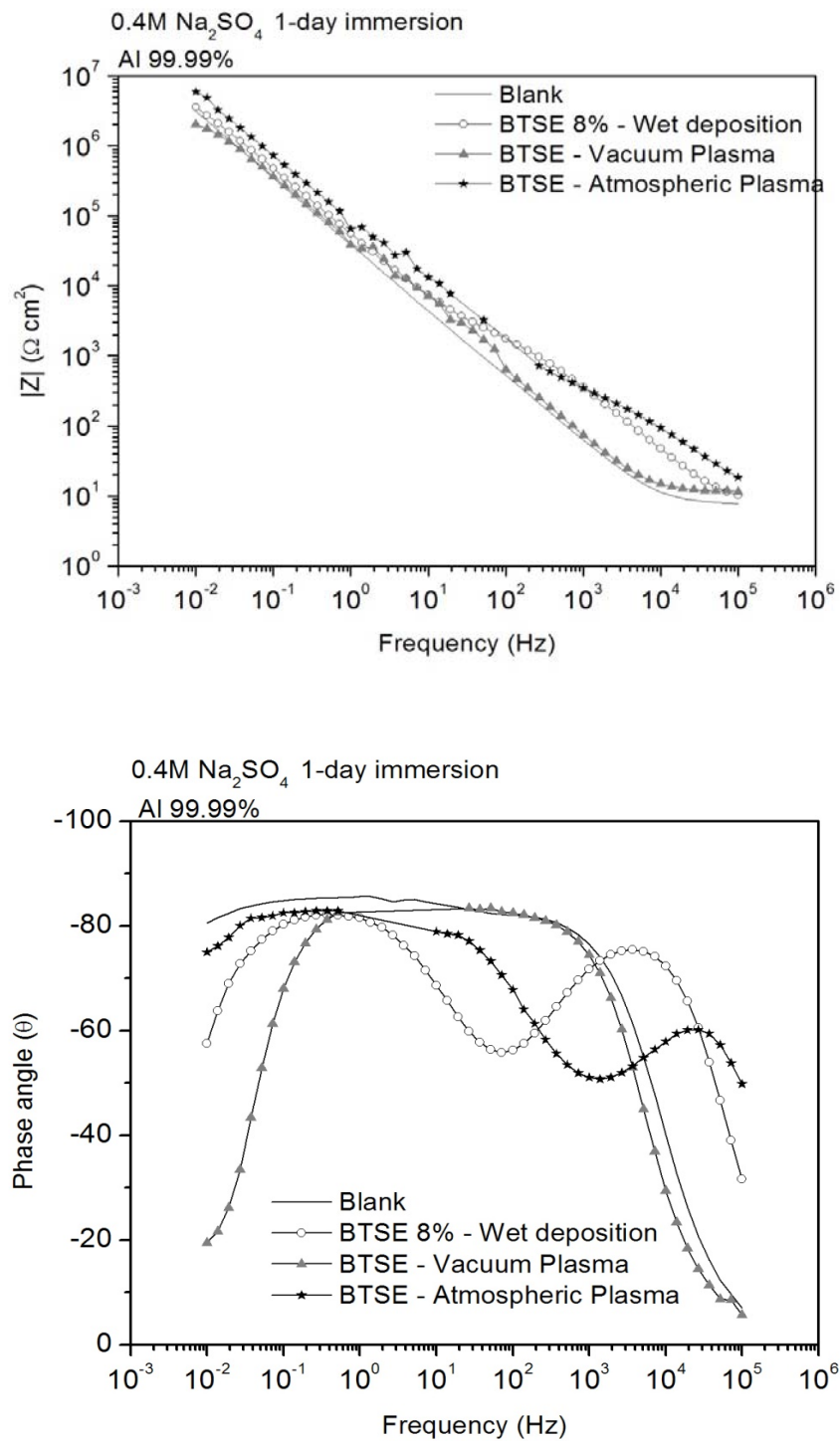
Figure 19 - *Bode diagram of an alkaline pre-treated blank AA2024-T3, and the same substrate coated with BTSE, through dipcoating (BTSE 7.5%), vacuum and atmospheric plasma, at immersion in Na₂SO₄.*

System 2

System 2 is studied through vacuum and atmospheric plasma deposition. The IR and photoelectron spectra of plasma-polymerized HMDSO are strongly dependent on the plasma parameters and on the plasma process. Therefore, it is crucial to characterize the films deposited by these techniques in detail.

Vacuum plasma deposition

X-ray photoelectron analysis was used to determine the relative amounts of O, C, and Si at the surface of the polymer film deposited from a HMDSO precursor. According to XPS analysis, there is a much lower C content in the polymer deposited under the influence of additional O_2. This is shown in Figure 20(a-b) and summarized in Table 5. The composition of the outer surface region of the films was $SiC_{2.1}O_{0.95}$ for the film deposited with pure HMDSO plasma and $SiC_{0.07}O_{2.4}$ for the film deposited with a higher oxygen partial pressure. The chemical composition of the films was also characterized by curve-fitting of the Si_{2p}, O_{1s} and C_{1s} peaks. The assignment of the peaks is summarized in Table 5. The photoelectron spectra show that for the film with the higher oxygen content silicon was mostly bound to four oxygen atoms, while for the films with low oxygen content the coordination number was between one and three. The chemical formula of this coating is very close to the PDMS one. This suggests that oxygen selectively binds to the silicon atom of the organosilicon species in the plasma.
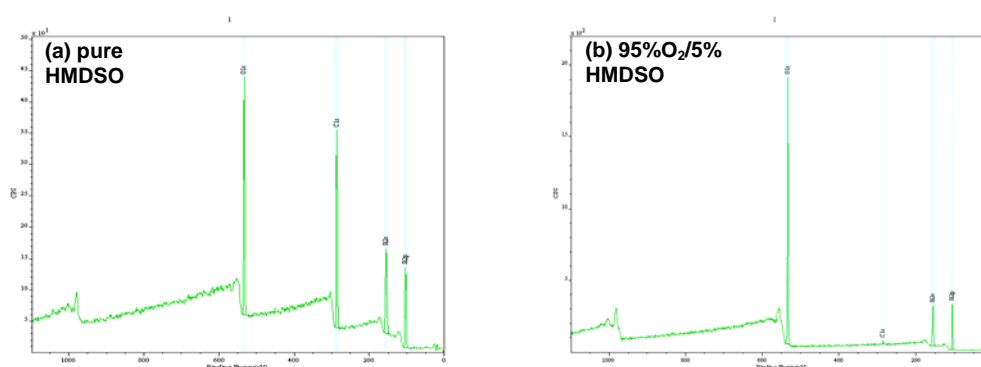
Figure 20 - XPS survey spectra of pp-HMDSO film, (a): 300 W, 300 mTorr, 10 min, (b): 200 W, 300 mTorr, 5 min.

Reflection absorption infrared spectra of HMDSO and HMDSO/O_2 plasma polymers are shown in Figure 21(a-b). For better comparison, the wavenumber regions have been divided into two parts. The peak assignment is given in Table 6. Comparison of the IR spectra of HMDSO and HMDSO/O_2 plasma polymers in Figure 21 reveals a strong increase in the intensity of the asymmetric Si–O–Si stretching vibration and a decrease of the peak intensity in the CH_x stretching region between 2800 and 3000

cm^{-1} when the oxygen was added to the plasma. Figure 21(a) shows the low wavenumber region. For the film deposited with HMDSO plasma, the Si–CH$_3$ bending band is clearly visible at 1255 cm^{-1} together with the asymmetric stretching of Si–O–Si at 1100 cm^{-1}. XPS data show that the oxygen in the plasma polymer films is bound to silicon (Table 5), so that the existence of Si–O–Si groups is confirmed. A band at 847 cm^{-1} originates from the rocking vibration of the methyl groups of Si(CH$_3$)$_3$. The methyl rocking band at 806 cm^{-1} indicates the presence of dimethylsilyl groups. The film deposited with HMDSO/O$_2$ plasma shows a strong, asymmetric, Si–O–Si peak at 1260-1000 cm^{-1}. The high frequency band is indicative of silica-like structures, which is in agreement with the observed +IV states in the Si$_{2p}$ spectrum (Table 5). A Si–OH peak at 926 cm^{-1} was observed in samples deposited with HMDSO/O$_2$. This peak is likely to be due to non-bridging Si–O units in the film [56]. Trimethylsilyl groups were still incorporated in the film, as can be deduced from the peaks at 1275 and 837 cm^{-1}. Figure 21(b) shows the CH stretch region. In both films, the CH$_3$ bands at 2960 and 2903 cm^{-1} are significantly more intense than the CH$_2$ bands at 2920 and 2872 cm^{-1}. This is to be expected as the monomer contains CH$_3$ groups and these are retained in the plasma polymer. The existence of few CH$_2$ groups and the observation that carbon is not bound to oxygen shows that a small amount of methylene groups acts as a link between silicon atoms.

		Polymer		Fitted peaks		
		Element (peak)	Atomic concentration (%)	Binding energy (eV)	Assignment	Percentage (%)
HMDSO		Si2p	24.5	100.9 102 102.8	Si(-O)$_1$ Si(-O)$_2$ Si(-O)$_3$	27 56 17
		C1s	52.1	284.2 285	Si-CH$_x$ O-Si-CH$_x$	63 37
		O1s	23.4	530.9 532.4	- Si-O-Si	2 98
HMDSO/O$_2$		Si2p	29	103.7	Si(-O)$_4$	100
		C1s	2	285	-	-
		O1s	69	532.3	Si-O-Si	100

Table 5 - *Chemical composition of HMDSO plasma polymer (plasma polymerization from HMDSO and HMDSO/O$_2$) evaluated by a fitting procedure of XPS from Alexander [48].*

Wavenumber (cm-1)		Group	Assignment
HMDSO	HMDSO/O$_2$		
2960	2970	Si-CH$_3$	v_{as}(CH$_3$)
2903	-	Si-CH$_3$	v_s(CH$_3$)
1255	1275	Si-(CH$_3$)$_x$	δ_s(CH$_3$)
1200-1000	1260-1000	Si-O-Si	v_{as}(Si-O-Si)
-	927	Si-OH	
847	837	Si-(CH$_3$)$_3$	r(Si-CH$_3$)
806	807	Si-(CH$_3$)$_2$	r(Si-CH$_3$)

Table 6 - *Assignment of the IR peaks of the HMDSO plasma polymer films deposited without and with O$_2$ gas feed.*

Atmospheric plasma deposition

HMDSO films were deposited at a plasma power varying from 60 W to 100 W, with Ar/O_2 as the main process gas. XPS analysis showed that the films were composed of 28 to 34 at.% silicon, 63 to 66 at.% oxygen and 9 at.% carbon. After a short sputtering with argon ion bombardment in the XPS chamber the carbon peak disappears, suggesting that the contamination is only superficial. The silicon and oxygen peaks from the film deposited at 100 W were de-convoluted into one main peak at 103.4 eV and 532.9 eV, which are values typically indicating the presence of SiO_2. The chemical composition of these films is similar to the one obtained for the vacuum plasma deposition ($SiC_{0.07}O_{2.4}$).

Figure 22 shows a series of infrared spectra of films grown at different power and deposition times. The peaks at 784, 1070, 1150 and 1234 cm^{-1} are due to the bending and asymmetric stretching modes of siloxane bridges, respectively [57].

Further examination of the infrared spectra reveals that some of them contain a well defined peak at 930 cm^{-1}. This peak may be assigned to the O-H deformation mode. It should be noted that no peaks are detected at 2900 and 1730 cm^{-1} (C-H and C-O stretching vibrations), due to C-H and C-O stretching vibrations, indicating that the ethoxide ligands do not incorporate into the film, whatever the experimental conditions. Figure 22(a-c) show that the composition and the porosity of the films change with the plasma power and with time. Increasing the input power from 60 to 100 W reduces the incorporation of hydroxyl groups and results in a significant decrease in the feature at 930 cm^{-1}, suggesting that the porosity of the films has significantly decreased [57, 58].
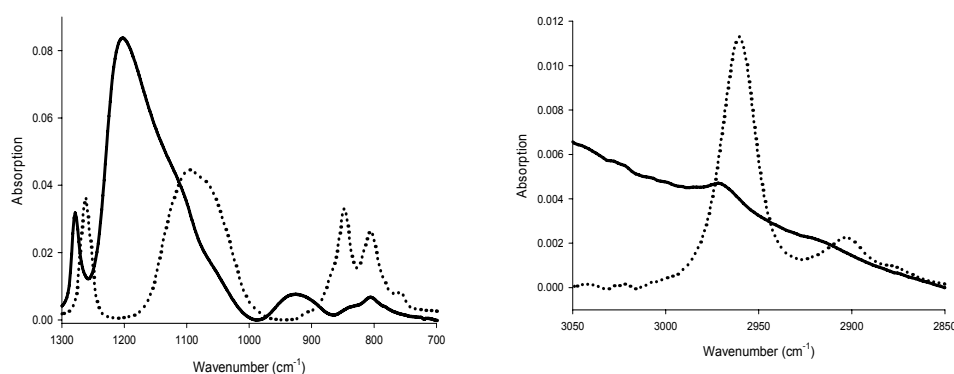
Figure 21 - Infrared spectra of the plasma polymers deposited with (a) HMDSO (…) and with (b) HMDSO/O_2 (─) for different wavenumber regions.
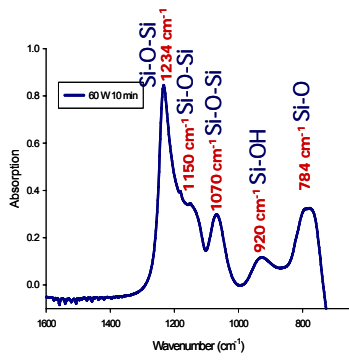
(a) 60 W, 10 min
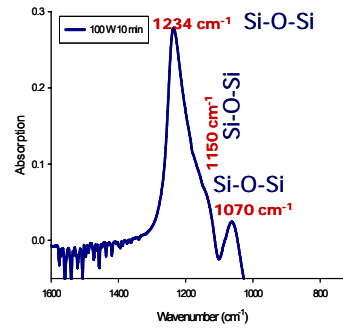
(b) 100 W, 10 min
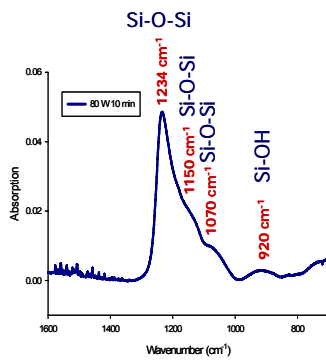
(c) 80 W, 10 min
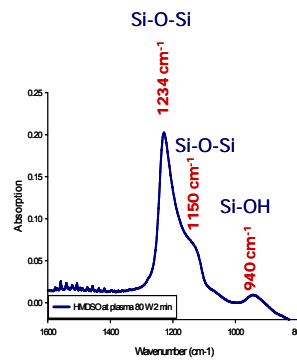
(d) 80 W, 2 min

Figure 22 - IR spectra of pp-HMDSO film (Atmospheric pressure) at different conditions (a-d).

System 3

<u>*Wet deposition*</u>

Thickness of the films

The thickness of the silane films with the incorporation of CeO_2 nanoparticles has been estimated through VISSE analysis, and confirmed by looking at the cross section of the films with FE-SEM and TEM. It depends on the BTSE concentration, as reported in previous studies [38, 40, 59, 60].

Figure 23 shows the VISSE spectra of the electropolished substrate coated with BTSE 5% and 10%, with the addition of CeO_2 nanoparticles. To extract the actual thickness of the coatings from these spectra, an optical model has been built and fitted to the experimental data by using simulation and non-linear least squares regression analysis [61]. The spectrum of the bare electropolished substrate (not shown here) allowed calculating its optical constants and using them in the model for the coated one. A Cauchy dispersion relation, valid for a transparent material in the used spectral range, has been applied to model the refraction index of the silane film. A Bruggeman effective medium approximation (EMA) layer has been used to correct for roughness of the film/substrate interface [60]. This represents an interface layer between the metal and the Cauchy layer. Finally, to model the coating with CeO_2 particles in it, another EMA type of layer has been considered. The optical constants for the nanoparticles have been calculated by analyzing the spectrum of a CeO_2 pellet made in the laboratory starting from the same nanopowder used in the coating. The described model gave a film thickness of 67 nm for 5% BTSE and 94 nm for 10% BTSE, which are in agreement with the results obtained with the other methods (below).

The FE-SEM image of a silane coating's cross section (Figure 24) confirms the above data for a BTSE concentration of 5% and nano-dispersed CeO_2 particles in the matrix. The thickness of the sample has been estimated using the SmileView software from JEOL Ltd. on several parts of the cross sections (only one image shown here).

FIB-TEM analysis was also performed on a sample coated with BTSE 8% and 250 ppm CeO_2, as nano-suspension. A cross section of the sample was prepared by FIB, and mounted in the TEM for imaging and analysis of the BTSE coating. The image in Figure 25 gives the thickness estimated for a BTSE 8% film, with an average of 84 nm, hence comprised between the thickness of the 5% and 10% films.

(a)

(b)
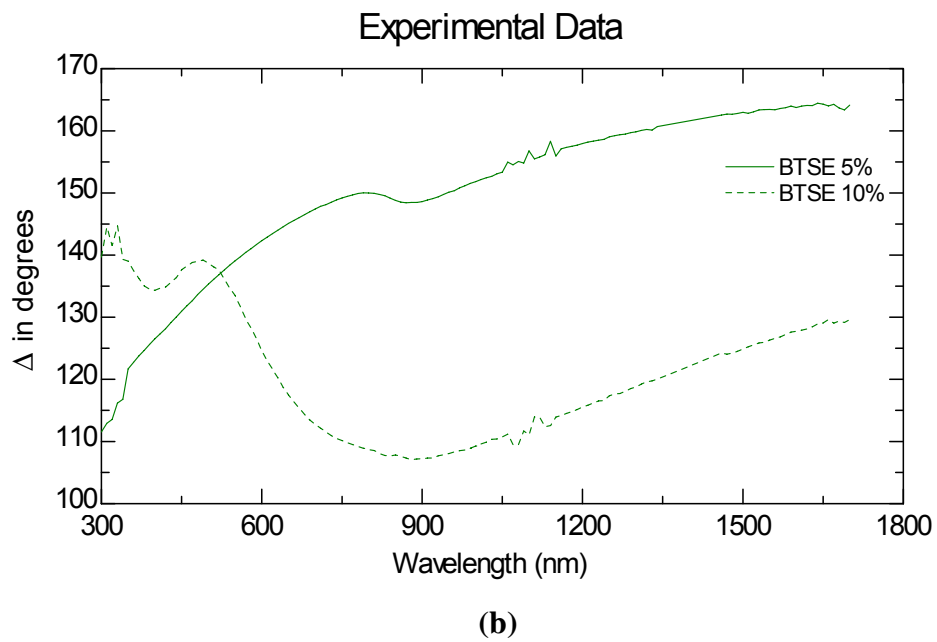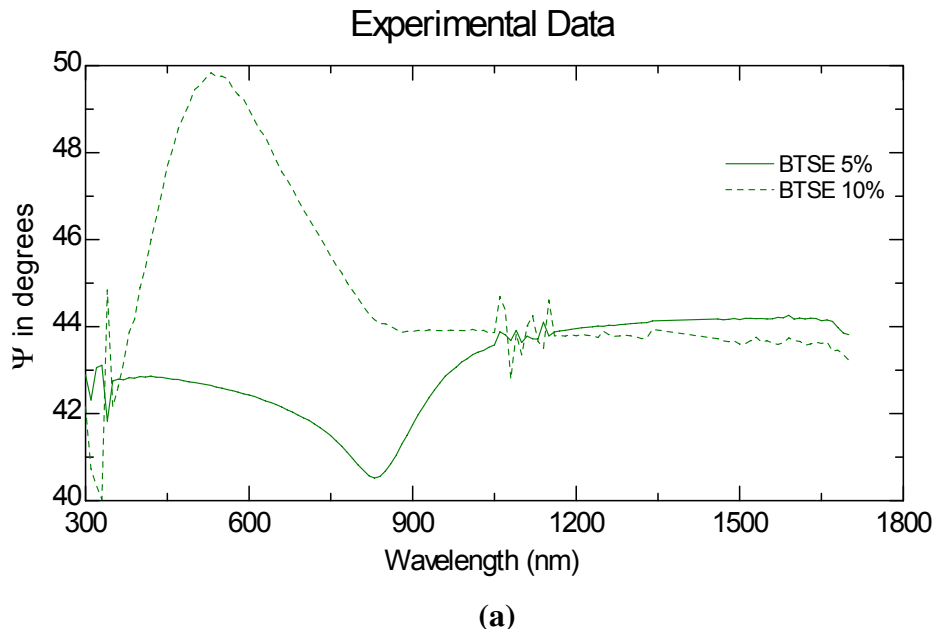
Figure 23 - Ψ (a) and Δ (b) VISSE spectra (measured at 65° incidence angle) of the electropolished substrate (Al 99.99%) coated with BTSE 5% and 10%, with the addition of CeO₂ nanoparticles.
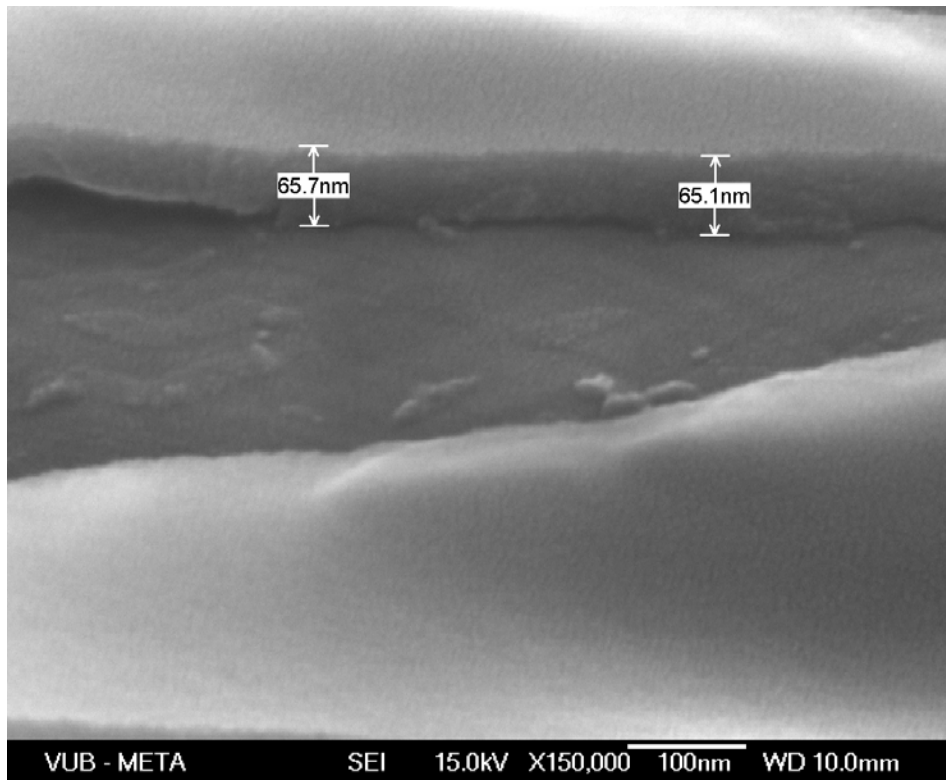
Figure 24 - ***FE-SEM image of a cross section of a BTSE 5% coating with nano-dispersed CeO$_2$ on Al 99.99% substrate. The thickness of the coating has been estimated using SmileView software.***
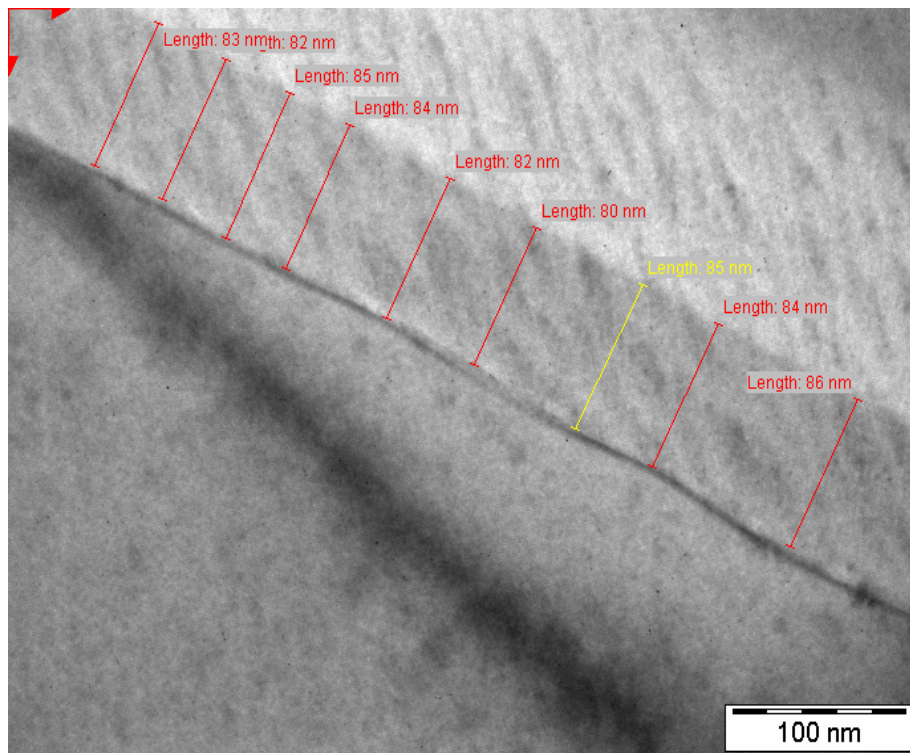
Figure 25 - ***FIB-TEM image of a cross section of a BTSE 8% coating with nano-dispersed CeO$_2$ on Al 99.99% substrate.***

Interactions between BTSE and CeO$_2$

The coating solutions have been analyzed by ^{29}Si NMR in order to study how the presence of CeO$_2$ nanoparticles affects the BTSE solution in terms of reactivity and stability, which are mainly determined by the hydrolysis and condensation reactions taking place in the solution, as described in the introduction. In particular, condensation would reduce the active sites responsible for the bonding with the substrate, and should not be accelerated.

^{29}Si NMR measurements were performed on freshly prepared solutions and after their storage for a pre-defined time. In the spectra shown in Figure 26 (BTSE alone and BTSE with CeO$_2$ nanoparticles, at time zero and after one week respectively) three resonances can be observed between -44 and -52 ppm: these can be assigned to hydrolyzed condensed species, such as dimers and trimers or cyclic monomers, dimers and trimers. The less resolved signal between -52 and -72 can instead be assigned to silicon atoms in more condensed species with higher molecular weight. The increasing degree of condensation and hence decreasing tumbling mobility gives rise to a range of signals with different chemical shifts and line-broadening. The absence of a resonance around -40 ppm implies that no fully hydrolysed monomers are present [41].

Table 7 shows the percentage of dimers and trimers, and that of larger condensed species, estimated from the integrated areas of the signals between -44 and -52 ppm and between -52 and -72 respectively. For all solutions, the amount of larger condensed species increases with storage time, up to 2.5 months, due to the ongoing condensation of the molecules, after which the relative amount of different species remains constant (accuracy on the integration values should be estimated at 2%). This confirms the results of previous research performed by De Graeve et al. [39] on water based BTSE solutions. The present work shows that the addition of ceria particles does not affect the speciation and ageing of the BTSE solutions in the time range under study. The values recorded at 2.5-month storage time for BTSE + CeO$_2$ are slightly outside the trend and this is probably just due to the lower accuracy (shorter accumulation time) of these specific measurements. The above results are also in agreement with the recent work of Montemor et al. [62], where it was shown that ceria particles do not influence the ageing of BTESPT (bis-[triethoxysilylpropyl] tetrasulfide, alcohol-based), another bis-functional organosilane molecule.
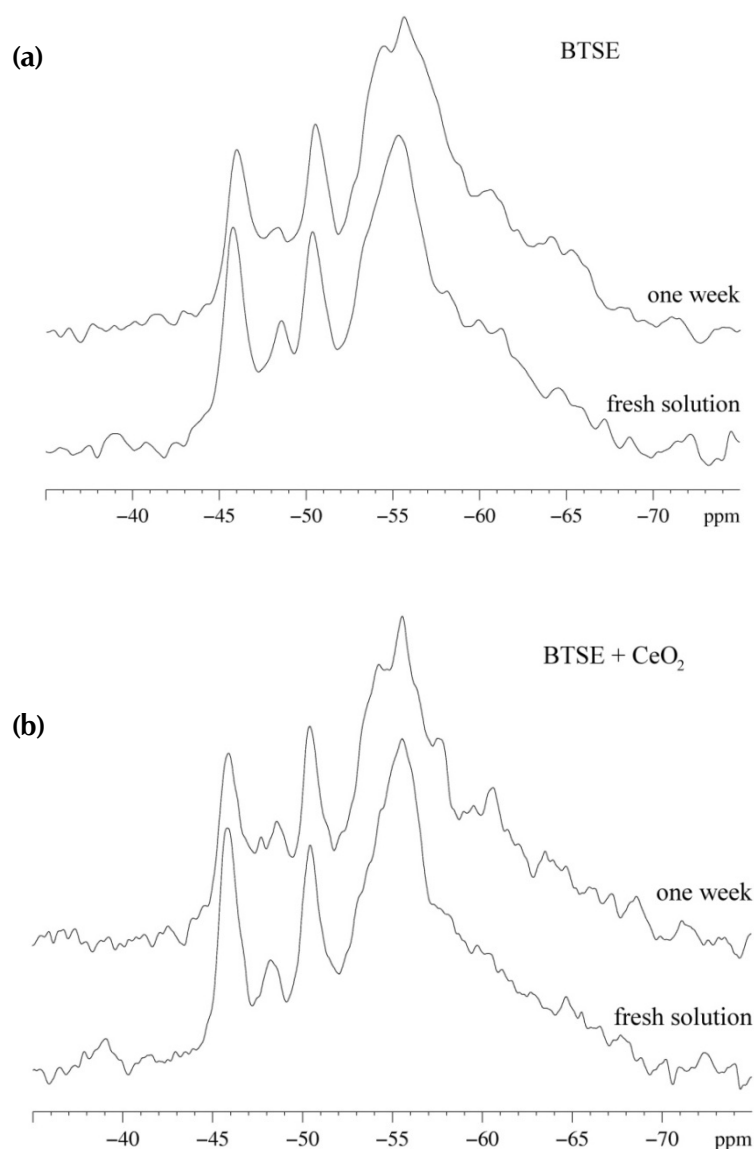
Figure 26 - ^{29}Si NMR spectra of (a) 8% BTSE solution, and (b) 8% BTSE solution with 250 ppm CeO$_2$ nanoparticles; both as freshly prepared and aged for one week.

Time	BTSE		BTSE + CeO$_2$	
	dimers and trimers	Larger condensed species	dimers and trimers	Larger condensed species
0	32	68	31	69
1 week	26	74	28	72
2.5 months	20	80	16	84
4 months	18	83	22	78
1 year	21	80	20	80

Table 7 - Ratio of oligomers to larger condensed species as a result of the ^{29}Si NMR study.

The chemical interaction between CeO_2 nanoparticles and the BTSE in the cured coating was investigated by XPS. The measurements could not be performed directly on the deposited films, because the presence of Ce could not be detected in the spectra of the samples as introduced (in agreement with [19, 26, 42]). This is due to the low concentration and to the nanostructure of the CeO_2 particles; in addition, as shown by the results in the following section, the CeO_2 particles are always covered by a layer of BTSE, but argon sputtering of the sample in the XPS chamber was intentionally avoided as it might affect the Ce status (from Ce(IV) to Ce(III)) [63].

The XPS analysis was hence performed on CeO_2 nanoparticles spread over the sample holder; on a mix of nanoparticles and BTSE 5% dried in the oven at $200^{\circ}C$ for 2 hours; and on a layer of BTSE 5% dip-coated on aluminium and cured as described above. The attention was focused on the energy ranges of oxygen (O_{1s}), silicon ($Si_{2p3/2}$) and cerium (Ce_{3d}), in order to check how they are affected by the simultaneous presence of the two compounds. Chemical shifts of the binding energies of core electrons can in fact be explained by the redistribution of charge of the outer electrons when a chemical bond is formed. Table 8 shows the energy values of the peaks observed in the respective spectra.

Figure 27 shows the spectra of the three compounds in the O_{1s} energy range. For the CeO_2 nanopowder, a peak at 529.0 eV appears, which is typical of the lattice oxygen in this compound [62-64]. The typical peak of O in BTSE is also shown at 532.4 eV. Finally, in the spectrum of CeO_2 with BTSE it is clear that two forms of oxygen are present due to the appearance of two peaks (as in [65]): these peaks are slightly shifted and with different shapes from the ones of the individual components, which might point to the presence of a Ce-O-Si bond [64].

The BTSE spectrum in the $Si_{2p3/2}$ energy range (Figure 28) shows a peak at 102.4 eV, which corresponds to the SiO_x in the silane film [62]. This peak is slightly shifted and with a different shape when CeO_2 nanoparticles are added to the silane. This can be explained by the interaction of silicon from BTSE with the cerium ions present on the nanoparticles surface, and it is in agreement with the results of Montemor and Cui [62, 65].

Finally, Figure 29 shows the spectra in the Ce_{3d} core level for CeO_2 and for the same compound modified by BTSE. The chemical state of cerium is a key parameter in the interaction of ceria with other compounds. The XPS spectra of cerium compounds exhibit complex features due to hybridization with ligand orbitals and partial occupancy of the valence 4f orbital. The electronic configuration of CeO_2 (Ce(IV)) is characterized by unoccupied 4f orbitals ($4f^o$) and Ce_2O_3 (Ce(III)) by a $4f^1$ configuration. The differences influence the shape of the core level photoelectron spectra. The presence of satellite peaks is an important feature for the identification of the cerium species. The peak at ~917 eV, which is the most intense of the three

final states (multiplet splitting) of the Ce_{3d} spin orbit doublet, appears only for Ce(IV) (CeO_2), while it is absent for Ce(III) species [63, 64, 66]. The spectrum of CeO_2 in Figure 29 is in agreement with other authors, and it clearly evidences the presence of Ce(IV) [62-66]. When silane is added to the CeO_2 particles, some peaks of the new compound are shifted (Table 8), a peak disappears (Table 8), and the signal at 917 eV has lower intensity.

To conclude, the XPS data present three main evidences that something is changing in the electronic structure of the BTSE film when CeO_2 nanoparticles are added to it (if compared to the pure BTSE layer or to the pure CeO_2): the Si_{2p} signals are different in shape and binding energy; the O_{1s} signals are quite different; and the Ce_{3d5} signals show some peak shifts, a peak disappearance and the attenuation in intensity of the peak at 917 eV. These different features are an indication of the possibility of the formation of a bond between SiO_3^{2-} and Ce(IV) [62, 64-66].
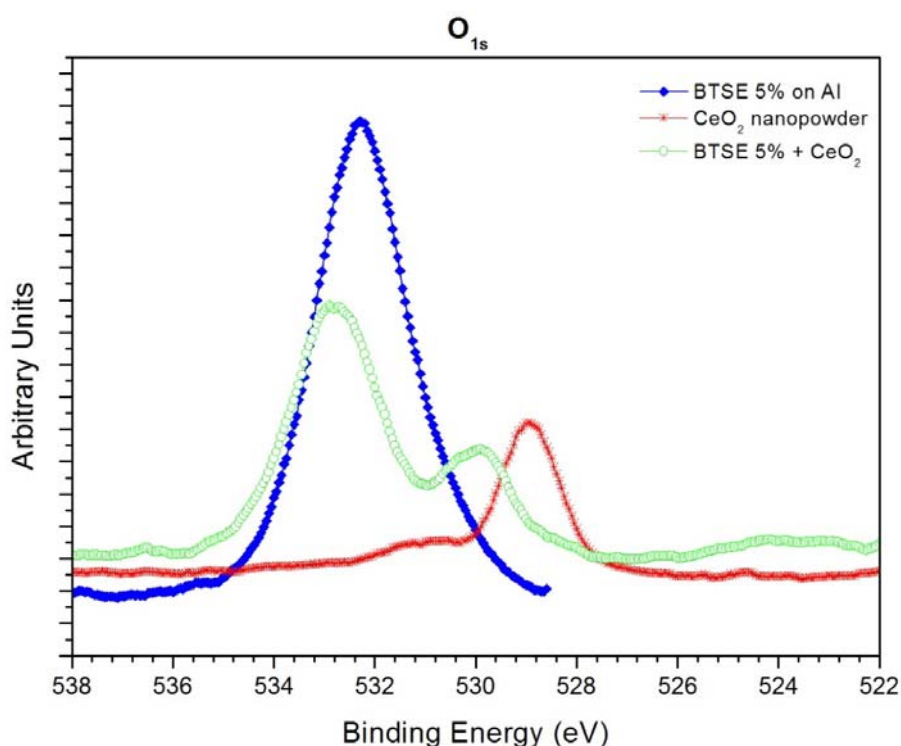
Figure 27 - XPS high resolution spectra in the O_{1s} region of a layer of BTSE 5% deposited over Al 99.99%; of CeO_2 nanopowder; and of a mix of CeO_2 nanopowder and BTSE 5%, dried in the oven at 200^oC.
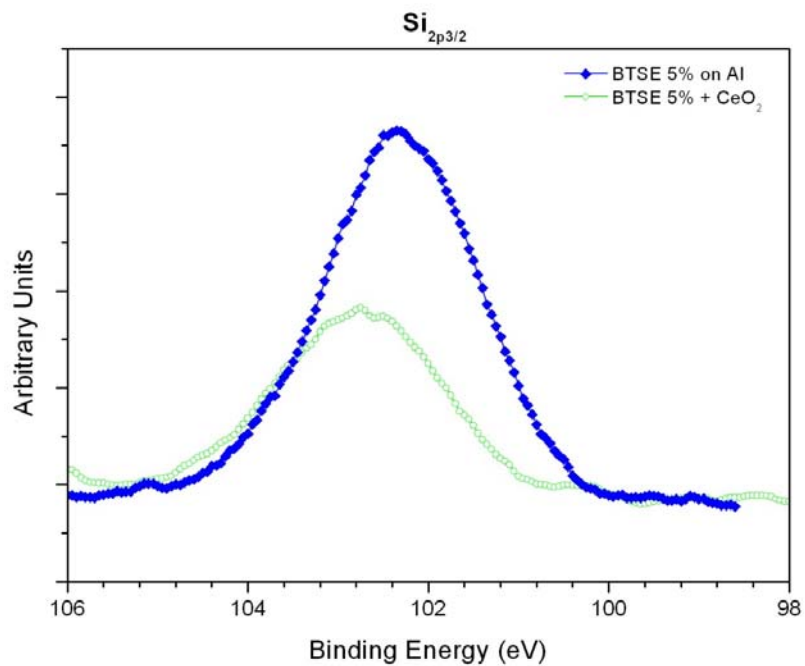
Figure 28 - XPS high resolution spectra in the Si$_{2p3/2}$ region of a layer of BTSE 5% deposited over Al 99.99% and of a mix of CeO$_2$ nanopowder and BTSE 5%, dried in the oven at 200°C.
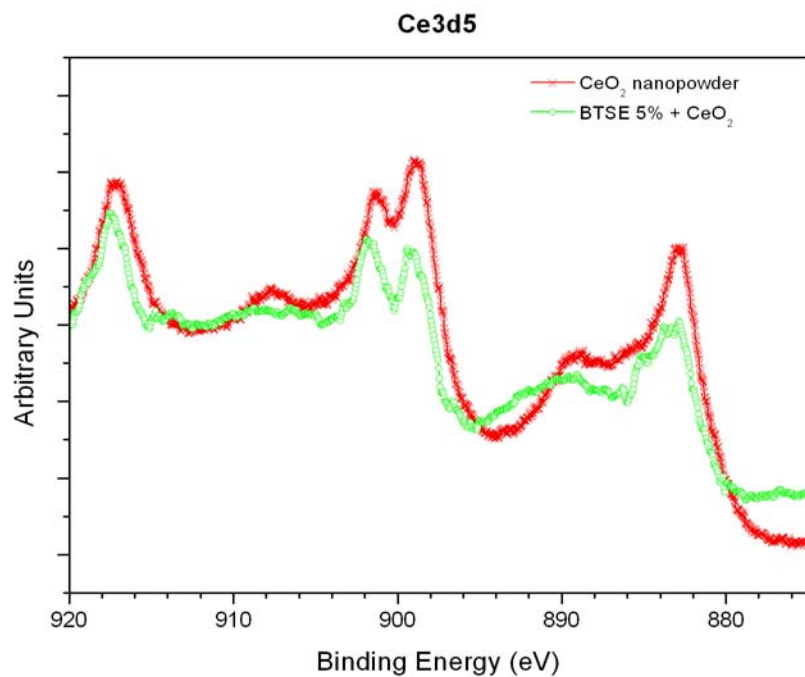
Figure 29 - XPS high resolution spectra in the Ce$_{3d}$ region of CeO$_2$ nanopowder and of a mix of CeO$_2$ nano-powder and BTSE 5%, dried in the oven at 200°C.

Energy range Core level	CeO_2	CeO_2 + BTSE	BTSE
$Ce_{3d\,5/2}$ (Figure 29)	882.9	882.7	N/A
	889.3	891.8	N/A
	898.5	899.1	N/A
$Ce_{3d\,3/2}$ (Figure 29)	901.3	901.6	N/A
	908.8	N/A	N/A
	917.0	917.5	N/A
O_{1S} (Figure 27)	529.0	529.8	N/A
	N/A	533.1	532.4
$Si_{2p3/2}$ (Figure 28)	N/A	102.6	102.4

Table 8 - Energy values (eV) of the peaks observed in the XPS spectra.

Film structure and distribution of CeO_2 nanoparticles

The crucial point in the formation of a BTSE layer with the inclusion of CeO_2 nanoparticles is to avoid the formation of nanoparticles agglomeration, which may reach a size comparable to the thickness of the layer. Figure 30, (a) and (b), shows the FE-SEM images (cross section and top view, respectively) of a cured film made with a solution prepared with CeO_2 nanopowder: the particles' agglomerates are present in all dimensions and create hillocks on the surface, hence disturbing the homogeneity of the silane film. The presence of agglomerates was also observed in the coating solution through dynamic light scattering measurements (not shown here): the data highlighted the presence of large agglomerates (up to a few hundred nanometers), which are then clearly observed in the cured coatings.

This issue has been acknowledged but not emphasized in previous work because these agglomerates are smaller than was thickness of the layers under study (as referred to in the introduction), but it represents a considerable challenge in the present work because of the thin nature of the film. The problem has been overcome by adding CeO_2 to the BTSE in the form of water nano-suspension. CPS (Centrifuge Particle Size) measurements in Figure 31 show a comparison of the size distribution between a solution prepared from dry nanoparticles and one prepared with the nano-suspension: in the latter, the particles size is much smaller, with an average of about 25 nm, and with less than 30% of the particles above 50 nm. The film prepared with the nano-suspension is shown in the FE-SEM micrographs of Figure 24 (cross section) and of Figure 32 (top view): no particles agglomerates can be observed in the silane coating, which looks homogeneous. The white spots in Figure 32 represent

some of CeO_2 nanoparticles and their sizes are in agreement with the CPS measurements.

A comparison of the samples prepared using the dry nanopowder and the nano-suspension can be done by looking at the two top-view FE-SEM micrographs (backscattered electrons) in Figure 33 (a) and (b). The image in (a) reveals white spots (CeO_2 particles) of a few hundred nanometers, while the white spots in (b) appear to be smaller, in agreement with the above results. The top view of the film with nano-dispersed CeO_2 (Figure 33(b)) also highlights the challenge of working with nano-dispersed particles, which are not easily detectable at this magnification.

A proof of the presence of CeO_2 particles in the samples has been obtained by chemical analysis through FE-SEM/EDX. These tests (not shown here) could only be performed on the wider particles because of the instrument limitation and the nano-size nature of the individual particles. The nanoparticles, though, could be successfully analyzed by TEM-EDX measurements, with a higher lateral resolution. EDX spectra were collected on some of the nanostructures pointed in the TEM image (Figure 34). Only one of the collected spectra is reported here (Figure 34) and it shows the peaks corresponding to the binding energy of Ce, evidencing the presence of Ce-rich particles in the layer. Similar results were obtained from the TEM-EDX analysis performed on the other particles. The Cu-peaks around 7 keV are coming from the interior of the TEM and cannot be used to identify Cu in the sample. The inside of the TEM is in fact built with electromagnetic lenses made of Cu windings.

Another proof of the presence of Ce in the BTSE coating prepared with the CeO_2 nano-suspension is obtained through wide scans and Auger mappings performed with the FE-AES equipment. The only possibility of detecting Ce, though, was in the presence of an agglomerate of particles (Figure 35(a), circled area). The peak corresponding to Ce (671 eV, circle in Figure 35(b)) was visible only after about 9 nm of material was sputtered out from the surface, while no cerium was detected in the wide scans of the samples "as introduced", that is before sputtering with argon ions to remove the superficial layers. An Auger mapping of the entire area in Figure 35(a) was also performed and it revealed the presence of Ce (Figure 36(a)) and O (Figure 36(b)) after the same sputtering time. These data also give information on the structure of the coating, revealing that the CeO_2 particles, even when forming an agglomeration, are always covered by a thin BTSE layer. This implies that the CeO_2 is well embedded in the silane matrix, resulting in a compact structure, which could be responsible for the increased barrier properties, as resulted in the EIS analysis reported below.
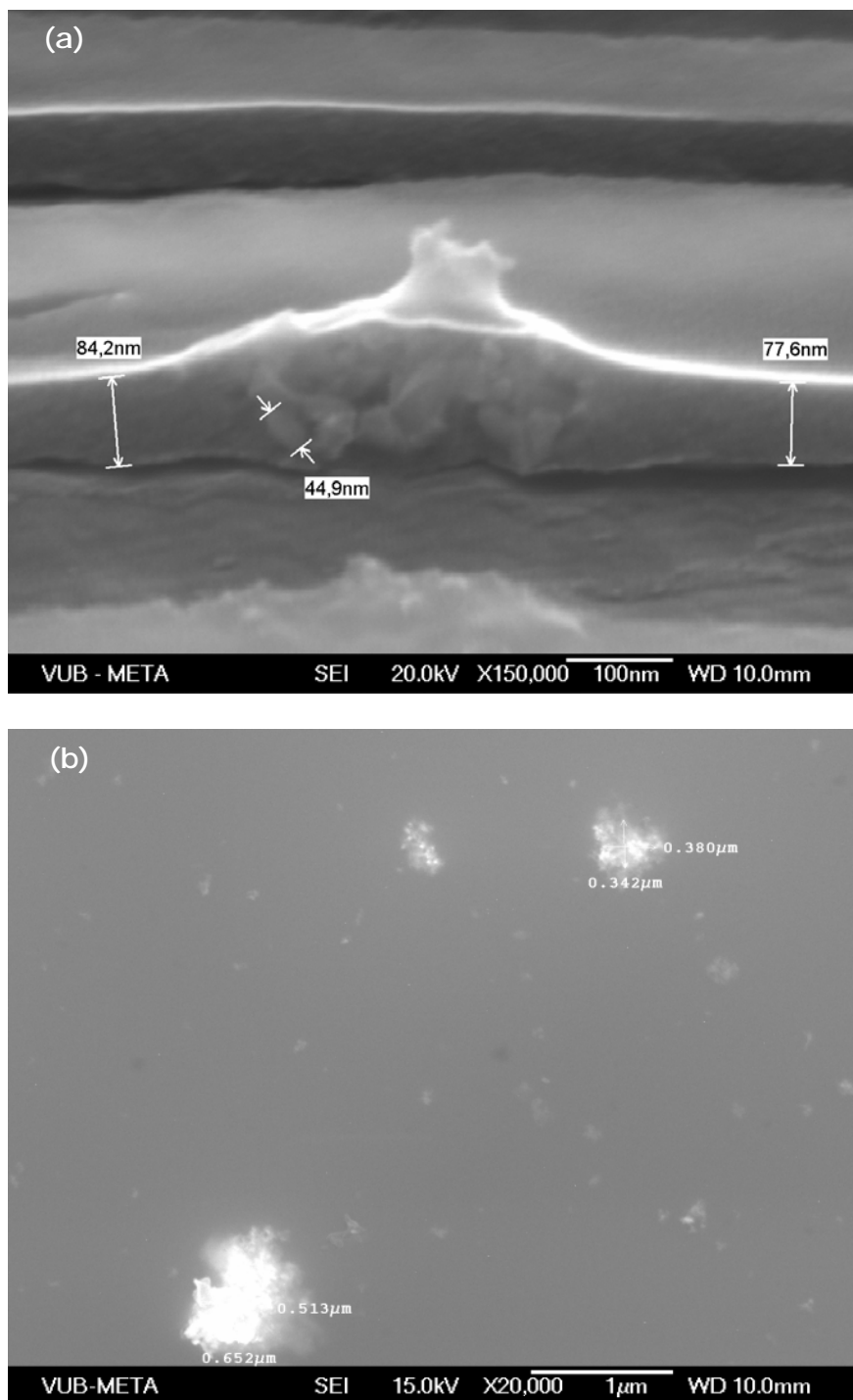
Figure 30 - FE-SEM micrographs of Al 99.99% electropolished and dip-coated with BTSE 5% + 250 ppm CeO₂ (as dry nanopowder): (a) cross section, (b) top view.
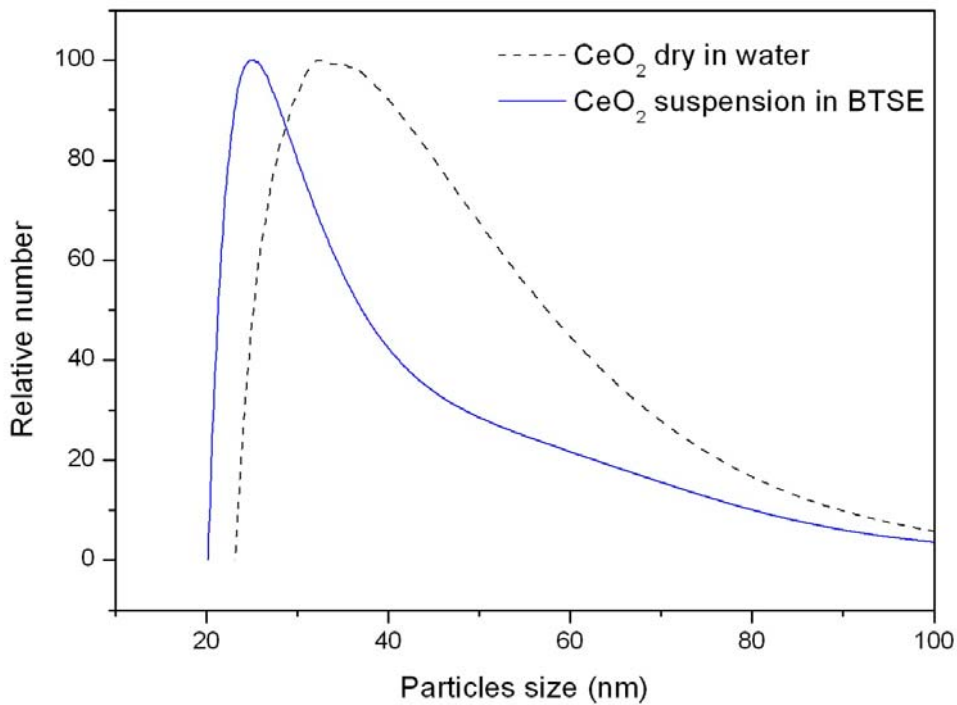
Figure 31 - Particle size distribution (CPS) of two solutions prepared with CeO₂ nano-suspension provided by Umicore and with CeO₂ nanopowder.
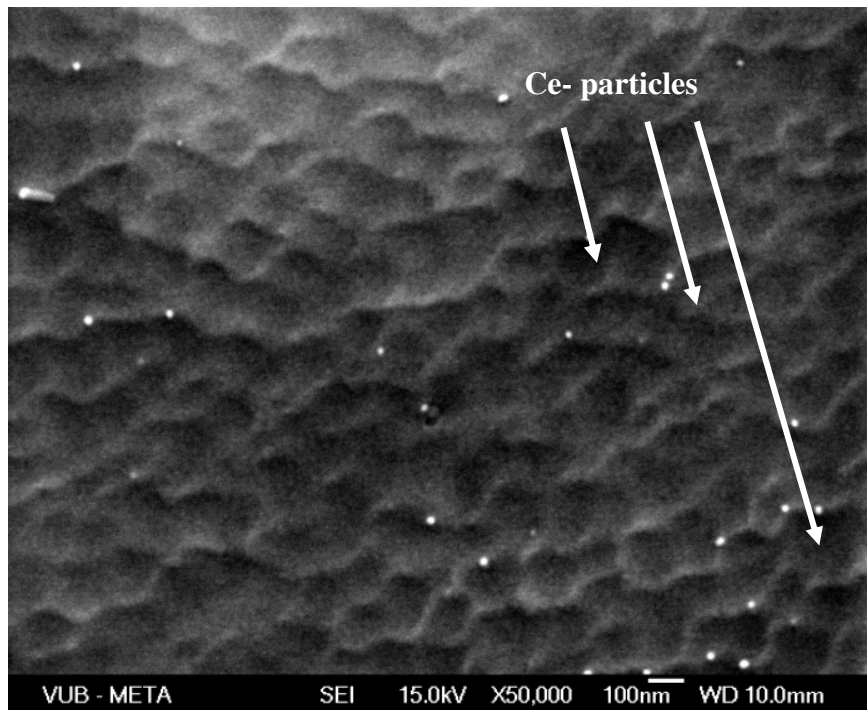
Figure 32 - FE-SEM micrograph (top view) of Al 99.99% electropolished and dip-coated with BTSE 5% + 250 ppm CeO₂ (as nano-suspension). The arrows show some of the nano-dispersed CeO₂ in the coating.
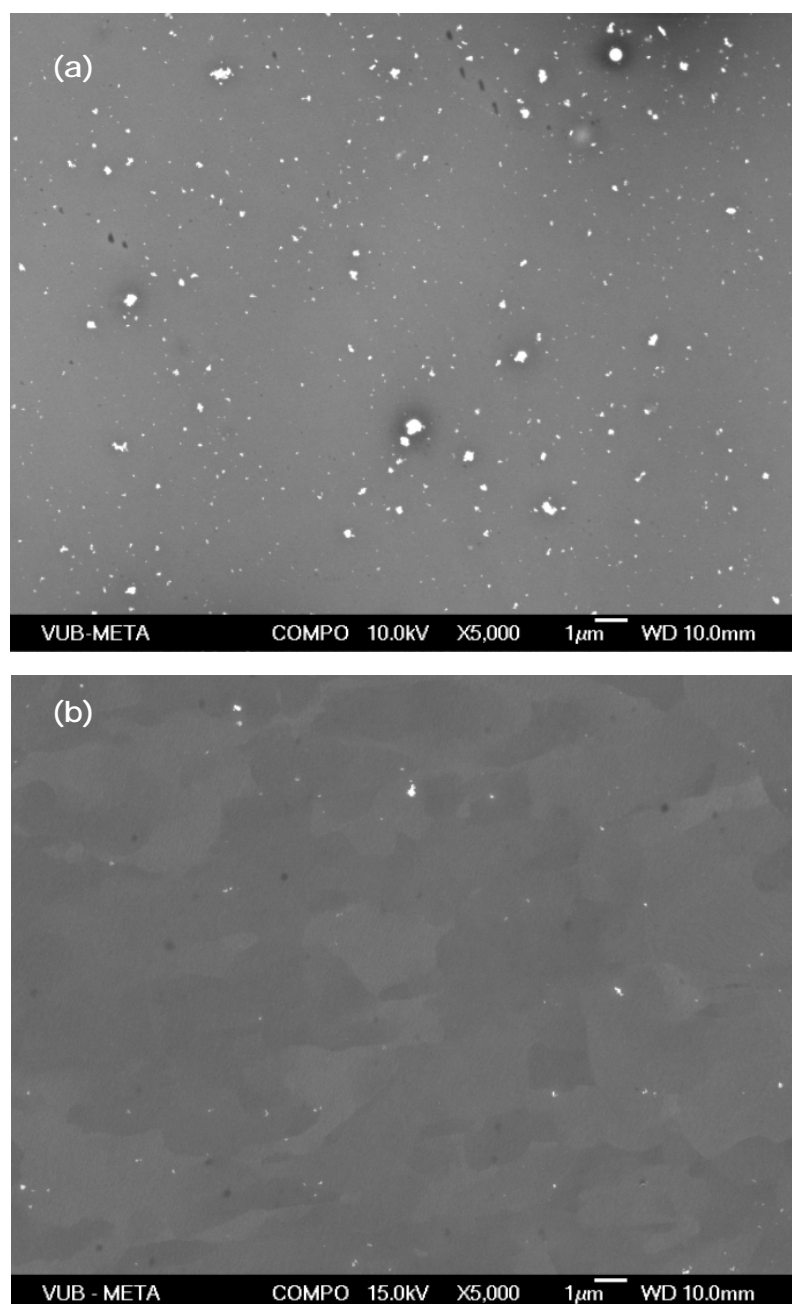
Figure 33 - FE-SEM micrographs (backscattered electron image) of BTSE 5% films with inclusion of CeO$_2$ nanoparticles, as (a) dry nanopowder and as (b) nano-suspension.
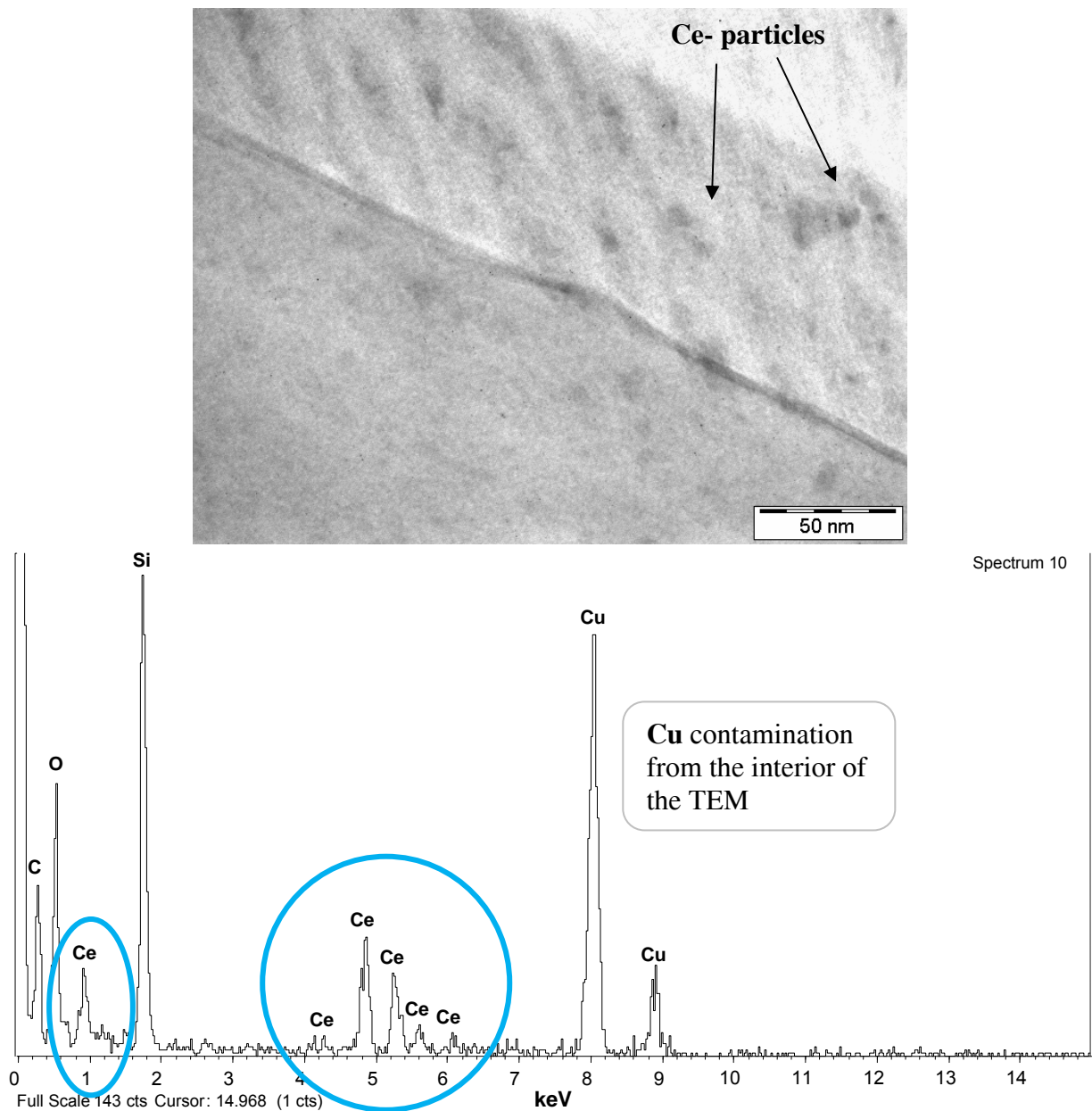
Figure 34 - Above: TEM image of a sample prepared by FIB (Al 99.99% substrate coated with BTSE 8% with inclusion of CeO$_2$ nanoparticles, added as nano-suspension). Below: TEM-EDX spectrum performed on one of the Ce particles indicated by arrow in the image above.
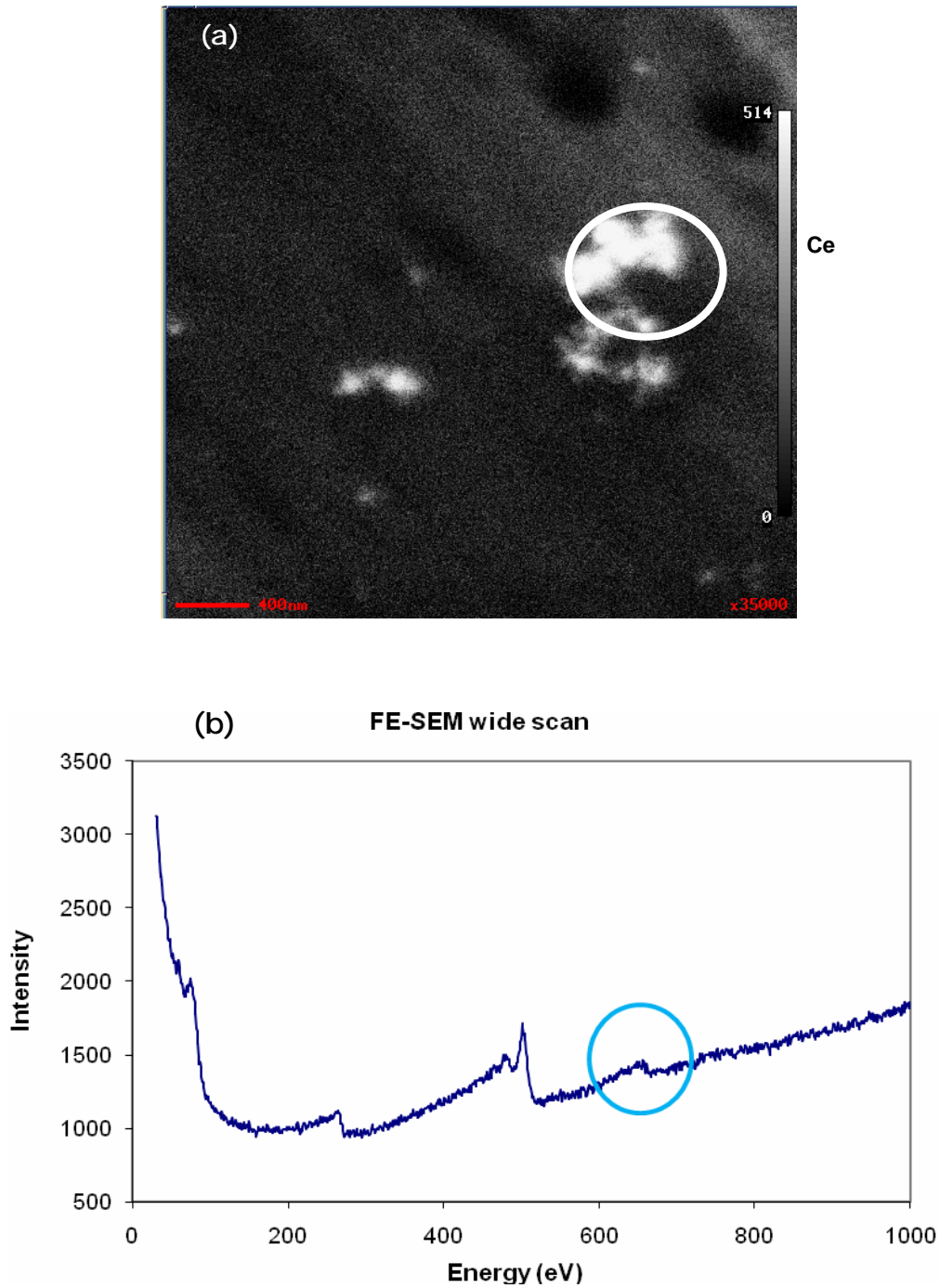
Figure 35 - SEM picture (a) and FE-AES wide scan (b) performed on an Al 99.99% substrate coated with BTSE 5% and CeO₂. The wide scan is performed on the white agglomeration circled in part (a), after a sputtering time equivalent to about 9 nm of materials removed.
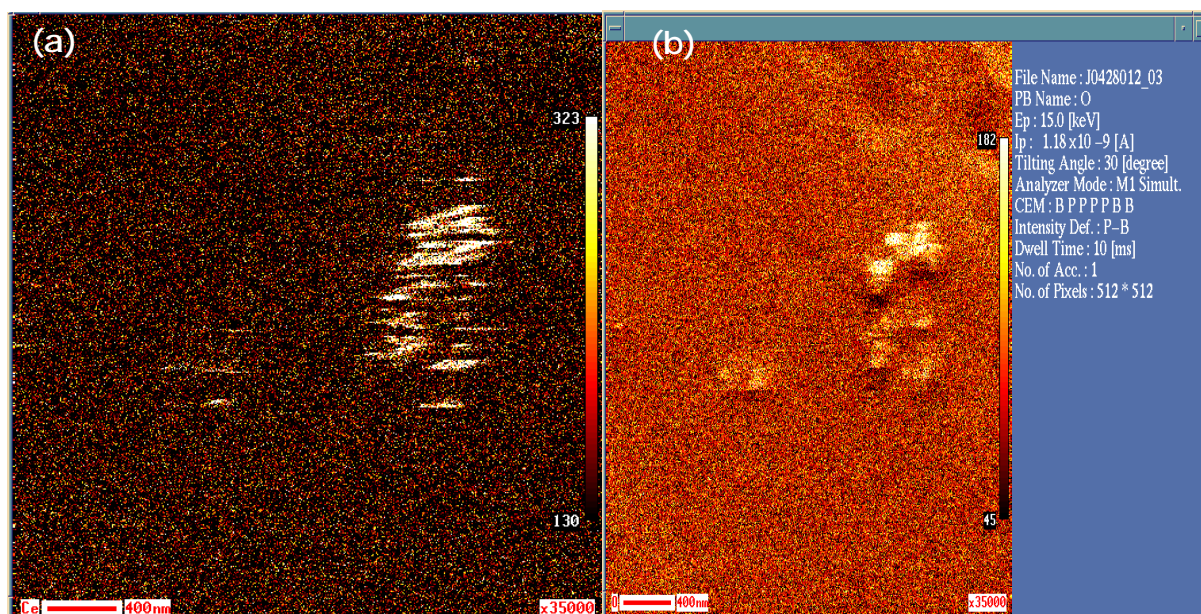
Figure 36 - *Auger mapping of the area shown in Figure 35(a) of an Al 99.99% substrate coated with BTSE 5% and CeO$_2$ after a sputtering time equivalent to about 9 nm of materials removed. (a) and (b) represents respectively the mapping for Ce and O.*

Barrier and corrosion properties of the coatings

The main aim of the Electrochemical Impedance Spectroscopy (EIS) measurements in the present work was to check how the barrier properties of the silane films varied with the presence and distribution of the CeO$_2$ nanoparticles. The EIS analysis was performed in Na$_2$SO$_4$ in order to characterize the silane layers and avoid pitting of the metallic substrate.

The attention was focused on the medium frequency range of the EIS diagrams. De Graeve et al. [1] showed that EIS measurements on a bare aluminium substrate present only one relaxation (clearly visible in the Bode phase angle diagram) attributed to its native oxide layer. The presence of a cured silane film on the sample results in an extra relaxation in the medium-high frequency domain, which can be attributed to the densification of the layer, well shown through IR-SE data. A study of EIS response with the variation of curing temperature showed a progressive increase of the impedance modulus and phase shift for the high frequency relaxation with increasing crosslinking. This resulted in an increase of the layer impedance in proportion to its decrease in permeability, hence indicating the progressive improvement of the silane barrier properties. A similar investigation was performed by Van Schaftinghen et al. [67] to determine the effect of the molecular structure and curing of silane monomers on the barrier properties of the formed silane film. Spectroscopic Ellipsometry measurements showed the variation of thickness and chemical state (crosslinking) of the different silane products, which resulted in different EIS spectra in the intermediate frequency range.

Figure 37 shows the Bode diagram (impedance modulus and phase angle) of the bare substrate, of the substrate coated with BTSE (8%) only and with BTSE (8%) and of CeO_2, added as nano-suspension. As reported in literature [1, 24, 42, 67-70], the variation of impedance in the middle frequency range region, as clearly shown in the phase angle plot, can be directly linked to the barrier properties of the samples. The comparison of the three sets of curves in Figure 37 shows that the presence of a silane coating on the aluminium increases the barrier properties of the blank substrate, as evidenced by the presence of an extra relaxation in the Bode diagram of the coated samples. The impedance response of the BTSE coating is further enhanced by the addition of CeO_2 in the silane matrix.

While the results are well reproducible at medium to high frequencies (as checked by the authors with further experiments, not reported here), the curves show an unusual behaviour at low frequencies, where a consistent trend cannot be observed. This behaviour could be attributed to the characteristics of the substrate (pure Al) in contact with the electrolyte (Na_2SO_4) [71]; hence the analysis of the present data has been limited to the medium to high frequency range, where the properties of the silane layer can be observed. Further investigation of the impedance behaviour of Al 99.99% at lower frequencies is being performed by the authors, and it will be the object of a future paper. In addition, further work is being performed on AA 2024, to better study the corrosion mechanisms. Pure Al has been used in the present work because of the requirements for a thorough characterization of the surface properties of the substrate and the thin layer.

Figure 38 shows a comparison between the Bode plots of the silane film prepared with CeO_2 nanopowder (with agglomerates) and of the one prepared with CeO_2 nano-suspension (homogeneous film), after 2 hr immersion in Na_2SO_4. For completeness, the EIS data of a film with silane only and of the bare substrate are also shown in the plot. The curves show a plateau at high frequencies, which is characteristic of the electrolyte resistance; at low frequencies the behaviour of the Al in contact with the Na_2SO_4 is observed, as stated above; while the relaxation at medium to high frequencies is characteristic of the properties of the silane film. The data show that the best barrier is achieved with the sample with nano-dispersed CeO_2 as opposed to the one with agglomerated particles, and this is clearly shown in the modulus and phase angle diagrams (Figure 38), with a higher impedance modulus and a more pronounced relaxation. The thin nature of the films (about 67 nm for the curves shown in Figure 38) is a limiting factor for the barrier properties of the system and accounts for the small difference in impedance modulus between the three samples. Nevertheless the curves show that the electric properties of the BTSE coating are modified by the addition of CeO_2, independently of the formation of agglomerates in the film. This is probably due to the fact that even though the agglomerates might form hillocks on the film surface (Figure 30), the outmost layer is always covered by a

uniform BTSE film, as shown by the FE-AES analysis above. Hence the CeO_2 nanoparticles can be considered effective fillers of silane coatings, in agreement with the results of other authors [3-5, 12, 62]. These results are also in line with the XPS results, which show how the electronic structure of BTSE is modified by the addition CeO_2 and point at the possible presence of a bond between the two compounds.

A study of the impedance response of the film with agglomerated nanoparticles as a function of immersion time (Figure 39) shows a clear decrease of the barrier properties after 2 days, which is not observed in the sample with nano-dispersed particles (Figure 40). This is clearly visible in the Bode phase plot (Figure 39), where the relaxation attributed to the silane layer tends to disappear after two days, probably due to preferential paths created in the organic film by the agglomerates.

In conclusion, the EIS measurements show that the barrier properties of silane are modified by the presence of CeO_2 nanoparticles, and an enhancement of the properties is observed in the samples with nano-suspended particles. These layers appear uniform (Figure 24) and free from large agglomerates which might create cracks in the silane structure, resulting in preferential pathways for the penetration of aggressive species to the coating/substrate interface.

The dip-coated BTSE layers, with or without the addition of CeO_2 nanoparticles, were also investigated in terms of corrosion properties. For this purpose, the films were deposited on AA2024-T3 substrate and immersed in 0.5 M NaCl. EIS measurements were performed as a function of time.

Figure 41 shows the Bode diagram of the samples at immersion in NaCl. Scattering of data at low frequencies is due to the presence of pitting on the substrate as in the NaCl impedance data related to system 1. All the coated samples show a barrier behavior compared to the blank, as is clear from the higher impedance modulus and the shape of the phase shift. A sample coated with BTSE and Ce^{3+} (added as $Ce(NO_3)_3$) was also investigated to check if the presence of the additive would add extra corrosion protection (Ce^{3+} is a known corrosion inhibitor [3, 4, 10, 14, 15]).

These results, again, confirm how the very thin nature of these coatings does not allow a thorough investigation of the corrosion properties of the samples. The small thickness of the coating, in fact, is the main responsible of the poor corrosion behavior of the samples, over the specific coating composition and/or the presence of additives.

All samples, in fact, are subject to pitting, independently on the presence of additives in the film, as is clearly shown in Figure 42, which represents the Bode plot of the same samples after 1 day immersion in NaCl. Even though the coated samples still show a higher impedance than the blank (samples have same thickness and same dielectric characteristics), the shape of the curves show the absence of a barrier film.
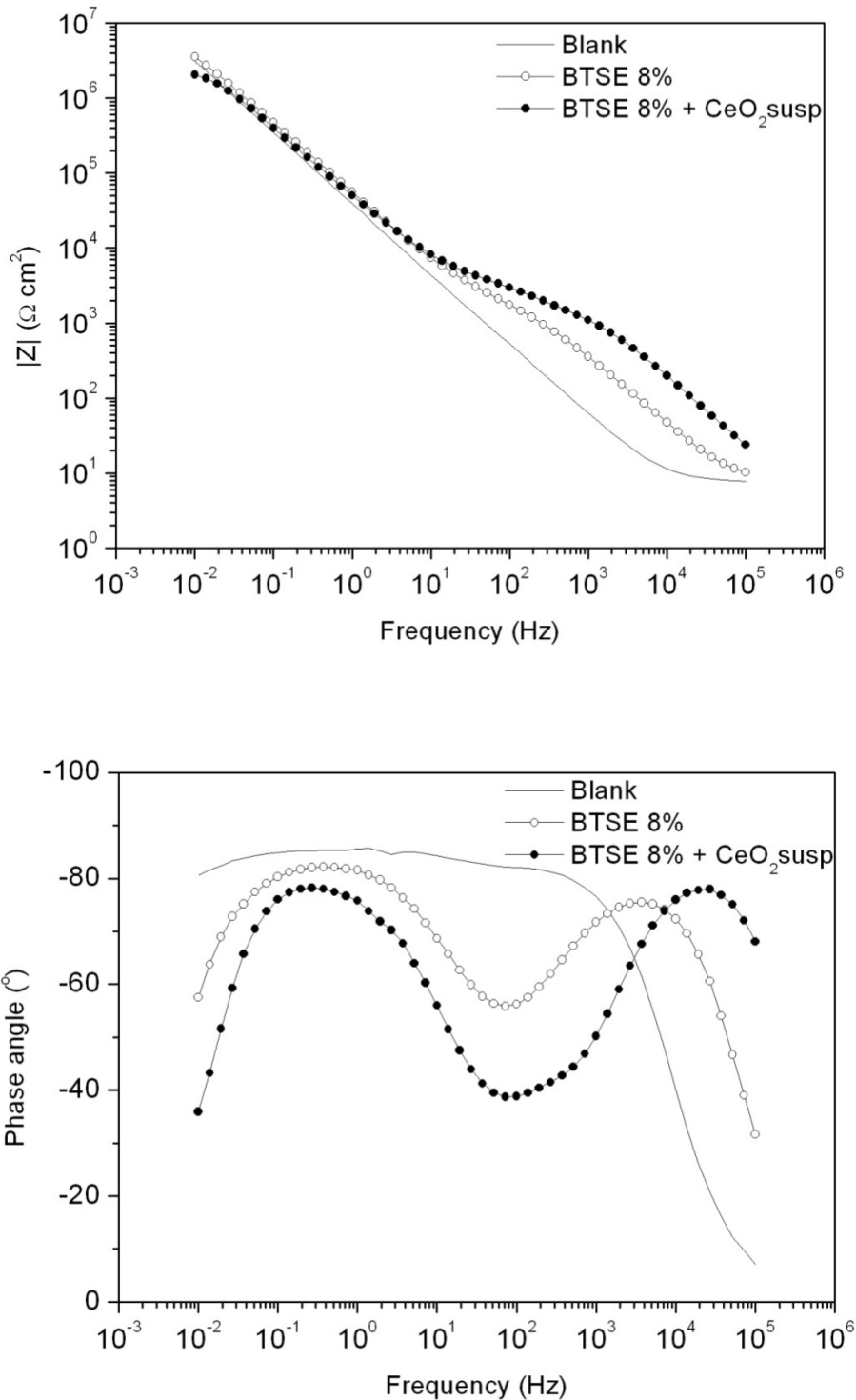
Figure 37 - Bode diagram of an alkaline pre-treated blank Al 99.99%; the same substrate coated with BTSE 7.5%; and with BTSE 7.5% + 250 ppm CeO₂ (as nano-suspension), after 24h immersion in Na₂SO₄.
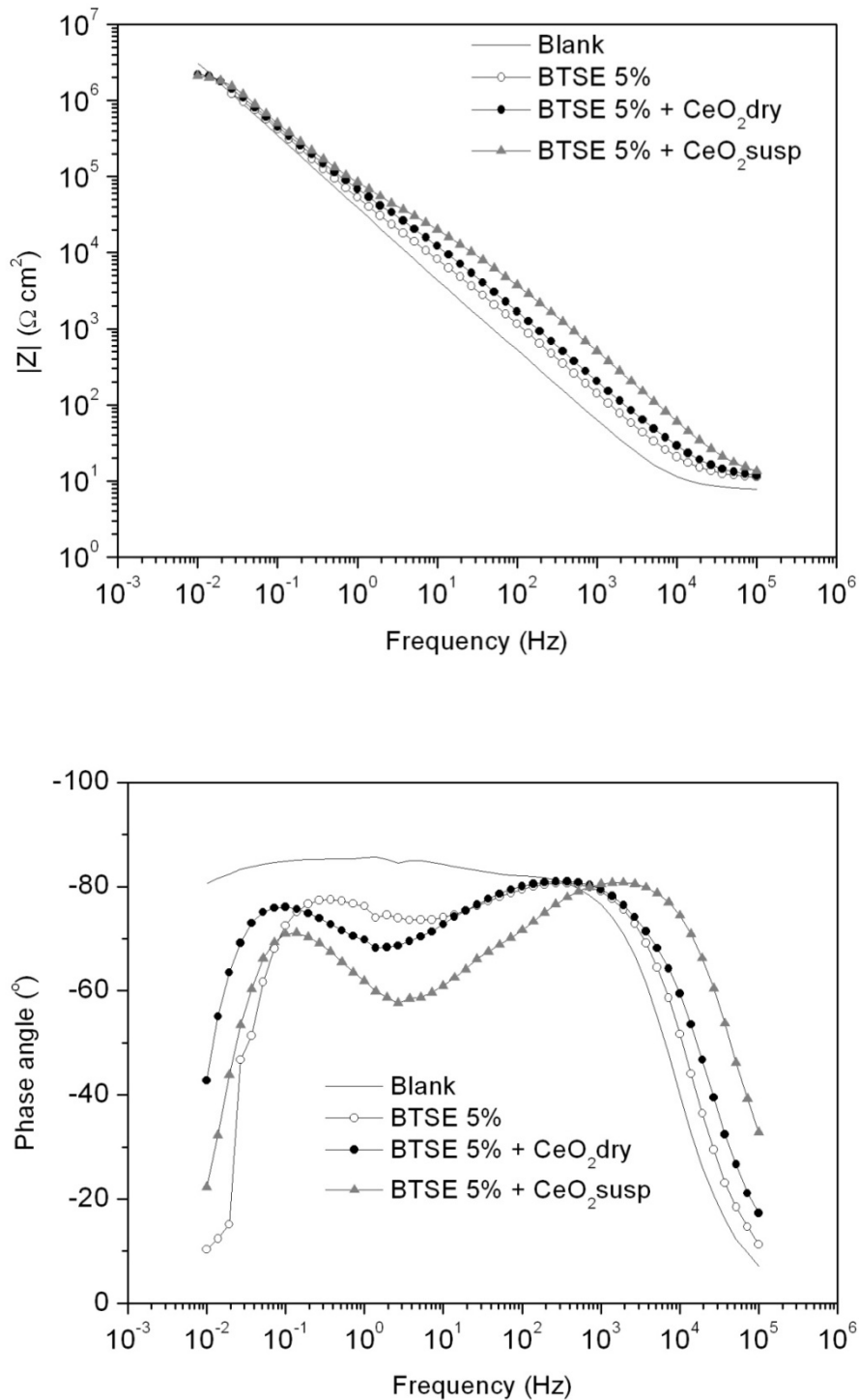
Figure 38 - Bode diagram of an alkaline pre-treated blank Al 99.99%; the same substrate coated with BTSE 5% and the same coating with addition of 250 ppm CeO$_2$ (dry or suspension), after 2h immersion in Na$_2$SO$_4$.
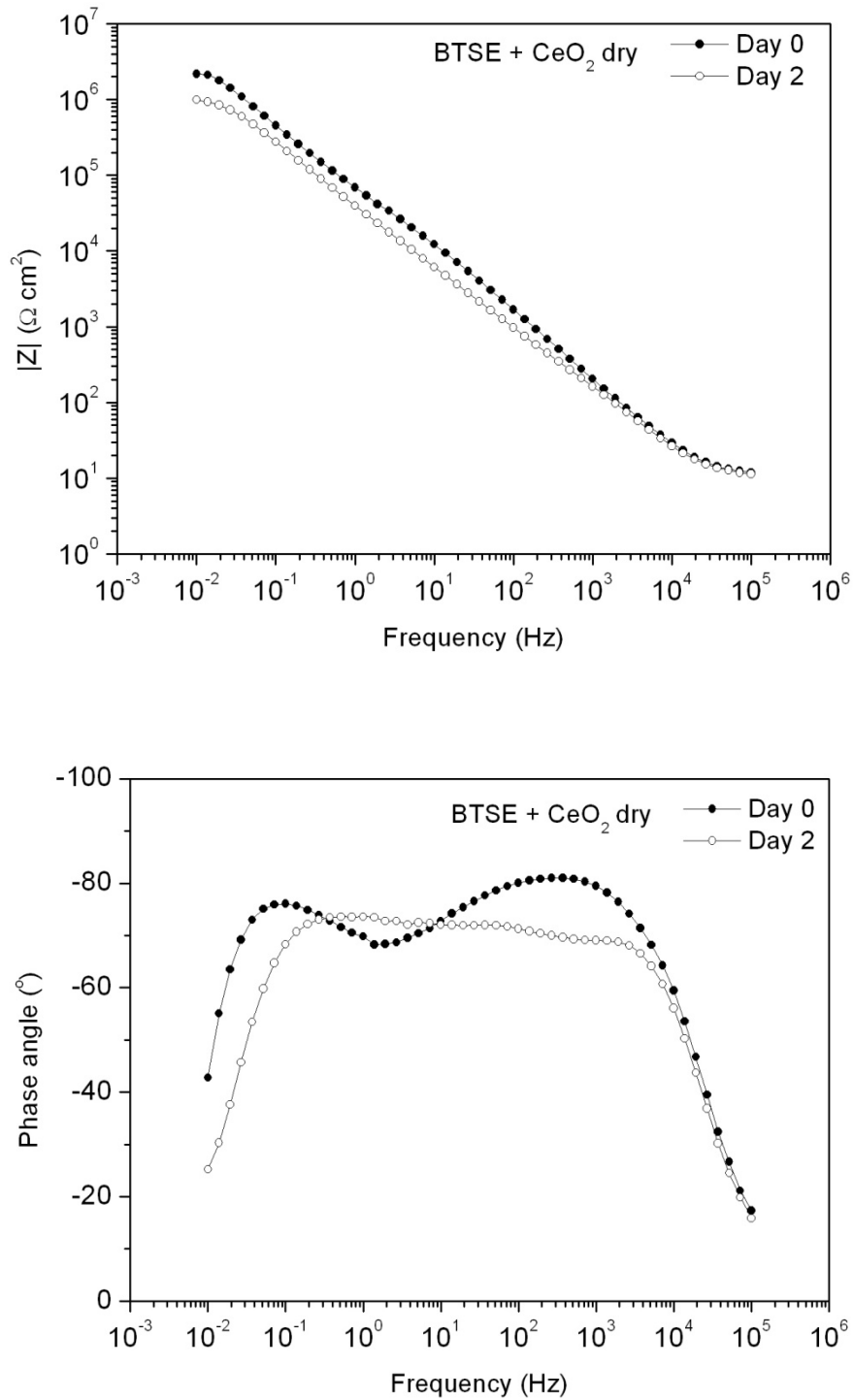
Figure 39 - Bode diagram of an alkaline pre-treated blank Al 99.99% coated with BTSE 5% (as nanoparticles) as a function of immersion time in Na₂SO₄.
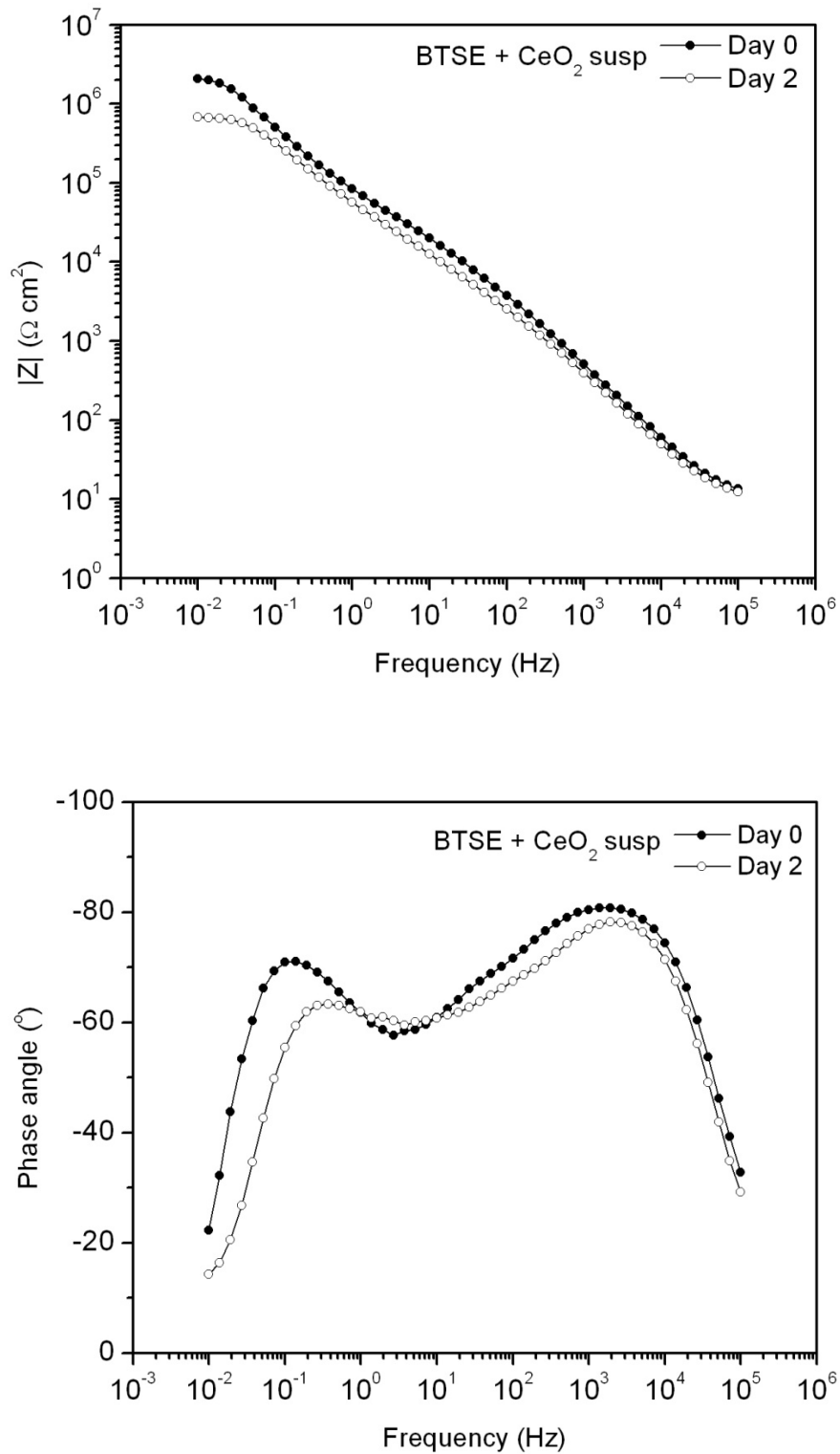
Figure 40 - Bode diagram of an alkaline pre-treated blank Al 99.99% coated with BTSE 5% (as nano-suspension) as a function of immersion time in Na$_2$SO$_4$.
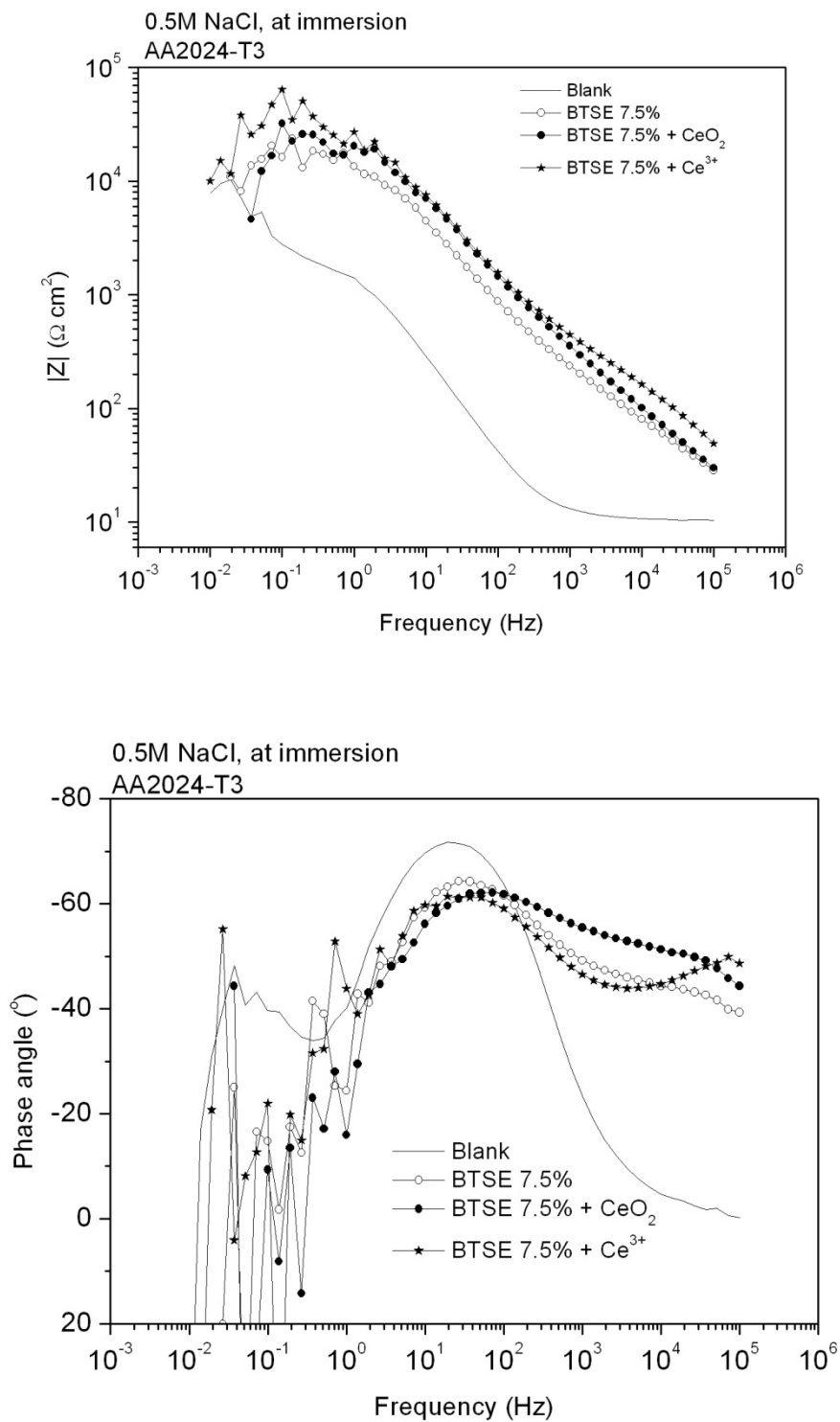
Figure 41 - Bode diagram of an alkaline pre-treated blank AA2024-T3, and the same substrate dip-coated with BTSE 7.5%; with BTSE 7.5% + 250 ppm CeO₂ (as nano-suspension) and with BTSE 7.5% + 250 ppm Ce³⁺, at immersion in NaCl.
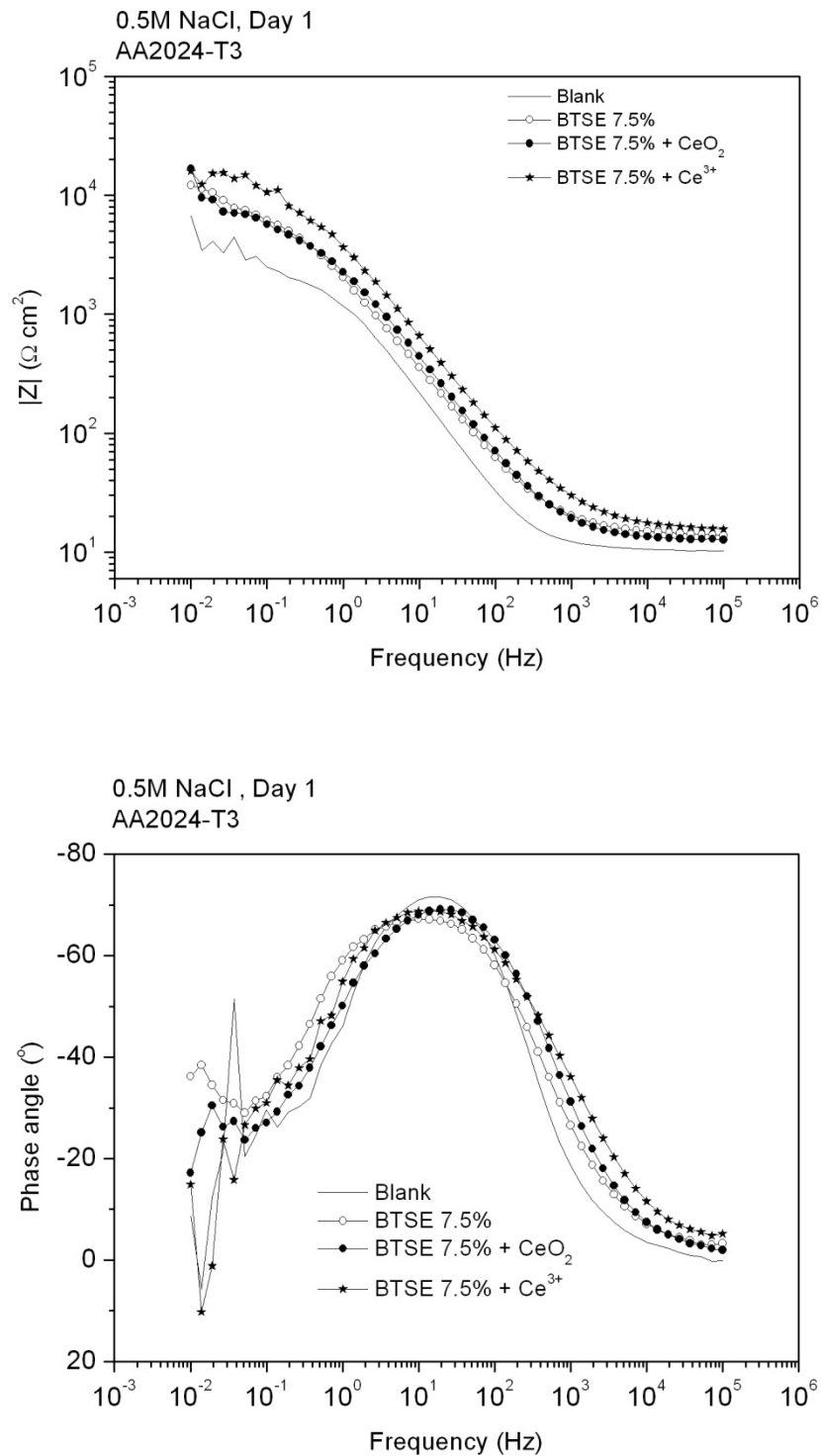
Figure 42 - Bode diagram of an alkaline pre-treated blank AA2024-T3, and the same substrate dip-coated with BTSE 7.5%; with BTSE 7.5% + 250 ppm CeO₂ (as nano-suspension) and with BTSE 7.5% + 250 ppm Ce³⁺, after 1 day immersion in NaCl.

Applied Properties

Dip-coated BTSE

Pull-off test and scanning electron microsocpy

The adherence of the dip-coated films was evaluated by pull-off tests. To perform this test the treated aluminium (Aludan AA H5005-H24 was used for this purpose) substrates were glued on thick steel plates. Afterward, a plot was glued on the free face of the treated aluminium substrates and a cut through the coating to the substrate was made around the plot (Figure 43). The force necessary to detach or to rupture the coating in a direction perpendicular to the substrate was then measured with an Instron equipment according to the ISO 4624 standard.
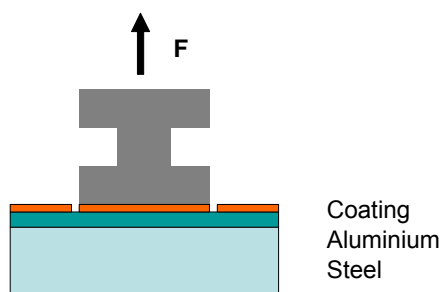
Figure 43 - Pull-off test.

The measured tensile stresses vary between 1 and 6 MPa. The reproducibility of the measurements was low due to heterogeneity of the coatings. The influence of the composition of the treatment on its adherence could not be determined at this stage.

The surface of the plot and the surface of the coated aluminium substrate were analysed by scanning electron microscopy (SEM) after the pull-off test to determine if the rupture is cohesive (in the coating thickness) or adhesive (at the interface coating-substrate).

System 1 (BTSE only, T0), or a mixture of silane and cerium, with or without the Ce^{3+} ions (system 3, T1 and T2) were detected on both surfaces (Figure 44 and Figure 45). Areas containing no Si and no Ce were also observed at the surface of the treated aluminium substrate after the pull-off test. These results suggest that both kinds of rupture occur.

Therefore, the tensile stress required to detach the plot is a measure of the coating adherence and of the coating cohesion.
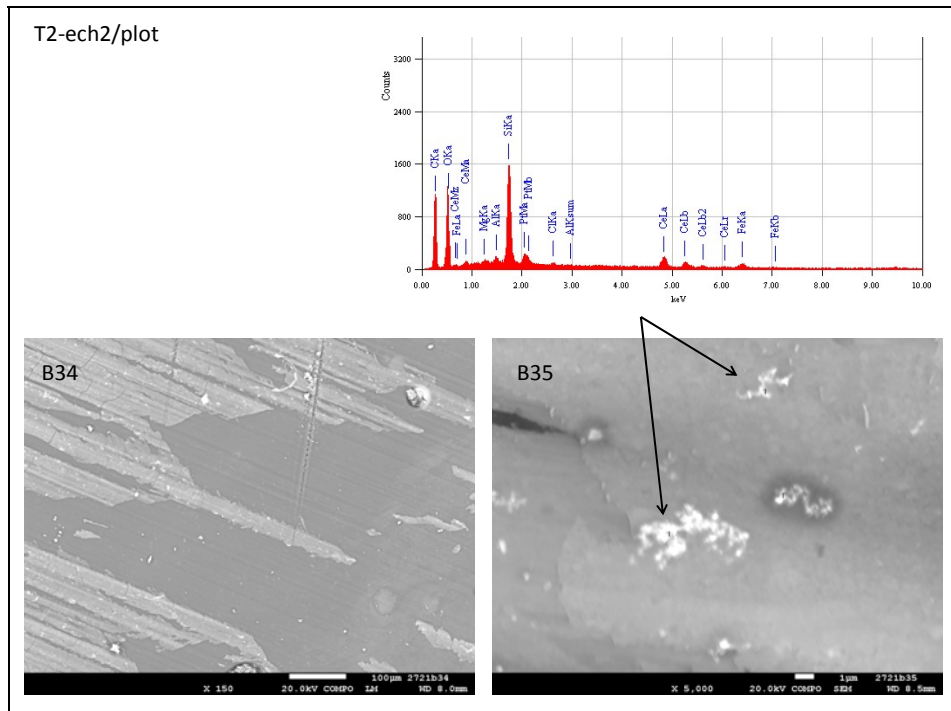
Figure 44 - SEM picture of the plot after the pull off test and EDX analysis (treatment 2).
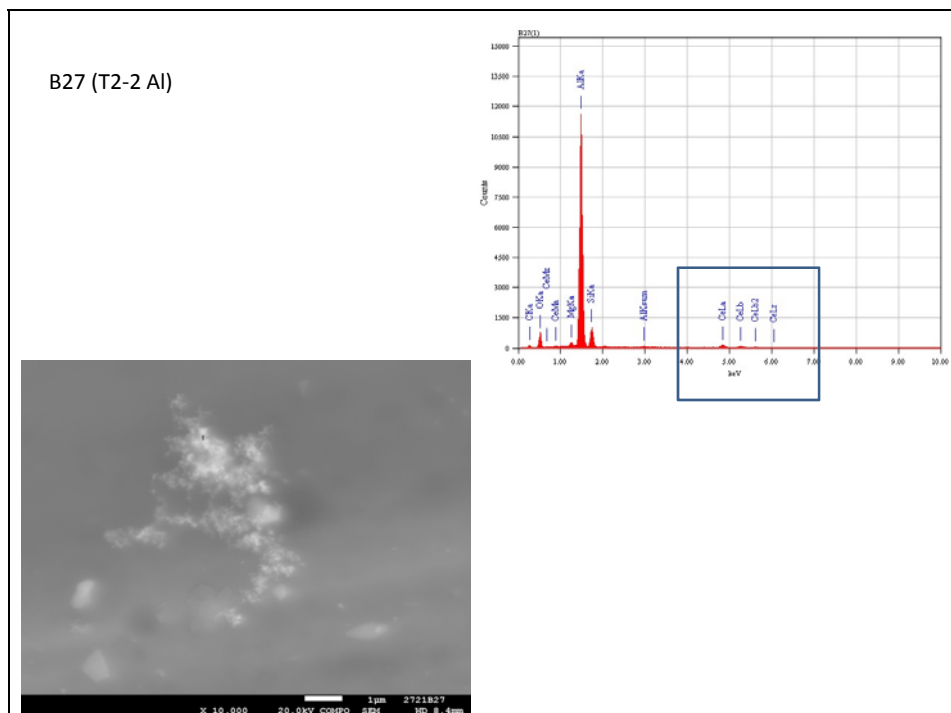
Figure 45 - SEM picture of the Al substrate after the pull off test and EDX analysis (treatment 2).

Acetic salt spray

Treated Al (AA2024-T3) substrates were scratched and exposed to salt spray. Figure 46 shows the surfaces of the panels after an exposure of 24h. The comparison of the bare Al surface with that of the treated samples show the protective properties of the treatments. However, due to the low thickness of the deposited silane, this protective effect doesn't last for a long time and corrosion is already observed after 24h.
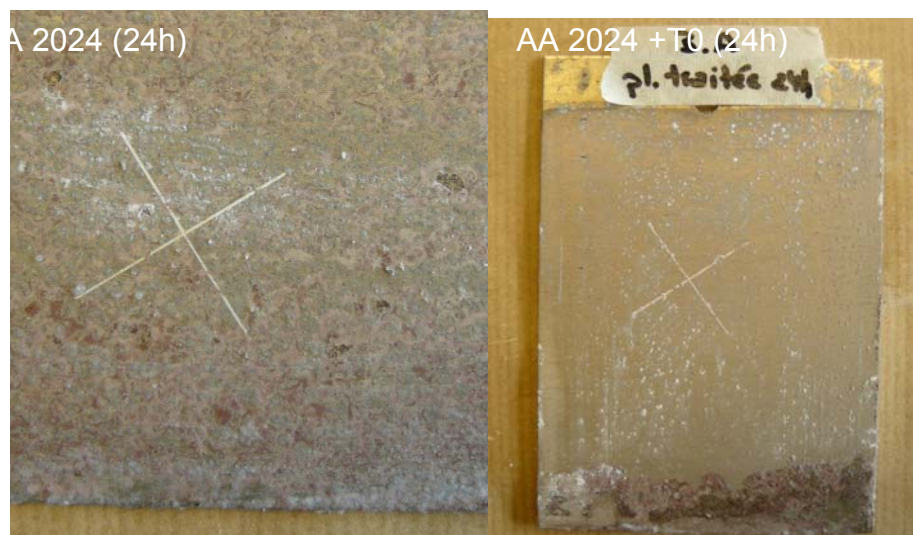
Figure 46 - Surfaces of Al and Al+T0 after exposure to acetic salt spray for 24h.

<u>Treatments by plasma</u>

Pull-off tests were performed on BTSE (system 1) and on HMDSO (system 2) deposited on Al 99.99% by vacuum or by atmospheric plasma in presence or in absence of oxygen. The measured tensile stresses are noted in Table 9.

The highest stresses were measured for P_{atm} BSTE. It can be assumed that the adherence of this treatment on the substrate is the most important even if the nature of the rupture (adhesive or cohesive) has not been checked. These values are high.

The influence of the deposition method of BTSE (plasma/dipcoating) on the adherence of the silane on Al could not be determined from the pull-off measurments since BTSE was deposited on different substrates: Aludan AA H5005-H24 for BTSE deposited by dipcoating and Al 99.99% for BSTE deposited by plasma.

Treatment	Tensile stress at maximum charge (MPa)			
P_{atm} BTSE	7.1	8.7	8.7	7.3
P_{atm} HMDSO/O_2	0.7	1	1.6	
Vacuum HDMSO	0.7	1.4	0.7	0.3
Vacuum HMDSO/O_2	0.4	1.5	0.9	

Table 9 - Tensile stresses measured on treatments deposited by plasma on Al 99.99%.

Treatment covered by a paint

Four paints were applied on treated and on nude aluminum:

o Commercial waterborne adhesion primer, for interior or exterior use, based on acrylic resin dispersed in water. It can be applied on stainless steel, new galvanized steel, aluminum, copper, zinc, ... (application: dry thickness ~30 µm - drying: 1 month at 50% RH and 21°C);

o SPF650: 100% UV-curable paint for metal protection (application: dry thickness ~20 µm - curing: 2 passes under a UV lamp (Hg) at 7 m/min (3901 mJ/cm^2));

o P91PI94B : water-based UV curable paint (application: dry thickness: ~20 µm - drying : 10 min at AT and 5 min at 50°C - two passes under a UV lamp (Ga) followed by two passes under another UV lamp (Hg) at 7 m/min (6156 +3901 mJ/cm^2));

o PE52 : polyester powder paint (application: dry thickness: > 60 µm - curing: 10 min at 180°C).

The selected treatments were those deposited by dip coating: T0 (BTSE 7.5%), T1 (BTSE 7.5% + 250 ppm CeO_2) and T2 (BTSE 7.5% + 250 ppm CeO_2 + 250 ppm $Ce(NO_3)_3$).The powder paint PE52 was also applied on AA 2024 treated with Eskaphor H 4070. This Cr-free treatment is applied industrially on Al and was considered as a reference.

Two kinds of aluminum were used: Aludan AA H5005-H24 (thin and flexible) and AA 2024-T3 (thicker but similar to the substrate used by the other partners). Aludan was especially used for the flexibility measurements.

Mechanical properties

The tested properties were adherence (cross-cut test (ISO 2409) and pull-off test), flexibility (Erichsen ISO 1520) and resistance to methyl-ethyl-ketone (ASTM D5402). This last test was used to check the curing of UV paints. Results are listed in Table 10.

The cross-cut and the pull-off test results show that the adherence of the water-based paint on Aludan is improved by the silane treatment. The rupture is adhesive in absence of any treatment and essentially cohesive when the substrate has been treated with T2 (Figure 47). BTSE treatments tends to decrease the adherence of this paint on Al 2024.

The adherence of photocurable and of powder paints, measured with the cross-cut test, is not improved by the presence of silane. In the case of the powder paint, a strong detrimental effect of BTSE on adherence was even observed. Therefore, the pull-off tests were not performed on these systems.

To improve the adherence of the UV paints, a silane functionalized with methacrylate group (Figure 48) (Dynasilan MEMO - Evonik) was deposited on treatment 2 from an alcoholic solution (drying at 20°C and then at 100°C during 30 min) [72]. The UV irradiation of the paint induces the radical polymerization of the acrylates used to formulate the paint with the methacrylate functions present at the surface of the MEMO treatment. The formation of covalent bonds between the paint and the treatment increases drastically the adherence of SPF 650 on treated Al and a cross-cut result of 0 (0: good - 5: bad) was obtained. Pull-off tests confirmed these results.

System (treatment)	Paint	Cross-cut (5: bad - 0: good)		Pull-off test (tensile stress (MPa))	Pull off test (nature of the rupture)
		Aludan AA H5005-H24	Al 2024	Aludan AA H5005-H24	
-	water-based	3	0	1,1 ± 0,77	~ 90% adhesive - ~ 10 % cohesive
system 1 (T0)	water-based	1	1	8,9 ± 1,3	~ 90% adhesive - ~ 10 % cohesive
system 3 (T1)	water-based	1	2	4,7 + 0,1	~ 60% adhesive - ~ 40 % cohesive
system 3 (T2)	water-based	1	1	8 ± 0,6	~ 10% adhesive - ~ 90 % cohesive
-	UV paint	0	5		
system 1 (T0)	UV paint	5	5		
system 3 (T1)	UV paint	5	5		
system 3 (T2)	UV paint	4	4		
system 3 (T2)	UV paint	4	4	3,2 ± 0,5	100 % adhesive
T2 + MEMO	UV paint	0	0	8,3 ± 4,3	adhesive - cohesive
-	UV-water-based	4	3		
system 1 (T0)	UV-water-based	3	5		
system 3 (T1)	UV-water-based	5	5		
system 3 (T2)	UV-water-based	5	5		
-	powder paint		0		
Eskaphor H 4070	powder paint		0		
system 1 (T0)	powder paint		5		
system 3 (T1)	powder paint		5		
system 3 (T2)	powder paint		3		

Table 10 - Mechanical properties of the coated panels.
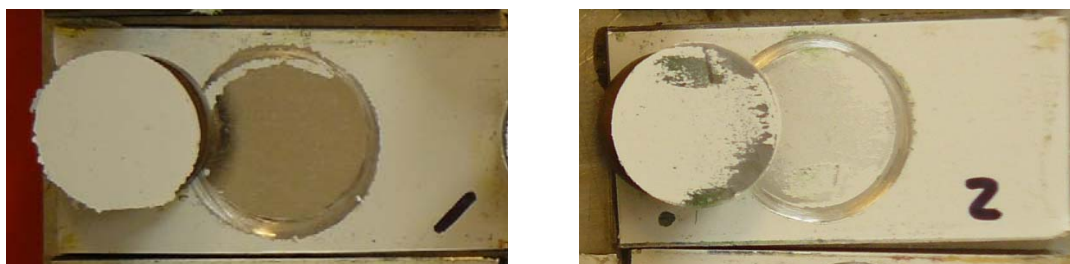
Figure 47 - Surfaces of aludan/no treatment/water-based paint (left) and aludan/T2/ water-based paint (right) after the pull-off test.

Figure 48 - 3-methacryloxypropyl trimethoxysilane.

Resistance to acetic salt spray

Coated panels were exposed to acetic salt spray (5% wt NaCl – CH_3COOH). Three coated panels of each system were exposed and observed after 24, 48h and 7d (Figure 49).

T2 improves very slightly the resistance to salt spray of the water-based paint, of SPF650 and of P91PI34B (Figures 49 (a) to (f)). The resistance of the powder paint is also improved by T2 (comparison of nude Al2024/powder paint and Al2024/T2/powder paint - Figures 49 (g) and (h). However, the resistance to acetic salt spray of the system Al2024/industrial treatment/powder paint is significantly better than those of the system Al2024/T2/powder paint (Figures 49 (h) and (i)).

a: water-based paint T0 (24h)	b: water-based paint T2 (24h)
c: SPF 650 T0 (24h)	d: SPF 650 T2 (24h)

e: P91PI34B T0 (24h)	f: P91PI34B T2 (24h)
g: Powder paint no treatment (7d)	h: Powder paint T2 (7d)
i: Powder paint industrial treatment (7d)	
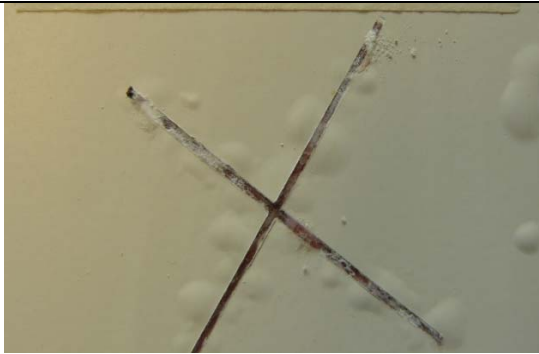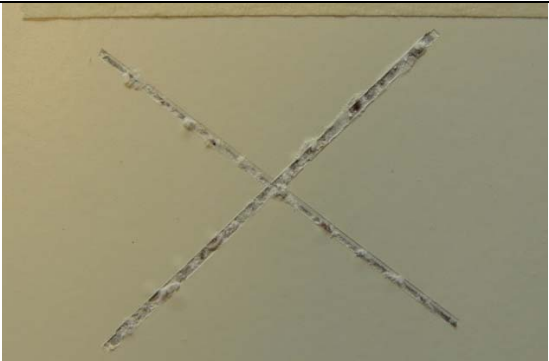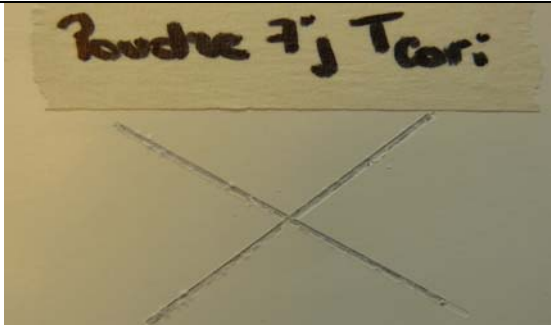
Figure 49 - Coated panels after an exposure to acetic salt spray.

Electrochemical Impedance Spectroscopy (EIS)

Coated panels were characterized by EIS (NaCl concentration: 3% - frequency range: 3.10^5 to 5.10^2 Hz - perturbation signal amplitude: 15 mV). Measurements were started immediately after the samples immersion. They were performed after 1d, 4d, 7d, 14d and 21d. The immersed area was 1.13 cm^2. The thickness of the paint was:

o ~30 μm for the water based paint,

o ~20 μm for the photocurable water-based paint P91PI34B,

o ~20 μm for the 100% photocurable paint SPF650 and

o at least 60 μm for the powder paint.

Bode diagrams (Figure 50) show that the protective properties of the photocurable paint SPF650 and of the powder paint are essentially determined by the formulation of the coating and not by the treatment. They are highly protective. At low frequencies, their impedance is still higher than 10^7 Ω.cm^2 after 7 days of immersion.

The protective effect of the water-based paint seems to be improved by the presence of treatment 2 on the aluminum substrate. The system water-based paint/T2 is still protective after 7d whereas this paint on T0 and on T1 is not protective anymore after 4 days.

The protective properties of the photocurable water-based paint are increased when the treatments contain cerium oxide and/or cerium nitrate. P91PI34B/T1 and P91PI34B/T2 are more resistant than P91PI34B/T0. At d0, their impedances are higher than 10^7 Ω.cm$^{2.}$
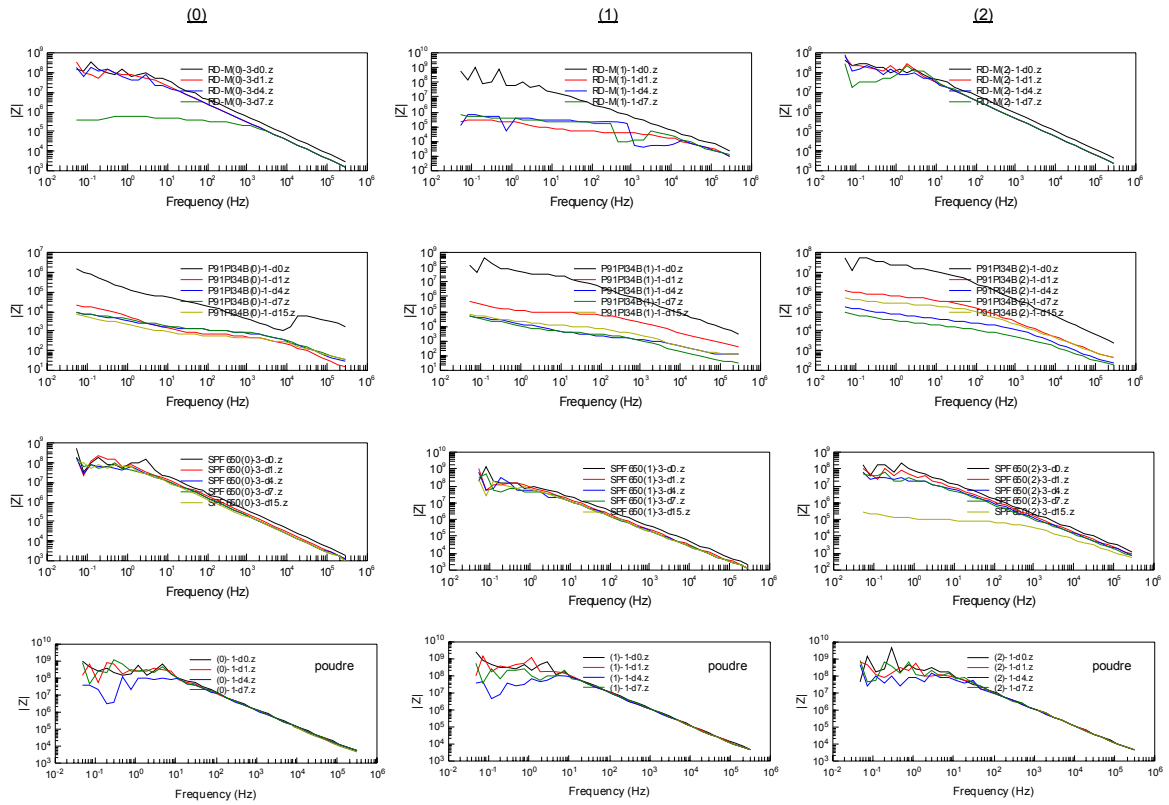
Figure 50 - Bode diagrams of coated Al2024 panels (paints: acrylic water-based paint (RD-M) and photocurable paints P91Pl34B and SP650, and powder paint).

CONCLUSIONS

System 1

The object of this study is the comparison among BTSE films (system 1) deposited with three different techniques: dipcoating (water-based silane), vacuum plasma and atmospheric plasma.

Atmospheric and vacuum plasma deposition of BTSE films has never been reported in the literature before. XPS and IR measurements show the presence of silicon under Si-O state in the layers deposited by the different methods. IRRAS highlights groups such as Si-O-Si, Si-O-C, Si-O and Si-CH$_3$.

XPS is used to quantify the silicon environments present in the different coatings. For dipcoated layers, a high proportion of Si(-O)$_2$ environment is obtained. The silicon atoms in the plasma BTSE films deposited by vacuum plasma are in the Si(-O)$_3$ environment. For atmospheric plasma method, 43% of the silicon atoms are in the Si(-O)$_4$ environment and 57% are bonded to three oxygen (Si(-O)$_3$).

The layers deposited by vacuum plasma can be considered as more organic-inorganic films, comparable to the silane layers obtained by dipcoating. Atmospheric plasma treatments, however, lead to the formation of oxidized films richer in Si-O bonds, hence more inorganic than those deposited by vacuum plasma and dipcoating.

The interfacial bonding of plasma polymer BTSE films deposited by vacuum and atmospheric plasma on the aluminum (99.99%) substrate has been assessed with ToF-SIMS and XPS combined to a sonication test.

The existence of a fragment at nominal mass 71 in the ToF-SIMS spectrum at the interface between the plasma polymer BTSE film and the substrate is assigned to AlOSi$^+$. This ion evidences a specific interaction -a true chemical covalent bond-between the aluminium and plasma polymer BTSE film. The AlOSi$^+$ fragment is present through an interfacial layer on top of the aluminium oxide layer.

The strength of the plasma polymer BTSE films bonding to the aluminium substrate has been assessed and positively confirmed by comparing the XPS Si 2p signals before and after an ultrasonic rinse.

The BTSE films deposited with the three different deposition methods were also compared in terms of barrier and corrosion properties, through EIS measurements in Na$_2$SO$_4$ and NaCl. The three films showed only minor differences and in all cases their corrosion protective behavior disappeared after 1-day immersion, due to the very thin nature of these layers. The small thickness, in fact, affects the corrosion properties of the samples more than their chemistry and composition do.

System 2

Part of this project also dealt with vacuum and atmospheric plasma deposition of SiO_x films (system 2). Work performed in this direction showed that SiO_2, SiO_x, and SiO_xC_y films can be selectively grown by PECVD at low and atmospheric pressure using HMDSO as precursor. The $HMDSO/O_2$ ratio in the gas mixture has a crucial effect on the silicon chemical bond inside the deposits. The films obtained with a pure HMDSO plasma are polymeric with a surface rich in carbonated species; whereas the films obtained from a $HMDSO/O_2$ plasma are silica-like with a very small amount of carbon. An interesting feature is that the films deposited at low pressure and at atmospheric pressure have a similar composition. Finally, the porosity of the deposited films can be followed by the presence of hydroxyl groups (IR-spectra).

System 3

The novelty and originality of this work is the investigation of thin films of water-based BTSE (less than 100 nm), with the incorporation of nano-dispersed CeO_2 particles (system 3), uniformly distributed in the layer, for improved barrier properties. The small thickness of the film and the water-based nature of the silane are both key issues for industry, in the aim of saving on costs and material weight and reducing the impact on human health and the environment.

Measurements were performed in order to understand how the presence of the nano-oxides might affect the silane under study. ^{29}Si NMR analysis on the coating solutions shows that the presence of CeO_2 does not affect the stability and ageing of the BTSE solution over a period of 4 months. The chemical interactions between the CeO_2 nanoparticles and the silane in the cured coating were investigated by XPS. Shifts of binding energies and change in peaks' shape in the spectra of the individual compounds and of the mixed coating point to the possible formation of a bond between the Si from BTSE and the Ce in the cured film.

A critical issue in the formation of these hybrid thin coatings is the nanoparticles agglomeration to a size comparable to the film thickness, leading to the presence of hillocks on the sample surface, which affect its uniformity and might create preferential paths for corrosion attack. The formation of uniform and homogeneous thin films was successfully achieved by adding the CeO_2 nanoparticles to the coating solution in the form of an aqueous nano-suspension.

Information on the coating structure was collected by combining the results of FE-SEM, FE-AES, FIB-TEM/EDX analyses. They confirm the presence of nano-dispersed CeO_2 particles in the BTSE coating and reveal that these nano-oxides are always covered by a uniform BTSE film, or in other words, well embedded in the silane matrix. This explains the results obtained by EIS investigation in Na_2SO_4, which shows that the incorporation of CeO_2 nanoparticles modifies the barrier properties of the thin BTSE

layers, with a better performance observed for the coatings where the particles are nano-dispersed, hence providing a more uniform and homogeneous layer.

Further EIS measurements on these films deposited on AA2024-T3 were performed in NaCl, in order to study their corrosion properties, also in the presence of corrosion inhibitors (Ce^{3+}). Even though at first the samples showed a (minor) barrier behavior compared to the blank, they all lost their protection behavior after 1-day immersion in the NaCl solution. This is a further confirmation that the small thickness of the coating is the main responsible of the poor corrosion behavior of the samples, over the specific coating composition and/or the presence of additives.

Applied Properties

Pull-off tests measurements were performed on all systems to check the adherence of the films to the substrate: on BTSE (system 1) and on HMDSO (system 2) deposited on Al 99.99% by vacuum or by atmospheric plasma in presence or in absence of oxygen; and on Aludan AA H5005-H24 treated by dip coating (BTSE 7.5% alone, BTSE 7.5% + 250 ppm CeO_2, and BTSE 7.5% + 250 ppm CeO_2 + 250 ppm $Ce(NO_3)_3$).

The highest stresses were measured for P_{atm} BSTE. It can be assumed that the adherence of this treatment on Al 99.99% is the most important even if the nature of the rupture (adhesive or cohesive) has not been checked.

The influence of the presence of Ce oxide and/or of Ce nitrate on the adherence of the BTSE treatment deposited by dip coating was not established. The nature of the rupture was cohesive and adhesive.

Four paints were applied on aluminum (Al 2024-T3 and Aludan AA H5005-H24): an acrylic water-based paint, a photocurable water-based paint, a 100% photocurable paint and a polyester powder paint. The mechanical properties of the coated panels and their resistance to corrosion were measured.

The BTSE treatments (system 1) deposited by dipcoating do not increase the adherence of the selected paints on aluminum substrate (except for water-based paint on Aludan). A strong decrease of adherence was even observed when the powder paint was applied on the treated panels.

The presence of CeO_2 and Ce^{3+} improves the resistance of all the coated substrates to acetic salt spray. EIS measurements show that the protective properties of the water-based paint are the highest when both CeO_2 and Ce^{3+} are present in the silane layer and those of the water-based UV paint are the highest both when CeO_2 is alone in the silane and together with Ce^{3+}. The UV paint SPF 650 and the powder paint are the most protective systems. Their properties are not influenced by the nature of the treatment.

SUPPORT TO INNOVATION AND TRANSFER OF KNOWLEDGE

The most innovative aspect of this project is the comparison of coatings deposited by wet and plasma methods, in terms of their surface characterization, composition and applied properties, depending on the deposition parameters. In particular, it has been shown for the first time that pp-BTSE films can be successfully deposited by atmospheric and vacuum plasma.

Another innovative aspect is the inclusion of nanoparticles in the silane matrix, which is also investigated with plasma deposition.

The main channel for transfer of knowledge is through the follow-up committee. The meetings have been quite successful: all representatives of the industries involved showed interest in the various aspects of the project and took active part in providing material and/or setting up collaborations, already ongoing or planned just for the purpose of this project.

A lot of emphasis has been placed on the preparation of the coating solutions with inclusion of nanoparticles, which is an issue of general concern among people working in the field. The topic was also widely discussed with Umicore (there is an ongoing collaboration on the matter) and at various international conferences. The solution finally came from Umicore, which provided the project members with a water based nanosuspension of CeO_2.

Related to this is also the issue of solution stability and environmental impact, which are crucial points for industrial applications. These were both investigated through the use of water-based and plasma-polymerized coating systems. Deposition parameters (time, temperature, power, etc.) were optimized in order to meet industrial requirements for a final cost-effective product (thin films).

Constant effort has been made by the partners to intensify national and international collaborations with both academic institutions and industry partners.

FOLLOW-UP COMMITTEE

Users committee meetings were being held regularly and they always have been quite successful. In particular, the first users committee meeting was fundamental in order to choose the main parameters of the project, such as the substrate and the coating solution. All industry representatives agreed that silane with inclusion of oxide nanoparticles was the best model to be investigated, and they were all interested in the CeO_2. Further discussions concerned the thickness range of the films (set at less than 1 μm), the stability of the coating solution and deposition time. These are all crucial factors in the preparation of samples and should be adapted for more practical feasibility in the industry. The agreement of all industry members on these aspects was a great starting point, and kept the entire committee constantly interested in the project.

All discussions raised during the meetings were followed by action plans, and collaboration with various members.

In specific, collaborations have been very active with the following:

Chemetall GmbH supplied BTSE solutions (both pure, 98%, and water-based, 10% and 15%). In addition, interesting discussion and exchange of ideas rose on the issue of mixing such solutions with oxide nanoparticles.

There are ongoing interactions with **Umicore** for the issue of nanoparticles agglomerations into the coating solution. Their suggestion was that particles agglomeration can be avoided by using a high energy ultrasonic probe and of by functionalizing them, but this would imply not having them pure into the film. Finally, they supplied a water-based suspension of CeO_2 nanoparticles, agglomerates-free, which will be used to make the silane-based coating solution. This led to more uniform coatings with a constant thickness, not altered by the presence of oxide clusters. In addition, CPS (Centrifuge Particle Sizer) measurements were performed at their facility on FOMOS suspensions for a more detailed analysis of the particles distribution.

Interactions with **OCAS-Arcelor Mittal** are also ongoing. Preliminary GDOES (Glow Discharge Optical Emission Spectroscopy) experiments have been performed at their facility, but the samples analyzed did not give significant results. Focused Ion Beam (FIB) and Transmission Electron Microscopy (TEM) measurements were performed to characterize the samples and they gave very good results.

PUBLICATIONS

F. BRUSCIOTTI, A. BATAN, I. DE GRAEVE, M. WENKIN, M. PIENS, F. RENIERS, J.J. PIREAUX, J. VEREECKEN, H. TERRYN
Characterization of thin BTSE coatings on aluminium with the inclusion of nano-dispersed CeO$_2$ particles
On Review in Surface and Coatings Technology (Submitted on February 11th 2010)

A. BATAN, N. MINE, B. DOUHARD. F. BRUSCIOTTI, I. DE GRAEVE, J. VEREECKEN, M. WENKIN, M. PIENS, H. TERRYN, J.J. PIREAUX, F. RENIERS
Covalent bond formation at the silane-metal interface: the case of plasma polymerization of bis-1,2-(triethoxysilyl)ethane (BTSE) on aluminium
Chemical Physics Letters, Volume 493 (2010) pp. 107-112

A. BATAN, F. BRUSCIOTTI, I. DE GRAEVE, J. VEREECKEN, M. WENKIN, M. PIENS, J.J. PIREAUX, F. RENIERS, H. TERRYN
Comparison between wet deposition and plasma deposition of silane coatings on aluminium
Progress in Organic Coatings (In Press, DOI: 10.1016/j.porgcoat.2010.04.009)

ORAL PRESENTATIONS

ELSPEC 2010 (4ème Conférence Francophone sur les Spectroscopies d'Electrons) 3-6 May 2010, Fes (Morocco)

AVS 56 (International Symposium and Exhibition) 8-13 November 2009, San Jose, CA (USA)

ECASIA 2009 (13th European Conference on Application of Surface and Interfaces Analysis) 18-23 October 2009, Antalya (Turkey)

EUROCORR 2009 (The European Corrosion Congress) 6-10 September 2009, Nice (France)

ASST 09 (Vth Aluminium Surface Science & Technology) 10-14 May 2009, Leiden (The Netherlands)

AETOC 2009 (International Workshop Application of Electrochemical Techniques to Organic Coatings) 15-18 April 2009, Grado (Italy)

ICTF14 & RSD 2008 (14th International Conference on Thin Films & Reactive Sputter Deposition) 17-20 November 2008, Ghent (Belgium)

CoSI 2008 (Coating Science International) 23-27 June 2008, Noordwijk (The Netherlands)

I-SUP 2008 (Innovation for Sustainable Production) 22-25 April 2008, Bruges (Belgium)

ACKNOWLEDGEMENTS

REFERENCES

[1] I. De Graeve, J. Vereecken, A. Franquet, T. Van Schaftinghen, H. Terryn, Prog. Org. Coat., 59 (2007) 224-229.

[2] M.F. Montemor, A.M. Cabral, M.L. Zheludkevich, M.G.S. Ferreira, Surf. Coat. Technol., 200 (2006) 2875-2885.

[3] M.F. Montemor, M.G.S. Ferreira, Electrochim. Acta, 52 (2007) 6976-6987.

[4] M.F. Montemor, M.G.S. Ferreira, Prog. Org. Coat., 63 (2008) 330-337.

[5] M.F. Montemor, W. Trabelsi, S.V. Lamaka, K.A. Yasakau, M.L. Zheludkevich, Electrochim. Acta, 53 (2008) 5913-5922.

[6] L.M. Palomino, P.H. Suegama, I.V. Aoki, M.F. Montemor, H.G. De Melo, Corros. Sci., 51 (2009) 1238-1250.

[7] M. Garcia-Heras, A. Jimenez-Morales, B. Casal, J.C. Galvan, S. Radzki, M.A. Villegas, J. Alloys Compd., 380 (2004) 219-224.

[8] M.F. Montemor, A.M. Simões, M.G.S. Ferreira, Prog. Org. Coat., 43 (2001) 274-281.

[9] M.L. Zheludkevich, R. Serra, M.F. Montemor, M.G.S. Ferreira, Electrochem. Commun., 7 (2005) 836-840.

[10] M.L. Zheludkevich, R. Serra, M.F. Montemor, K. Yasakau, I.M. Miranda Salvado, M.G.S. Ferreira, Electrochim. Acta, 51 (2005) 208-217.

[11] N.E. Cant, K. Critchley, H.-L. Zhang, S.D. Evans, Thin Solid Films, 426 (2003) 31-39.

[12] V. Palanivel, D. Zhu, W.J. van Ooij, Prog. Org. Coat., 47 (2003) 384-392.

[13] C. Sanchez, G.J.D.A.A. Soler-Illia, F. Ribot, D. Grosso, Comptes Rendus Chimie, 6 (2003) 1131-1151.

[14] K. Aramaki, Corros. Sci., 44 (2002) 1621-1632.

[15] K. Aramaki, Corros. Sci., 45 (2003) 1085-1101.

[16] L.S. Kasten, J.T. Grant, N. Grebasch, N.N. Voevodin, F.E. Arnold, M.S. Donley, Surf. Coat. Technol., 140 (2001) 11-15.

[17] M.F. Montemor, A.M. Simões, M.G.S. Ferreira, Prog. Org. Coat., 44 (2002) 111-120.

[18] M.F. Montemor, W. Trabelsi, M.L. Zheludkevich, M.G.S. Ferreira, Prog. Org. Coat., 57 (2006) 67-77.

[19] W. Trabelsi, P. Cecilio, M.G.S. Ferreira, M.F. Montemor, Prog. Org. Coat., 54 (2005) 276-284.

[20] K.A. Yasakau, M.L. Zheludkevich, S.V. Lamaka, M.G.S. Ferreira, J. Phys. Chem., 110 (2006) 5515-5528.

[21] D. Zhu, W.J. Van Ooij, Electrochim. Acta, 49 (2004) 1113-1125.

[22] V. Palanivel, Y. Huang, W.J. Van Ooij, Prog. Org. Coat., 53 (2005) 153-168.

[23] L. Liu, J.-M. Hu, J.-Q. Zhang, C.-N. Cao, Electrochim. Acta, 52 (2006) 538-545.

[24] A.M. Cabral, W. Trabelsi, R. Serra, M.F. Montemor, M.L. Zheludkevich, M.G.S. Ferreira, Corros. Sci., 48 (2006) 3740-3758.

[25] W. Trabelsi, P. Cecílio, M.G.S. Ferreira, K. Yasakau, M.L. Zheludkevich, M.F. Montemor, Prog. Org. Coat., 59 (2007) 214-223.

[26] W. Trabelsi, E. Triki, L. Dhouibi, M.G.S. Ferreira, M.L. Zheludkevich, M.F. Montemor, Surf. Coat. Technol., 2006 (2006) 4240-4250.

[27] C. Tendero, C. Tixier, P. Tristant, J. Desmaison, P. Leprince, Spectrochim. Acta, B (2006).

[28] R. d'Agostino, Plasma Processing of Polymers, NATO ASI Series, Kluwer, Academic Publishers, 1997.

[29] K.G. Sachdev, H.S. Sachdev, Thin Solid Films, 107 (1983) 245-250.

[30] I. Tajima, M. Yamamoto, Journal of Polymer Science Part a-Polymer Chemistry, 25 (1987) 1737-1744.

[31] N. Inagaki, M. Taki, J. Appl. Polym. Sci., 27 (1982) 4337-4343.

[32] A. Sabata, W.J. Vanooij, H.K. Yasuda, Surf. Interface Anal., 20 (1993) 845-859.

[33] A.M. Wrobel, M.R. Wertheimer, J. Dib, H.P. Schreiber, Journal of Macromolecular Science-Chemistry, A14 (1980) 321-337.

[34] V. Barbarossa, S. Contarini, A. Zanobi, J. Appl. Polym. Sci., 44 (1992) 1951-1957.

[35] Ph. Supiot, C. Vivien, A. Granier, A. Bousquet, A. Mackova, D. Escaich, R. Clergereaux, P. Raynaud, Z. Stryhal, J. Pavlik, Plasma Processes and Polymers, 3 (2006) 100-109.

[36] R. Prikryl, V. Cech, R. Balkova, J. Vanek, Surf. Coat. Technol., 174-175 858-862.

[37] D. Susac, C.W. Leung, X. Sun, K.C. Wong, M. K.A.R., Surf. Coat. Technol., 187 (2004) 216-224.

[38] A. Franquet, Characterisation of silane films on aluminum, in: PhD Thesis - Department of Metallurgy, Electrochemistry and Materials Science, Vrije Universiteit Brussel, Brussels, 2002.

[39] I. De Graeve, E. Tourwé, M. Biesemans, R. Willem, H. Terryn, Prog. Org. Coat., 63 (2008) 38-42.

[40] A. Franquet, C. Le Pen, H. Terryn, J. Vereecken, Electrochim. Acta, 48 (2003) 1245-1255.

[41] A. Franquet, M. Biesemans, R. Willem, H. Terryn, J. Vereecken, J. Adhes. Sci. Technol., 18 (2004) 765-778.

[42] L.M. Palomino, P.H. Suegama, I.V. Aoki, M.F. Montemor, H.G. De Melo, Corros. Sci., 50 (2008) 1258-1266.

[43] P.H. Suegama, H.G. de Melo, A.V. Benedetti, I.V. Aoki, Electrochim. Acta, 54 (2009) 2655-2662.

[44] S. Hee Lee, D. Chool Lee, This Solid Films, 325 (1998) 83-86.

[45] D. Landheer, J.E. Hulse, T. Quance, This Solid Films, 293 (1997) 52-62.

[46] G. Bräuer, Surface and Coating Technology, 112 (1999) 358-365.

[47] K. Suzuki, This Solid Films, 351 (1999) 8-14.

[48] M.R. Alexander, R.D. Short, F.R. Jones, W. Michaeli, C.J. Blomfield, Appl. Surf. Sci., 137 (1999) 179-183.

[49] S. Reichlmaier, J.S. Hammond, M.J. Hearn, D. Briggs, Surf. Interface Anal., 21 (1994) 739-746.

[50] M. Gettings, A.J. Kinloch, J. Mater. Sci., 12 (1977) 2511-2518.

[51] M.L. Abel, R.P. Digby, I.W. Fletcher, J.F. Watts, Surf. Interface Anal., 29 (2000) 115-125.

[52] R.A. Cayless, D.L. Perry, The Journal of Adhesion, 26 (1988) 113 - 130.

[53] M.-L. Abel, R.P. Digby, I.W. Fletcher, J.F. Watts, Surf. Interface Anal., 29 (2000) 115-125.

[54] U. Bexell, M. Olsson, Surf. Interface Anal., 31 (2001) 223-231.

[55] K. Shimizu, M.L. Abel, J.F. Watts, J. Adhes., 84 (2008) 725-741.

[56] I. Montero, L. Galan, O. Najmi, J.M. Albella, Physical Review B, 50 (1994) 4881-4884.

[57] W.J. Patrick, G.C. Schwartz, J.D. Chapple-Sokol, R. Carruthers, K. Olsen, Journal of Electrochemical Society, 139 (1992) 2604-2613.

[58] M.S. Haque, H.A. Naseem, W.D. Brown, Journal of Electrochemical Society, 144 (1997) 3265-3270.

[59] C. Le Pen, B. Vuillemin, S. Van Gils, H. Terryn, R. Oltra, Thin Solid Films, 483 (2005) 66-73.

[60] A. Franquet, J. De Laet, T. Schram, H. Terryn, V. Subramanian, W.J. Van Ooij, J. Vereecken, Thin Solid Films, 384 (2001) 37-45.

[61] T. Schram, Characterisation of thin coatings on aluminium by means of visible and infrared spectroscopic ellipsometry, in: PhD Thesis - Department of Metallurgy, Electrochemistry and Materials Science, Vrije Universiteit Brussel, Brussels, 1999.

[62] M.F. Montemor, R. Pinto, M.G.S. Ferreira, Electrochim. Acta, 54 (2009) 5179-5189.

[63] X. Yu, G. Li, J. Alloys Compd., 364 (2004) 193-198.

[64] E. Bêche, P. Charvin, D. Perarnau, S. Abanades, G. Flamant, Surf. Interface Anal., 40 (2008) 264-267.

[65] H. Cui, G. Hong, X. Wu, Y. Hong, Mater. Res. Bull., 37 (2002) 2155-2163.

[66] T. Skála, F. Sutara, K.C. Prince, V. Matolín, J. Electron. Spectrosc. Relat. Phenom., 169 (2009) 20-25.

[67] T. Van Schaftinghen, C. Le Pen, H. Terryn, F. Hörzenberger, Electrochim. Acta, 49 (2004) 2997-3004.

[68] M.L. Zheludkevich, R. Serra, M.F. Montemor, I.M. Miranda Salvado, M.G.S. Ferreira, Surf. Coat. Technol., 200 (2006) 3084-3094.

[69] F. Deflorian, L. Fedrizzi, S. Rossi, P.L. Bonora, Electrochim. Acta, 44 (1999) 4243-4249.

[70] C. Le Pen, J. Vereecken, J. Appl. Electrochem., 35 (2005) 1303-1309.

[71] E. Van Gheem, J. Vereecken, C. Le Pen, J. Appl. Electrochem., 32 (2002) 1193-1200.

[72] Z. Jovanovic, J.B. Bajat, R.M. Jancic-Heinemann, M. Dimitrijevic, V.B. Miskovic-Stankovic, Prog. Org. Coat., 66 (2009) 393-399.